INVESTIGATION OF TURBULENT HEAT TRANSFER AND PRESSURE DROP CHARACTERISTICS IN THE ANNULI OF TUBE-IN-TUBE HEAT EXCHANGERS (HORIZONTAL LAY-OUT)

by
FRANCOIS P.A. PRINSLOO

Submitted in the partial fulfilment of the requirements of the degree
MAGISTER INGENERIAE

in
MECHANICAL ENGINEERING

at the
Department of Mechanical and Aeronautical Engineering
Faculty of Engineering, Built Environment and Information Technology
University of Pretoria

Supervisors: Prof Jaco Dirker and Prof Josua P. Meyer

December 2016

ABSTRACT

Author: Francois Petrus Abraham Prinsloo

Student number: 28326441

Supervisors: Prof J Dirker and Prof JP Meyer

Department: Mechanical and Aeronautical Engineering

Degree: Master of Engineering (Mechanical Engineering)

Tube-in-tube heat exchangers are commonly used in many applications and are generally operated in a counterflow configuration. Unfortunately, existing correlations developed for heat transfer and pressure drop predictions for the outer annular flow passage have been found to sometimes produce large discrepancies between them.

In this experimental study research was performed to obtain experimental data with the lowest possible uncertainties associated with it in order to validate existing correlations and to identify the core aspects that influence the heat transfer and pressure drop characteristics in annular flow passages that have neither uniform wall temperatures nor uniform wall heat fluxes. Focus was placed on the turbulent flow regime and temperature and pressure drop measurements were taken at different fluid velocities, annular diameter ratios, and inlet temperature of water.

Four horizontal test sections with annular diameter ratios of 0.327, 0.386, 0.409 and 0.483 and hydraulic diameter of 17.00, 22.98, 20.20 and 26.18 respectively were constructed from hard drawn copper tubes. The test sections were equipped with industry standard inlet and outlet configurations and had pressure drop lengths of between 5.02 m and 5.03 m and heat transfer lengths of between 5.06 m and 5.10 m. This resulted in length to hydraulic diameter ratios of between 194 and 300. A wide range of annular flow rates were considered and Reynolds numbers ranges from 15 000 to 45 000 were covered for both heated and cooled annulus operating conditions. Specific attention was given to the influence of the inlet fluid temperature. For heated annulus cases an inlet temperature range of 10°C to 30°C was covered, while for cooled annulus cases an inlet temperature range of 30°C to 50°C was covered.

Since one of the main focuses of the study was to provide accurate temperature measurement, especially local wall temperature measurements of the inner tube, an *in-situ* calibration technique of the wall thermocouples were used. This enabled continuous verification of the measurement accuracy and allowed re-evaluation of readings.

Based on the processed experimental results, it was found that the direction of heat transfer did not affect the average heat transfer coefficient across the inner tube wall. Longitudinal local heat transfer coefficients were found to not be constant along the test section length, but continually decreased towards the annulus outlet, indicating undeveloped thermal flow. Heated annuli had a larger average heat transfer coefficients compared to cooled annuli at similar Reynolds numbers.

This can be attributed to a dependency on fluid properties, which were less at higher bulk temperatures. Analysis showed although both had about the same local Nusselt numbers at the exit region, the heated annuli had much larger Nusselt numbers at the entrance region of the test section. The friction factor was mostly affected by the fluid velocity, but at low velocities higher friction factors were detected when inlet temperatures were lower.

For the data sets considered in this study, the average Nusselt number and the Colburn *j*-factor decreased somewhat with increase in annular diameter ratio. It seemed that the friction factor was also not influenced by the annular diameter ratio.

Publications in journals and conferences

FPA Prinsloo, J Dirker, JP Meyer. *"Heat transfer and pressure drop characteristics in the annuli of tube-in-tube heat exchangers (horizontal lay-out)"*, Proceedings of the 15th International Heat Transfer Conference (IHTC-15), Kyoto, Japan, Paper Number IHTC15-9225, 10-15 August 2014.

Journal article under review:
FPA Prinsloo, J Dirker, JP Meyer. *"Heat transfer direction dependence of heat transfer coefficients in annuli"*, Submission ID: HAMT-D-17-00086, Heat and Mass Transfer

Acknowledgements

My parents for their continual support and motivation.

To Nerine, for the love and support through good and rough times.

My fellow post-grad colleagues, allowing me to know that we were all together in the trenches; trenches filled with occasional birthday cake, Friday lunch, as much fun as possible and long working hours.

To Madder Steyn, with whom I spent more time in the labs than we did at home, for the all-nighters, all the discussions and planning, always able to help me understand the complex theory.

Dr. Jaco Dirker for his guidance and advice as study leader, for his patience when things were going rough and his excitement when results looked good.

The funding obtained from the NRF, TESP, University of Stellenbosch/ University of Pretoria, SANERI/SANEDI, CSIR, EEDSM Hub and NAC is acknowledged and duly appreciated.

For our Lord, who gave me the strength, mind and will-power to complete this momentous task.

TABLE OF CONTENTS

LIST OF FIGURES

LIST OF TABLES

NOMENCLATURE

a	Annular diameter ratio	[-]
A_s	Surface area	[m^2]
A_o	Cross sectional area of annulus	[m^2]
C_o	Outer tube correlation coefficient	[-]
C_p	Specific heat	[J/kgK]
CV	Control Volume	[-]
D_h	Hydraulic diameter	[m]
EB	Energy Balance	[%]
f	Friction factor	[-]
F_{ann}	Factor taking into account the dependence on a	[-]
h	Convective heat transfer coefficient	[W/m^2K]
k	Thermal conductivity	[W/mK]
K	Factor to take into account the temperature dependence of fluid properties	[-]
L_{dp}	Pressure drop length	[m]
L_{hx}	Heat exchange length	[m]
$\dot{m}$	Mass flow rate	[kg/s]
N	Number of thermocouples	[-]
Nu	Nusselt number	[-]
n	Exponent	[-]
p	Exponent in j-factor calculation	[-]
P	Reynolds number exponent	[-]
Pr	Prandtl number	[-]
Δp	Pressure drop	[Pa]
$\dot{Q}$	Heat transfer rate	[W]
$\bar{Q}$	Average heat transfer rate	[W]
Re	Reynolds number	[-]
Re^*	Modified Reynolds number	[-]
T	Temperature	[°C]
ΔT_{LMTD}	Logarithmic mean temperature difference	[°C]
$\bar{T}$	Average temperature	[°C]
V	Fluid velocity	[m/s]
x	Axial length along the heat exchanger	[m]

Greek Symbols

μ	Kinematic viscosity	[m^2/s]
ρ	Density	[kg/m^3]
$\emptyset$	Factor in Equation (2.12)	[-]

σ	Standard deviation	[-]

Subscripts

1 *(one)*	Inner tube outer wall
avg	Average
b	Bulk property
D_h	Based on hydraulic diameter
i	Inner tube
ii	Inner tube inlet
io	Inner tube outlet
j	Index number
local	Local property
o	Annulus
oi	Annulus inlet
oo	Annulus outlet
w	Wall

Abbreviations

RTD	Resistance Temperature Detector
TC	Thermocouple
VSD	Variable Speed Drive

CHAPTER 1 - INTRODUCTION

1.1 Background

"Wisdom begins in wonder." – Socrates

Heat transfer is an important energy transmission phenomenon and is critical in all thermodynamic related processes found in society. These processes include cooling and heating in day-to-day devices such as fridges or freezers, kettles, stoves, air conditioners, computers and motor vehicles. Heat transfer also plays a central role in many processes in industry. For example, in a power plant operated on the Rankine cycle, heat is transferred to liquid water, turning it into steam. After the steam has been used to perform a task (driving a turbine), heat has to be removed from the steam via cooling to condense it back into liquid. Many more examples exist.

The fundamental modes of heat transfer are *conduction*, *convection* and *radiation*. Conduction refers to the heat transfer that occurs across a solid or stationary fluid. Convection refers to the heat transfer between a moving fluid and solid surface, which are at different temperatures. Radiation describes the net transfer of heat between two surfaces at different temperatures, by means of photons in electromagnetic waves. Thermal radiation occurs through any transport medium (solid or fluid) or vacuum.

When heat is to be transferred to or from a fluid, it is often done by using a heat exchanger of some sort, which allows heat to be transferred from one fluid to another, without direct contact between the fluids. Documented research into the improvement of such devices can be dated back to the early twentieth century. Scientists and investigators studied amongst others, fluid properties and fluid mechanics. Prandtl's ground breaking work on the boundary layer lead to the understanding of fluid flow over a surface. With this knowledge, researchers investigated flow mechanisms inside tubes and flow channels while giving special attention to aspects such as fluid velocity profiles, friction factors and heat transfer capabilities.

Many different types of heat exchangers were developed and experimentally tested in order to develop correlations with which to mathematically describe, for instance, heat transfer coefficients and friction factors. Such correlations aided in the design process by allowing the user to predict with some measure of certainty the required dimensions for a specific heat transfer duty, and to draw up other specifications of a heat exchanger.

One of the most common types of heat exchangers is the tube-in-tube or double-pipe heat exchanger, shown schematically in Figure 1-1. Such heat exchangers consist of one tube placed approximately concentrically into another. The inner tube can be smooth or finned on either, or both of its inner and outer surfaces depending on the heat transfer requirements. The annular space, formed by the cavity between the two tubes, can for instance receive heat from a heating element wrapped around the inner tube, or it could exchange heat (receiving or loosing heat) with a fluid of a different temperature flowing inside the inner tube. When exchanging heat between two fluids, the heat exchanger is usually operated in a counter flow configuration (as is depicted in Figure 1-1)

where the fluids flow in opposite direction. Many researchers treated the annular diameter ratio, defined as the inner wall diameter divided by the outer wall diameter, as an important parameter when calculating the capacity of a tube-in-tube heat exchanger.

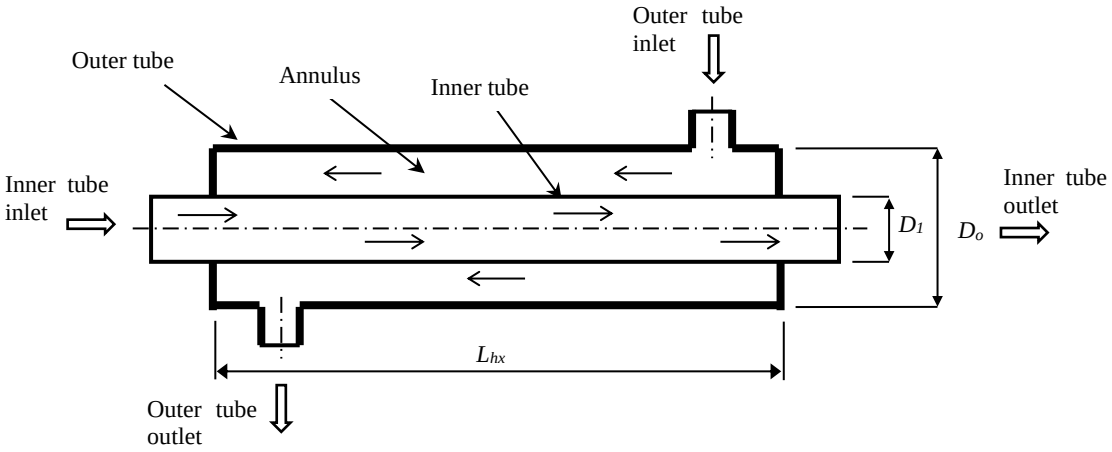

Figure 1-1: Representation of a tube-in-tube heat exchanger in counter flow configuration.

When operated in the turbulent flow regime, the most dominant mode of heat transfer in a tube-in-tube heat exchanger with fluid in both tubes is forced convection at both the inner and outer surfaces of the inner tube. This is due to the temperature difference between the inner tube surfaces and the fluids, as well as relative velocity of the fluids in terms of the stationary surfaces.

The study of convective heat transfer also requires interest in fluid mechanics. As fluid flows through a tube or passage, it experiences resistance to flow due to frictional forces at the interface between the fluid and the tube or passage surface. This results in a pressure drop over the length of the flow passage. The most important factors used to determine the magnitude of pressure drop are the fluid velocity, fluid viscosity, surface roughness and changes in tube geometry. Higher fluid velocity and fluid viscosity result in increased pressure loss over a tube section.

Research has shown that fluid mechanics has a direct impact on the heat transfer and friction factor, but the magnitude of the effect is not always quantifiable. One of the problems encountered in research on heat exchangers is the ability to, without affecting the fluid mechanics of the fluid in the tubes, accurately measure flow velocity, pressure drop and local temperature.

Having direct correlations that describe the convective heat transfer coefficient and the friction factor is useful to thermal design engineers. It allows them to make heat transfer and pressure drop predictions without being required to go through the costly time consuming process of experimentally measuring such values. Numerous heat transfer and friction factor correlations are available in literature. These correlations attempt to describe the dependence of such coefficients on geometric, thermal and flow parameters. Unfortunately, there are large discrepancies between some of these correlations. Dirker and Meyer (2004) found that some of these heat transfer-and friction factor predictions might differ by up to 20%. Authors differ on whether the ideal correlation for heat transfer in fully developed turbulent annular flow need to account for the annular diameter ratio, ratio between annulus wall and bulk fluid properties, the constant relation between the fluid

properties (represented by the Prandtl number) and Reynolds number, or the exponents necessary for each factor.

1.2 Problem Statement

It seems there is uncertainty as to whether a single correlation exists that can be used to accurately predict the heat transfer rate or the friction factor for annular flow at any combination of heat exchanger dimensions and fluid conditions. Additionally, there are opposing opinions regarding whether the effects of the direction of heat flux and the fluid temperatures is important when evaluating the heat transfer coefficient and friction factor. The role of the annular diameter ratio in correlations is disputed as well. These discrepancies have necessitated additional investigation to be conducted in order to attempt to address some of the disagreement and to remedy some of the shortfalls of existing experimental data-sets.

1.3 Research Objectives

The purpose of this experimental study was to:

- Design and build tube-in-tube heat exchanger test sections in such a way as to minimise the geometric effects on the fluid mechanics and heat transfer properties of the annular flow.
- Obtain reliable local wall temperature measurements on the outer tube and inner tube of the heat exchanger.
- Measure and record average fluid velocities and annular pressure drops over the length of the heat exchanger.
- Test the effects of different flow velocities, the inlet temperatures of the fluid in the annuli and the heat flux directions on the heat transfer and friction factor.
- Describe trends in experimentally obtained and analysed data, which could aid in improving existing correlations.

1.4 Delineation and limitations

The extent of the study was restricted by available equipment and space and time, as is the case with most experimental investigations. Only four annular diameter ratios were tested, reason being that each diameter ratio required the building of a complete heat exchanger and conducting a large array of experiments on it. The time required to achieve this for additional annular diameter ratios was not viable.

This study only considered turbulent annular flow in the Reynolds number range of 10 000 to 50 000. The design of the heat exchanger limited the inlet temperature to a maximum of 50ºC. Ambient temperatures and equipment capacity limited the cooling of the water to a minimum of 10ºC.

1.5 Significance of the study

It is believed that this study will improve researchers' understanding of the annular heat transfer phenomenon. The research can solve queries regarding the influence of heat flux direction and the fluid inlet temperatures on the heat transfer rate and friction factor. New design and construction techniques can yield accurate data to be used in development of correlations. Local wall

temperatures can help to get a better understanding of the growth of local heat transfer rate along the length of a tube-in-tube heat exchanger.

1.6 Chapter overviews

This dissertation consists of seven main chapters. The first (and current) chapter introduces the reader to the nature of the study and the content of the report. Chapter 2 contains the literature survey in which a review is given on topics that include Nusselt number correlations and friction factor correlations. Chapter 3 contains a description of the experimental test facility, a discussion on the design and construction of the test sections, and an overview of the calibration of instruments. Chapter 4 contains a description of the experimental procedure followed. Chapter 5 contains details on the data processing methods. Chapter 6 contains the experimental results and a discussion there-of. Chapter 7 list the major findings of the investigation and supplies the reader with the conclusions that were drawn from the study.

CHAPTER 2 - LITERATURE SURVEY

2.1 Introduction

In the past century there has been a wealth of research conducted into the heat transfer and pressure drop characteristics of annular flow. However, as measuring techniques evolved and accuracies improved, researchers developed new correlations in an attempt to create predictions with superior accuracy. There has been contradicting opinions on what factors have an influence on the predictions.

This chapter includes a review of literature covering topics pertinent to this study, including Nusselt number correlations and friction factor correlations.

2.2 Nusselt Number Correlations

Possibly the first person to establish a method to predict heat transfer was Wilhelm Nusselt [1]. He proposed a dimensionless group, later named after him as the Nusselt number, with which the convective heat transfer can be presented. The Nusselt number can be computed as the ratio of the product of the convective heat transfer coefficient with the characteristic length (often the hydraulic diameter), to the conductive heat transfer coefficient as:

$$\mathrm{Nu} = \frac{hD_h}{k} \tag{2-1}$$

The Nusselt number shows the enhancement of heat transfer through the layer as a result of convection relative to conduction across the same fluid layer. The larger the Nusselt number, the more effective the convection. A Nusselt number equal to unity for a fluid layer signifies heat transfer across the layer by pure conduction [2].

2.2.1 Work from the 1900's

In 1915 Nusselt [1] proposed the use of a power function to predict the convective heat transfer characteristic in an enclosed flow channel:

$$\mathrm{Nu} = c\mathrm{Re}^{m1}\mathrm{Pr}^{m2}\left(\frac{d}{L}\right)^{m3} \tag{2-2}$$

where Re was the Reynolds number, Pr the Prandtl number, d the diameter and L the tube length. Many researchers after him worked on attaining reliable values for his proposed coefficient c and exponents m_1, m_2 and m_3 used in Eq. (2-2).

Sieder and Tate [3] realised in 1936 that at that time, correlations used either main stream properties or film properties. They then improved Eq.(2-2) to account for the heating or cooling of the fluid by including the viscosity ratio at the wall:

$$\mathrm{Nu} = 0.02\mathrm{Re}^{0.8}\,\mathrm{Pr}^{1/3}\left(\frac{\mu}{\mu_w}\right)^{0.14} \tag{2-3}$$

The proposed correlation showed less than 10% absolute mean deviation between predicted and measured results for Reynolds numbers up to 90 000. Beyond this point the equation starts to over predict by as much as 25% at Reynolds number of 150 000.

In 2005 Dirker and Meyer [4] investigated eleven correlations available in literature developed in the 20th century for the calculation of heat transfer in smooth concentric annuli with fully developed turbulent flow and compared it to data obtained from their own work. The correlations are given in Table 2-1, adapted from [4]. The predictions they evaluated included the works of Davis (1943), McAdams (1954), Foust and Christian (1940), Monrad and Pelton (1942), Wiegand *et al.* (1945), Kays and Leung (1963), Petukhov and Roizen (1964), Dittus - Boelter (1930), Stein and Begell (1958) and Crookston *et al.* (1968). Some of the works mentioned above are more applicable to this study than the rest and will be considered more extensive below.

Davis (1943)

In 1943 Davis [5] aimed to create a correlation to predict the heat transfer in an annular space, irrespective of the annular diameter ratio or fluid medium:

$$\mathrm{Nu} = 0.038a^{-0.15}\mathrm{Re}^{0.8}\,\mathrm{Pr}^{1/3}\left(\frac{\mu}{\mu_w}\right)^{0.14} \tag{2-4}$$

where the annular diameter ratio was $a = D_1/D_o$ with D_1 the annulus inner wall diameter and D_o the annulus outer wall diameter. The above equation can also be rewritten in such a way that both the Reynolds and Nusselt numbers are based on the hydraulic diameter of the annulus ($D_h = D_o - D_1$), rather than the annulus inner diameter:

$$\mathrm{Nu}_{Dh} = 0.038a^{-0.15}(a-1)^{0.2}\mathrm{Re}_{Dh}{}^{0.8}\,\mathrm{Pr}^{1/3}\left(\frac{\mu}{\mu_w}\right)^{0.14} \tag{2-5}$$

It can be noted that the correlation proposed by Davis is based on the equation proposed by Sieder and Tate, only differing by the addition the factor $0.038a^{-0.15}(a-1)^{0.2}$ to accommodate for the influence of the annular diameter ratio.

This particular correlation is of importance to this study due to its ability to include the influence of different annular ratios on the heat transfer capabilities of a tube in tube heat exchanger.

McAdams (1954)

McAdams [6] published a textbook where he discussed and compared various proposed correlations for the prediction of Nusselt number in annular spaces. He stated that heat transfer over the inner wall of an annulus can be best predicted with

$$\mathrm{Nu} = 0.023\mathrm{Re}^{0.8}\,\mathrm{Pr}^{1/3}\left(\frac{\mu}{\mu_w}\right)^{0.14} \tag{2-6}$$

Notice that he did not include a factor to compensate for different annular diameter ratios, but similar to Sieder and Tate proposed a correlation which takes into account the effect of difference in temperature between the bulk fluid and the annular inner wall. In fact, his correlation is almost identical to that of Sieder and Tate, except for the constant factor being 0.023. No account was given on the accuracy of his proposed equation.

Important to this study is McAdams' notion that the annular diameter ratio had such a little effect on the predicted Nusselt number that it could be omitted from the equation.

Dittus - Boelter (1930)

Dittus - Boelter [7] derived an equation for the calculation of the local Nusselt number in fully developed turbulent flow in smooth circular tubes. Adjusted for hydraulic diameter, their proposed equation was:

$$\mathrm{Nu}_{Dh} = 0.023{\mathrm{Re}_{Dh}}^{0.8}\mathrm{Pr}^{n} \tag{2-7}$$

where $n = 0.3$ for cooling of the annular fluid and $n = 0.3$ for heating of the annular fluid.

It was stated that the equation should be used for moderate temperature differences between the inner annulus wall and the fluid. This equation is of importance to this study due to the fact that although it was not developed for annuli, it is often accepted that it can be used by employing the hydraulic diameter instead of the circular diameter.

2.2.2 Recent Works

Work done in recent years produced more correlations, included in Table 2-2 adapted from [8]. Some of these were based on previous correlations using new data measured with modern equipment, while others are new semi-empirical type correlations. These proposed correlations will be discussed in more detail below.

Dirker and Meyer (2005)

After comparing their own work to that of others, Dirker and Meyer [4] found differences of up to 20% between the correlations and as a result presented their own correlation. Their correlation was developed using the modified Wilson plot method, as developed by Briggs and Young [9], and included factors to account for the annular geometry influences dependent on the annular diameter ratio. Their data was collected from nine different test sections, each with a different annular diameter ratio. This equation proofed to be accurate to within 3% from their experimental data. The equation as proposed by Dirker and Meyer:

$$\mathrm{Nu}_{Dh} = C_o{\mathrm{Re}_{Dh}}^{P}\,\mathrm{Pr}^{\frac{1}{3}}\left(\frac{\mu_o}{\mu_{iw}}\right)^{0.14} \tag{2-8}$$

where the exponent *P* was calculated as

$$P = 1.013e^{-0.067/a} \tag{2-9}$$

and the coefficient C_o determined by

$$C_o = \frac{0.003a^{1.86}}{0.063a^{-3} - 0.0674a^{-2} + 2.225/a - 1.157} \tag{2-10}$$

Swamee et al (2008)

In 2008 Swamee *et al* [10] developed a correlation using fundamental equations of heat transfer to incorporate a compensation for annular ratio into the Sieder and Tate correlation, given in Eq.(2-11). They used this equation to optimize the tube diameters and flow rates of tube-in-tube heat exchangers.

$$\mathrm{Nu}_{Dh} = \frac{0.027}{(1+1/a)^{0.2}} \mathrm{Re}_{Dh}{}^{0.8} \mathrm{Pr}_o{}^{1/3} \left(\frac{\mu_o}{\mu_{iw}}\right)^{0.14} \tag{2-11}$$

Lu and Wang (2008)

Lu and Wang [11] investigated different orientations of tube-in-tube heat exchangers. They performed experiments on heat exchangers with horizontal flow, upward flow and downward flow. From this data, they produced a Dittus-Boelter type equation (Eq.(2-12)).They did not investigate the effect of annular diameter ratio on the heat transfer.

$$\mathrm{Nu}_{Dh} = 0.0022 \mathrm{Re}_{Dh}{}^{0.8} \mathrm{Pr}_o{}^{0.4} \tag{2-12}$$

Gnielinski (2009)

In 1993 Gnielinski [12] developed a correlation by modifying a semi-empirical type correlation intended for fully developed tube flow to accommodate annular flow. In 2009 [13] he revised the correlation with the inclusion of the published data of Dirker and Meyer [4]. He developed a semi-empirical type correlation, similar to that of Prandtl:

$$\mathrm{Nu}_{Dh} = \frac{(f/8)\mathrm{Re}_{Dh}\mathrm{Pr}_o}{\varphi + 12.7\sqrt{(f/8)}\left(\mathrm{Pr}_o^{2/3} - 1\right)} \left[1 + \left(\frac{D_h}{L_{hx}}\right)^{2/3}\right] F_{ann} K \tag{2-13}$$

where

$$\varphi = 1.07 + \frac{900}{\mathrm{Re}_{Dh}} - \frac{0.63}{(1 + 10\mathrm{Pr}_o)} \tag{2-14}$$

He incorporated the effect of the velocity profile of flow in an annular duct by acknowledging the dependency of the friction factor f on the annular diameter ratio ($a = D_1/D_o$):

$$f_{ann} = (1.8 \log_{10} \mathrm{Re}^* - 1.5)^{-2} \tag{2-15}$$

where

$$\mathrm{Re}^* = \mathrm{Re}\, \frac{(1+a^2)\ln a + (1-a^2)}{(1-a)^2 \ln a} \tag{2-16}$$

Furthermore, Gnielinski suggested that the direction of heat flux influences the heat transfer due to physical properties being temperature dependent. At that time, there was no available literature on this phenomenon for annular ducts. Therefore, he adopted correction factors developed for circular tubes. Variation in fluid properties due to temperature change was taken into account using

$$K = \left(\frac{\mathrm{Pr}}{\mathrm{Pr_w}}\right)^{0.11} \textit{for liquids} \tag{2-17}$$

where Pr is the Prandtl number of the liquid at bulk temperature and Pr_w at wall temperature respectively. For gasses the variation in fluid property was accounted for with

$$K = \left(\frac{T_b}{T_{iw}}\right)^n \tag{2-18}$$

where $n = 0.45\ for\ 0.5 < \frac{T_b}{T_{iw}} < 1.0$ and $n = 0$ if the gas was cooled. Gnielinski suggested that $n \approx 0.15$ for steam and carbon dioxide in the same range.

The annular diameter ratio dependence was taken into account with the factor F_{ann}:

$$F_{ann} = 0.75a^{-0.17} \tag{2-19}$$

Table 2-1: Correlations, as investigated by Dirker and Meyer, for the prediction of the Nusselt number in smooth annular flow.

Author(s)	Correlation	Diameter ratio Range (a)	Reynolds number range (Re_{Dh})	Medium
Davis [5]	$^{*}Nu_{Dh} = 0.038a^{-0.15}\left(\frac{1}{a}-1\right)^{0.2} Re_{Dh}^{0.8} Pr_o^{1/3}\left(\frac{\mu}{\mu_w}\right)_o^{0.14}$	0.000147-0.847	Not Specified	All media
McAdams [6] (quoted as Davis equation of 1943)	$Nu_{Dh} = 0.03105a^{-0.15}\left(\frac{1}{a}-1\right)^{0.2} Re_{Dh}^{0.8} Pr_o^{1/3}\left(\frac{\mu}{\mu_w}\right)_o^{0.14}$	0.000147-0.847	Not Specified	All media
Foust and Christian [6]	$^{*}Nu_{Dh} = \frac{0.04a}{\left(\frac{1}{a}+1\right)^{0.2}} Re_{Dh}^{0.8} Pr_o^{0.4}$	0.543-0.833	3 000 - 60 000	Water
McAdams [6]	$Nu_{Dh} = 0.023 Re_{Dh}^{0.8} Pr_o^{\frac{1}{3}}\left(\frac{\mu}{\mu_w}\right)_o^{0.14}$	Not specified	Not specified	Not specified
Monrad and Pelton [14]	$Nu_{Dh} = 0.023\left[\frac{2\,ln\frac{1}{a}-\frac{1}{a^2}+1}{\frac{1}{a}-a-2\frac{1}{a}ln\frac{1}{a}}\right] Re_{Dh}^{0.8} Pr_o^{n}$ where $n = 0.3\ for\ cooling, n = 0.4\ for\ heating$	0.606, 0.408, 0.0588	12 000 – 220 000	Water, air
Wiegard et al. [15]	$Nu_{Dh} = 0.023a^{-0.45} Re_{Dh}^{0.8} Pr_o^{n}\left(\frac{\mu}{\mu_w}\right)_o^{0.14}$	- 1.0	Not Specified	Fluids: $\mu_{material} \leq 2\mu_{water}$
Kays and Leung [16]	Results listed in tables for various conditions	0 - 1.0	10^4 - 10^6	Not specified
Petukhov and Roizen [17]	$^{*}Nu_{Dh} = \frac{0.06759a^{-0.16}}{\left(\frac{1}{a}+1\right)^{0.2}}\zeta Re_{Dh}^{0.8}$ where $\zeta = 1 + 1.75\left[\frac{\frac{1}{a}-5}{\left(\frac{1}{a}-1\right)Re_{Dh}}\right]$ for $a \geq 0.2$ $\zeta = 1$ for $a \leq 0.2$	0.07 – 1.0	10^4 – 3x10^5	Air
Dittus - Boelter [7]	$Nu_{Dh} = 0.023 Re_{Dh}^{0.8} Pr^{n}$ where $n = 0.3\ (Cooling), n = 0.4\ (Heating)$	Not specified	> 10 000	Not specified
Stein and Begell [18]	$Nu_{Dh,f} = 0.0200a^{-0.5} Re_{Dh,f}^{0.8} Pr_f^{\frac{1}{3}}$	0.812, 0.684, 0.59	30 000 – 390 000	Water
Crooksten et al. [19]	$Nu_{Dh} = 0.23a^{-\frac{1}{4}} Re_{Dh}^{\frac{3}{4}} Pr_o^{\frac{1}{3}}$	0.1, 0.0625, 0.0323	17 000 – 100 000	Air

*Original equations were rewritten to have the Reynolds and Nusselt numbers based on the annular hydraulic diameter, $D_h = D_o - D_1$.

Table 2-2: Correlations recently published for determining the heat transfer in a smooth concentric annulus.

Author(s)	Correlation	Diameter ratio Range (a)	Reynolds number range (Re_{Dh})	Medium
Gnielinski [12]	$\mathrm{Nu}_{Dh} = \frac{(f/8)\mathrm{Re}_{Dh}Pr_o}{1+12.7\sqrt{(f/8)}\left(Pr_o^{2/3}-1\right)}\left[1+\left(\frac{D_h}{L_{hx}}\right)^{2/3}\right]F_{ann}K$	Not specified	2300 - 10^6	Water
Dirker & Meyer [4]	$\mathrm{Nu}_{Dh} = C_o{\mathrm{Re}_{Dh}}^{P}\,\mathrm{Pr}^{\frac{1}{3}}\left(\frac{\mu_o}{\mu_{iw}}\right)^{0.14}$ $P = 1.013e^{-0.067/a}$ $C_o = \frac{0.003a^{1.86}}{0.063a^{-3}-0.0674a^{-2}+2.225/a-1.157}$	0.3125 -0.588	$4x10^3$ -$3x10^4$	Water
Swamee et al [10]	$\mathrm{Nu}_{Dh} = \frac{0.027}{(1+1/a)^{0.2}}{\mathrm{Re}_{Dh}}^{0.8}{\mathrm{Pr}_o}^{1/3}\left(\frac{\mu_o}{\mu_{iw}}\right)^{0.14}$	Not specified	Not specified	Not specified
Lu & Wang [11]	$\mathrm{Nu}_{Dh} = 0.0022{\mathrm{Re}_{Dh}}^{0.8}{\mathrm{Pr}_o}^{0.4}$	0.6911	> $3x10^3$	Water
Gnielinski [13]	$\mathrm{Nu}_{Dh} = \frac{(f/8)\mathrm{Re}_{Dh}\mathrm{Pr}_o}{\varphi+12.7\sqrt{(f/8)}\left(\mathrm{Pr}_o^{2/3}-1\right)}\left[1+\left(\frac{D_h}{L_{hx}}\right)^{2/3}\right]F_{ann}K$ $\varphi = 1.07+\frac{900}{\mathrm{Re}_{Dh}}-\frac{0.63}{(1+10\mathrm{Pr}_o)}$ $K = \left(\frac{\mathrm{Pr}_o}{\mathrm{Pr}_{iw}}\right)^{0.11}$ for liquids $K = \left(\frac{T_b}{T_{iw}}\right)^{n}$ for gasses with n = 0 for cooling $\mathrm{n} = 0.45 \text{ for } 0.5 < \frac{\mathrm{T_b}}{\mathrm{T_{iw}}} < 1.0$ $\mathrm{F_{ann}} = 0.75\mathrm{a}^{-0.17}$ $f = (1.8\log_{10}\mathrm{Re}^{*}-1.5)^{-2}$ $\mathrm{Re}^{*} = \mathrm{Re}\,\frac{(1+a^2)\ln a+(1-a^2)}{(1-a)^2\ln a}$	Not specified	Not specified	All mediums

Nusselt number correlation comparison

To compare the predictions of relevant correlations to one another, each was applied to an experimental data set (data collected in this study) for a double pipe heat exchanger with an annular ratio of 0.386, an inner Reynolds number of 30 000, an inner tube inlet temperature of 10°C and an annular fluid inlet temperature of 50°C. The annular fluid velocity had a range with a Reynold number of 15 000 to 45 000. The results are shown in Figure 2-1. The predictions of Lu & Wang was on average almost double that of the other correlations and was subsequently left out of the graph to enable a better comparison. The graph includes the average of the four correlations compared. It is noticed that the prediction from Dirker and Meyer was typically 5.9% above the Average, while Gnielinski's correlation predicted 10.3% above Average. The prediction from Swamee *et al* under predicted the Average by 12.6%, while Dittus - Boelter, published in 1930, was only 3.7% below the Average.

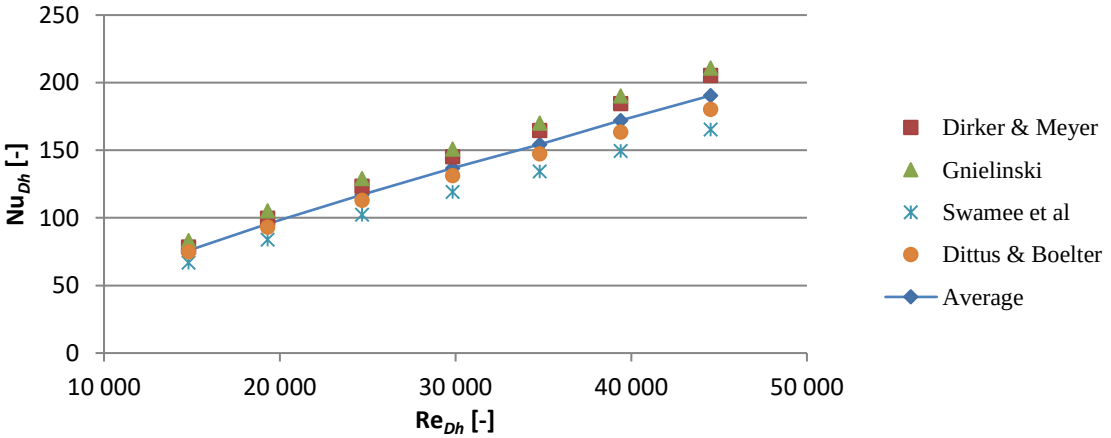

Figure 2-1: Comparison of predictions from Nusselt number correlations for a 0.386 annular ratio, Re_{Dh} of 15 000 to 45 000, T_{oi} of 50°C and T_{ii} of 10°C.

2.3 Conclusion: Nusselt number correlations

It is clear that there has been a lot of work on this topic in the past century, but unfortunately many different theories were developed and each proven by its author. It is thus not clear whether the ideal correlation for heat transfer in fully developed turbulent annular flow need to account for the annular diameter ratio, ratio between annulus wall and bulk fluid properties, the constant relation between the fluid properties (represented by the Prandtl number) and Reynolds number, or the exponents necessary for each factor. A set of data with small uncertainties, accommodating and alternating different variables, can assist in the comparison of existing correlations and development of new equations.

In the next section an overview is given of the literature review involving friction factor correlations.

2.4 Friction Factor Correlations

The friction factor in the annulus of a tube-in-tube configuration cannot be simplified as flow in a single circular tube. Specific correlations are needed due to the presence of an additional wall (inner

tube wall) which creates a more complex velocity profile in the annulus. Advancement of friction factor correlations has gone hand in hand with the development of Nusselt number correlations, in some instances using the same experimental setup. Unfortunately, so have the discrepancies between different works. Table 2-3 contains correlations for the prediction of the friction factor in smooth concentric annuli and will be discussed below.

Blasius (1912)

As early as 1912 Blasius [20], a student of Prandtl, did an investigation into the application of Prandtl's boundary layer concept. He found that friction in a tube was both a function of the Froude number and the viscosity. Therefore, he included the Reynolds number in the set of variables to account for viscosity, while the Froude number accounted for relative roughness.

Blasius found that for smooth annular pipe flow there existed a unique relation between f and Re, which he correlated as

$$f = 0.3164\mathrm{Re}_{Dh}^{-0.25} \tag{2-20}$$

Nobody would have assumed such a simple correlation, especially after the complexity of proposals made in the 19th century. To top it all, Blasius also stated that his correlation was not only valid for water flow in tubes, but for any Newtonian fluid.

Quarby (1967)

In 1967 Alen Quarby [21] did an experimental investigation into turbulent flow through concentric annuli. He reviewed the works of Davis [5], Rothfus *et al* [22], Lee and Barrow [23], Brighton and Jones [24], and Johnsson and Sparrow [25] and concluded his literature review with a statement often still applicable today: "*It is clear then that previous results, whilst covering a wide range of the parameters involved are somewhat inconclusive*." He deduced that the previous investigations had little agreement on whether the friction factor was a function of the diameter ratio and what its exact relation was to the hydraulic Reynolds number.

In his paper Quarby concluded from his own work that the friction factor was independent of the diameter ratio within the limits of his experimental accuracy (accuracy not stated). He found that his resulting correlation (of a Blasius form) was in close agreement with that of Brighton and Jones, with the best fit for his results given by

$$f = 0.0844\mathrm{Re}_{Dh}^{-0.255} \tag{2-21}$$

Quarby's correlation was developed for air as flow medium and he gives no indication as to its applicability to other fluids.

Jones and Leung (1981)

Jones and Leung [26] published a paper in 1981 wherein they investigated the data collected by Meter and Bird [27] and of Rothfus, Monrad and Secal [28]. Jones and Leung found an overall scatter of -25% to +35% about the Colebrook prediction for smooth tubes. They suggested that the Reynolds number was not the only parameter required to determine the friction factor. In addition,

some relation had to be made to the diameter ratio. They proposed an alteration of the Colebrook equation, which included a modified Reynolds number, Re^*, given by

$$\frac{1}{\sqrt{f}} = 2\log_{10} \mathrm{Re}^* \sqrt{f} - 0.8 \tag{2-22}$$

With the use of the modified Reynolds number, Re^*, their equation was developed for the prediction of friction factors in steady state, fully developed flow in smooth geometries, including concentric annuli, rectangular ducts and circular tubes. When applied to objectively confirmed data, the observed data had a scatter of approximately ±5%.

Kenada et al. (2003)

In 2003 Kenada *et al.* [29] created a predictive expression (not a correlation and not based on experimental laboratory data) by performing direct numerical simulations on flow inside an annulus:

$$\frac{f}{8} = \left[1.61 + \frac{1}{0.436} ln\left(\frac{\mathrm{Re}_{Dh}}{\sqrt{8/f}}\right) - \frac{550}{\mathrm{Re}_{Dh}\sqrt{f/8}}\right]^{-2} \tag{2-23}$$

They managed to eliminate the need of aspect ratio as a parameter in the algebraic predictive expression. It was reported that the diameter ratio only has an effect for flows closely approaching transitional flow. The prediction covered almost a complete range of flow and diameter ratio and was found to agree closely with the most reliable experimental data at the time of the study.

Table 2-3: Correlations to predict the friction factor for smooth annular flow.

Author(s)	Correlation	Diameter ratio Range (a)	Reynolds number range (Re_{Dh})	Medium
Blasius [20]	$f = 0.3164 Re_{Dh}^{-0.25}$	Not specified	3 000 - 200 000	All Media
Quarby [21]	$f = 0.0844 Re_{Dh}^{-0.255}$	0.347, 0.178 and 0.107	6 000 - 90 000	Air
Jones and Leung [26]	$\frac{1}{\sqrt{f}} = 2\log_{10}(Re^{*}\sqrt{f}) - 0.8$ $Re^{*} = \frac{Re_{Dh}\left((1+a^2)\ln a + (1-a^2)\right)}{(1-a)^2 \ln a}$	0.0 - 1.0	10 000 - 1 000 000	Based on data from other authors.
Kenada *et al* [29]	$\frac{f}{8} = \left[1.61 + \frac{1}{0.436} ln\left(\frac{Re_{Dh}}{\sqrt{8/f}}\right) - \frac{550}{Re_{Dh}\sqrt{f/8}}\right]^{-2}$	0.003 - 1.0	> 10 000	Not specified
Gnielinski [13]	$\frac{1}{\sqrt{f}} = 1.8\ \log_{10}(Re^{*}) - 1.5$	Not specified	Not specified	All Media

Gnielinski (2009)

Gnielinski [13] referred in his paper to the friction factor correlation as proposed by Kanokov (as referenced by Gnielinski [13]):

$$\frac{1}{\sqrt{f}} = 1.8 \log_{10} \mathrm{Re}^{*} - 1.5 \tag{2-24}$$

He used the above equation to calculate the friction factor for smooth annular flow. This prediction also makes use of a modified Reynolds number, Re^{*}, as the case with Jones and Leung [26].

Friction factor comparison

The friction factor correlations listed in Table 2-3, except for the correlation of Quarby, are compared to one another in Figure 2-2. The figure illustrates the predicted friction factor of each correlation for an annular diameter ratio of $a = 0.327$ and flow of $10\,000 \leq \mathrm{Re}_{Dh} \leq 50\,000$.

A clear scatter of about 7% difference is seen between the correlations. Of interest is the agreement between the correlations of Jones and Lang and Gnielinski, both of which includes a modified Reynolds number, Re^{*}, to account for the effect of the annular diameter ratio. The correlations of Blasius and Kenada *et al.* are also in agreement, down to a $\mathrm{Re}_{Dh} = 20\,000$. Below this the correlation of Kenada *et al.* seems to over predict the friction factor.

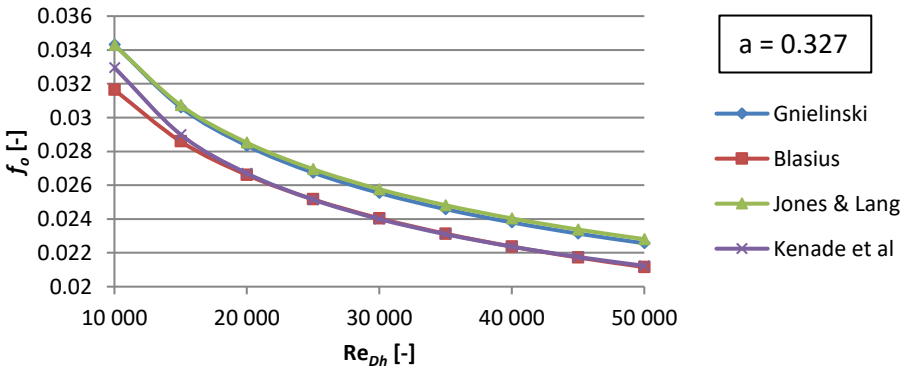

Figure 2-2: Comparison of existing friction coefficient correlations.

2.5 Conclusion: Friction factor correlations

There seem to be two schools of thought regarding friction factor correlations for smooth annular flow: either the friction factor takes into account the effect of the diameter ratio, or it is purely a function of the velocity and viscosity of the flow. It is seen above that there is about a 7% difference between the two schools of thought.

2.6 Chapter summary

In this chapter the reader was familiarised with previous work done to predict Nusselt numbers and friction factors for turbulent flow in concentric annuli. It is clear that there is a divide in opinions regarding the factors which should be included in the correlations. For both Nusselt number and friction factor, there seem to be disagreement in relation to the effect of the annular diameter ratio has on predicted values. Some researchers feel that it is not necessary to include the annular

diameter ratio in correlations, but instead only hydraulic diameter compensation will suffice for annular flow. The direction of heat flux might also have an influence on the heat transfer, as suggested by Gnielinski.

The next chapter will explain the experimental facility and processes to construct the test sections used in the experiments.

CHAPTER 3 - EXPERIMENTAL SETUP

3.1 Introduction

The experimental facility that was used to conduct the experiments was located in the Thermoflow Laboratories of the University of Pretoria. This chapter explains the layout of the experimental setup, with a description of the features and ranges of each apparatus. After this, the design process, manufacturing method and assembly of the test sections are also outlined.

3.2 Experimental Facility

The experimental facility was designed as a closed loop system consisting of a test bench onto which different test sections (tube-in-tube heat exchangers) could be coupled. The laboratory's existing test bench was modified to allow for the interchange of different test sections. Further modifications allowed the user to easily switch the flow direction in either the annulus or inner tube, or to change the water flow to allow either heating or cooling of the annulus.

Figure 3-1 gives a schematic representation of the experimental facility. It consisted of a hot water loop and a cold water loop. The shown configuration is that of a test section connected to the facility in order to allow hot water flow in the inner tube and cold water flow in the annulus, thus representing a heated annulus. If the hot water loop was to be connected to the annulus and the cold water loop connected to the inner tube, the heat exchanger would be configured to cool the annulus. Quick couplings and flexible hoses made this alteration swiftly if needed. Table 3-1 provides the reader with some basic technical detail of the components represented in Figure 3-1.

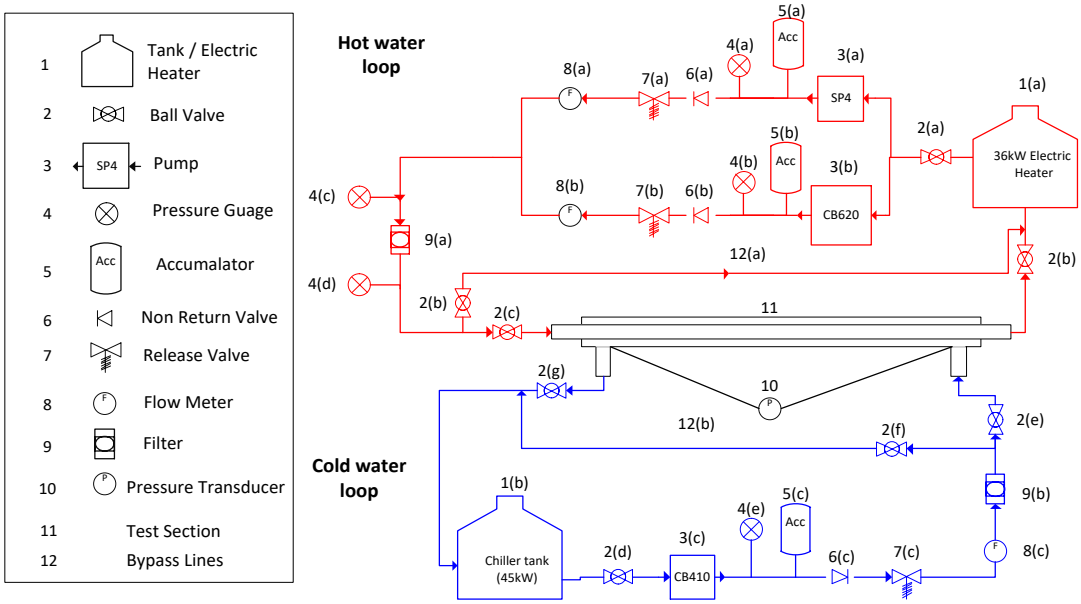

Figure 3-1: Diagram describing the layout of the experimental setup (Refer to Table 3-1).

Table 3-1: Technical information on equipment used on the test bench (Refer to Figure 3-1).

Item	Description
1(a)	36 kW electric heater, 1000 litre reservoir, thermally insulated.
1(b)	45 kW chiller, 2500 litre reservoir, thermally insulated.
2(a-g)	Ball valves.
3(a)	Positive displacement pump, CEMO SP4: Maximum flow rate of 2.8 m^3/h @ 1400 rpm, 6 m supply head, 0.24 kW power rating.
3(b)	Positive displacement pump, CEMO CB620: Maximum flow rate of 14 m^3/h @ 1400 rpm, 50 m supply head, 3.5 kW power rating.
3(c)	Positive displacement pump, CEMO CB410: Maximum flow rate of 5.8 m^3/h @ 1400 rpm, 12 m supply head, 0.5 kW power rating.
4(a-e)	Pressure dial gauges, 0-20 Bar.
5(a)	Accumulator, Capacity of 0.006 m^3.
5(b)	Accumulator, Capacity of 0.032 m^3.
5(c)	Accumulator, Capacity of 0.010 m^3.
6(a-b)	Non-return valves.
7(a-c)	Adjustable relieve valves to protect system from over pressure.
8(a)	Coriolis flow meter, CMF025, 0 – 0.606 kg/s, accuracy of 0.1% full scale.
8(b)	Coriolis flow meter, CMF100, 0.694 – 5.55 kg/s, accuracy of 0.1% full scale.
8(c)	Coriolis flow meter, CMF050, 0 – 1.833 kg/s, accuracy of 0.1% full scale.
9(a-b)	Inline filters.
10	Differential pressure transducers, accuracy of 0.25% full scale: 0 – 14 kPa, 0 – 22 kPa & 0 – 55 kPa
11	Test section
12	Bypass lines

First consider the hot water flow loop in Figure 3-1 (also refer to Table 3-1). A hot water reservoir, item *1(a)*, equipped with a 36 kW electric heater, serviced the hot water loop with a capacity of 1000 litres. The water temperature was set manually by adjusting the thermostat controlled switchgear which maintained the water within ±1ºC of the selected temperature. The water was pumped through the loop with either one of two positive displacement pumps, *3(a)* and *3(b)*,

depending on the flow rate required. The speed of each pump was controlled with a VSD (Variable Speed Drive). Each pump was connected to an accumulator, *5(a)* and *5(b)*, to dampen out the pulsations in the flow. Flow rates were measured with Coriolis mass flow metres, *8(a)* and *8(b)*. A filter, *9(a)*, was installed to trap loose particles in the water. The loop was equipped with pressure relieve valves, *7(a)* and *7(b)*, to protect against pressure surges and non-return valves, *6(a)* and *6(b)*, to protect the pumps. Pressure gauges, *4(a)* - *4(d)*, were installed throughout the loop to assist with in-time pressure monitoring. Valves, *2(b)* and *2(c)*, allowed the user to either pump through the test section *11*, or through the bypass line *12(a)* back to the reservoir.

The cold water loop was very similar to the hot water loop. However, a 45 kW chiller unit connected to a 2500 litre reservoir, *1(b)*, was used to service it. The temperature was thermostatically controlled to within ±1ºC of the selected temperature. A positive displacement pump, *3(c)*, controlled with a VSD, pumped the water through an accumulator, *5(c)*, before it entered the Coriolis mass flow meter *8(c)*. This loop was also equipped with a pressure relieve valve, pressure gauge, non-return valve, filter and bypass valves. All tubes and pipes conveying water were insulated to minimise heat exchange with the ambient. Details on the insulation will follow later in Section 3.3.4.

Pressure transducers, item *10*, fitted to take-off ports at both ends of the heat exchanger's outer tube measured the pressure drop over the length of the annulus. Since it was known that a pressure transducer has an accuracy of 0.25% of full-scale capability of the diaphragm used, three different sized transducers were installed to ensure optimum measurements. The pressure port design is discussed later.

Data was logged onto a desktop computer using equipment and software (Labview version 9.0.1) from National Instruments. Programming in Labview also enabled remote control of the VSDs, controlling the speed of each pump. Data was recorded at a rate of 10Hz. The Labview interface allowed the user to get real-time feedback of current conditions in the system.

3.3 Test Sections

Consider Figure 3-2 and Figure 3-3 giving schematic cross-sectional views of a concentric tube-in-tube test section constructed mainly from copper tube. The inner tube, which formed the inner wall of the annular space, had an inner diameter of D_i, and an outer diameter of D_1. The outer tube, which formed the outer wall of the annular space, had an inner diameter of D_0. As mentioned, the annular diameter ratio is defined as:

$$a = \frac{D_1}{D_0} \tag{3-1}$$

This ratio has a value smaller than 1 and will be used in this dissertation to identify and refer to the different test sections.

The inner and outer tubes were connected at both ends with industry standard T-piece fitting that was soldered onto the outer tube and tapered down to fit over the inner tube, as seen in Figure 3-4. The fluid entered the annular cavity through the T-piece, perpendicular to the heat exchanger,

resulting in definite undeveloped flow at the entrance region. The inlet of the T-piece was reduced to 7/8" to allow a standard 25 mm hose to fit over it.

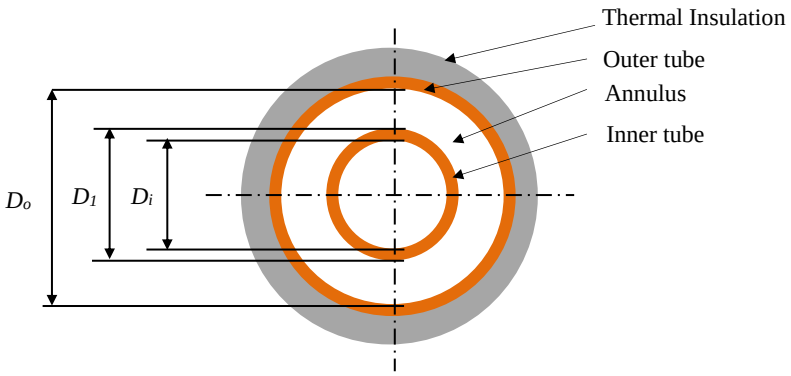

Figure 3-2: Cross section of heat exchanger

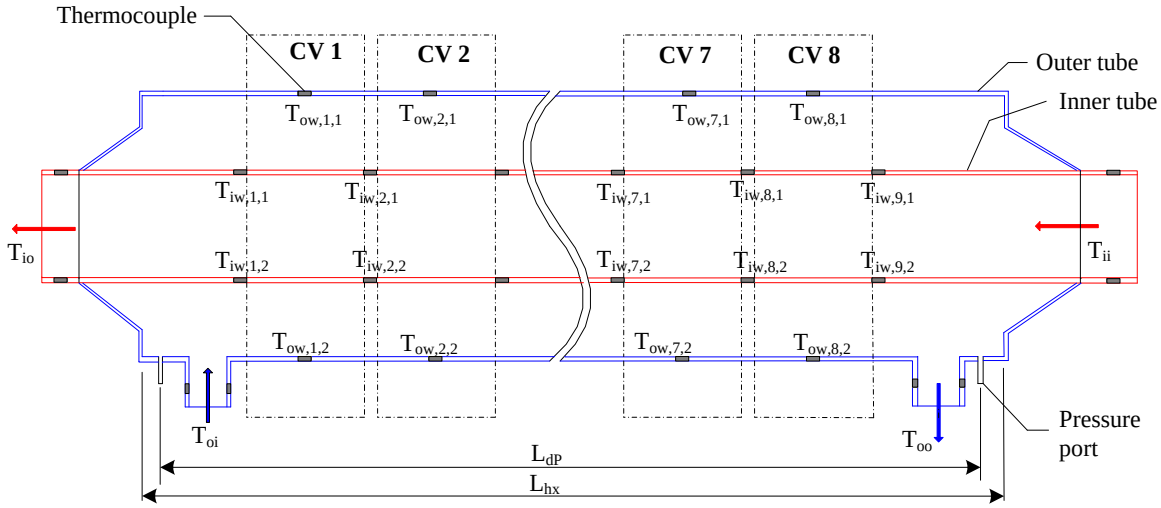

Figure 3-3: Axial schematic display of heat exchanger, showing inner tube, outer tube, inlets / outlets and division of control volumes (not to scale).

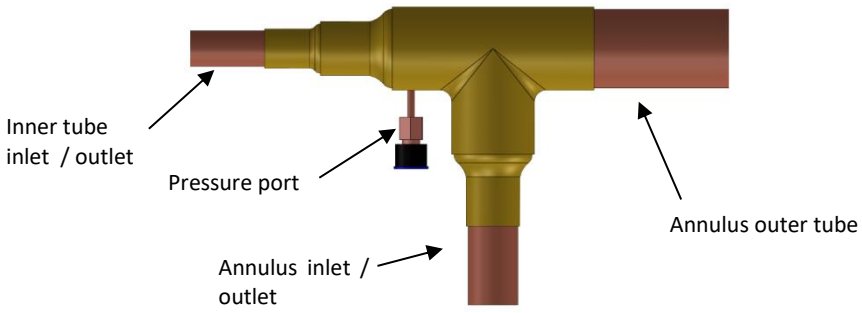

Figure 3-4: Model of inlet and outlet sections.

The outer tube was equipped with pressure ports at the inlet and outlet to allow for pressure drop measurement over the length of the tube, as seen in Figure 3-3 and Figure 3-4. These were constructed by soldering small copper tubes, with inner diameter of 2 mm and length of 25 mm,

positioned at the bottom of the annular passages in the stagnant flow regions, one before the inlet and the other after the outlet. A hole was then drilled through its centre into the outer tube wall. The diameters of the taps were far smaller than the recommended 10% of the hydraulic diameters of the annuli to avoid [30] significant influence on the pressure readings. Special care was taken to ensure no burrs were left behind after drilling the holes and that the tubes were smooth on the inside. Clear plastic hoses were run from the pressure ports to the pressure transducers. This resulted in length to diameter ratios (L_{dP}/D_h) ranging from 193.1 to 297.65.

Four different horizontally orientated heat exchanger test sections with lengths of approximately 5 m were built and tested in this experimental investigation. Table 3-2 gives a summary of the test section dimensions including each test section's relevant diameters, annular ratio, heat transfer length, L_{hx}, and pressure drop length, L_{dp}. The heat transfer length was measured as the full wetted length of the inner tube, while the pressure drop length was measured in axial direction from the inlet to outlet pressure taps.

Table 3-2: Summary of test section dimensions.

Test section	D_i (mm)	D_1 (mm)	D_o(mm)	D_h(mm)	a (-)	L_{hx} (m)	L_{dp} (m)
1	14.485	15.900	32.900	17.000	0.483	5.10	5.03
2	14.485	15.900	38.880	22.980	0.409	5.06	5.02
3	11.180	12.700	32.900	20.200	0.386	5.09	5.03
4	11.180	12.700	38.880	26.180	0.327	5.08	5.02

All the sections were built in an identical fashion having nearly the same dimensions, except for the inner and outer tube diameters. In total, only two inner tubes and two outer tubes were constructed. The four test sections were assembled by pairing different combinations of the two inner tube diameters and two outer tube diameters.

In order to measure the inlet and outlet temperatures of the water, both the inner tube and annular inlets and outlets were equipped with temperature measuring stations. Two 100 mm long transparent polyethylene hoses were used to connect the measuring stations to the inlets and outlets, thus avoiding axial heat conduction through the highly conductive copper tubing towards the measuring stations. These measuring stations each consisted of four circumferentially equally spaced T-type thermocouples attached to a short (80 mm) copper tube section which was thermally insulated from the ambient. The use of four thermocouples per measuring station was employed in order to reduce the relative uncertainty of the inlet and outlet fluid temperatures.

Considering the calculation of local heat transfer coefficients, the heat exchanger was divided into entrance, exit, and measurable area regions. This ensured fully developed flow in the measurable regions. For turbulent flow in a circular tube, the thermal entrance region is commonly approximated to be 10 times the tube's inner diameter [2]. However, for annular flow passages, there are no clear guidelines as the length of the thermal entry length. By taking the thermal entrance length to be 10 times the inner diameter of the largest outer tube, an entrance region of

390 mm was needed, while if the thermal entry length is taken to be 10 times the largest hydraulic diameter, an entrance region of 262 mm is obtained. Accordingly, it was decided that the hydraulic diameter could be used for estimating the lower limit of the thermal entry length. This resulted in entrance and exit regions of at least 300 mm. Having a heat exchanger with a planned length of 5 000 mm, this left 4 400 mm of measurable wetted length.

Originally, it was reasoned that measuring stations at intervals of 500 mm should allow for accurate local heat transfer analysis. More frequent measuring stations were regarded as redundant due to the fact that the measuring equipment might not be able to measure the small temperature differences between successive measuring stations with desired accuracy. Thus, the 4400 mm was divided into 8 control volumes (CVs), each with a length of 550 mm (refer to Figure 3-3). After attaching the inlet and outlet T-sections it was found that the lengths of the entrance and exit regions, measured from the centre of the T-section, were 315 mm.

As mentioned, one of the aims of the experiment was to investigate local and bulk annular passage heat transfer coefficient. Therefore, it was required to obtain local inner and outer tube wall temperature measurements. These local inner wall temperatures were measured using T-type thermocouples embedded in the inner tube wall, while outer wall temperatures were obtained by attaching thermocouples to the outer tube wall. The positioning of the inner tube thermocouples are shown in Figure 3-5 and are discussed in more detail in Section 3.3.1. Detail description of the outer tube thermocouple attachment is supplied in Section 3.3.2. The axial locations of the thermocouples were selected according to the eight equally sized control volumes (CV 1 to CV 8) that were used during the data-analysis process (this process will be discussed in a future chapter).

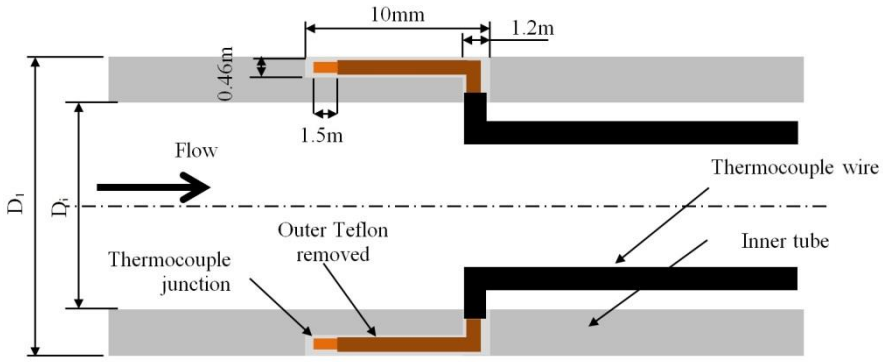

Figure 3-5: Attachment detail for thermocouples embedded in the inner tube wall (not to scale).

In total, inner tube wall temperature measurements were made at nine axial locations, at the beginning and at the end of each control volume, while the outer tube wall temperature measurements were made at eight axial locations, positioned in the axial centre of each control volume (halfway between the axial locations of the inner tube measuring positions). In order to decrease the temperature measurement uncertainty, more than one thermocouple was installed at each axial measuring location. In this study, two thermocouples spaced 180° apart were used for each axial location (one at the top and the other at the bottom). Therefore, each heat exchanger test section was equipped with 50 thermocouples that included those at the inlets and outlets as well as those installed on the inner and outer tubes, as is summarised in Table 3-3.

Table 3-3: Summary of thermocouple attachments

Location	Number of measuring stations	Number of thermocouples per station
Inlets and outlets	4	4
Inner tube wall	9	2
Outer tube wall	8	2
	Total number of thermocouples	**50**

3.3.1 Thermocouple Attachment on the Inner Tube Wall

The embedded thermocouples in the inner tube wall required special attention. The annular passage had to be as smooth as possible and free of unnecessary obstructions affecting the flow dynamics and ultimately, the heat transfer and pressure drop behaviour. Therefore, thermocouple wires could not be placed in the annular passage. Instead, the thermocouple wires had to run through the inside of the inner tube and the tips be embedded in the tube wall, as shown in Figure 3-5. As will be discussed in detail shortly, the thermocouple tips were soldered onto the inner tube within a groove and the leads passed through a hole that was later filled and sealed with a suitable epoxy resin.

In order to check the influence of the thermocouple tip attachment method on experimental results, a rudimentary first order CFD analysis was done with variables matching the experiment conditions. It was found that the thermocouple wire, running from the outside of the inner tube where it was in contact with the annular passage fluid to the inside where it was in contact with the inner fluid (at a different temperature), did conduct some heat. To prevent the effect of this conduction having a significant influence on the temperature measurement, the thermocouple junction was placed 10 mm away from the hole in the inner tube. Furthermore, the junction was placed upstream (in terms of the annular fluid) from the hole to avoid significant effects from the disturbance in flow caused by the small unevenness of the surface (caused by the embedding process).

Each T-type thermocouple consisted of two 0.30 mm wires (cobalt and copper), that were each insulated by a Teflon layer which increased the effective diameter of each wire to 0.4 mm. These two insulated wires were positioned side by side and covered with another outer protective Teflon layer, giving the thermocouple lead a total outer enveloped cross sectional size of 0.55 x 0.95 mm. In order to embed the thermocouple leads into the inner tube wall, a groove running in the axial direction was machined into the tube with a milling machine. On average, the inner tube wall had a thickness of about 0.7 mm. It was essential to mill the groove deep enough to embed the thermocouple wires completely, while allowing the remaining wall to withstand the tube pressures it would be subjected to. After doing tests, it was found that the optimum groove depth was 0.46 mm.

Refer to Figure 3-6 giving a schematic representation as well as a photograph of a machined groove and the associated 1.2 mm hole through the inner tube wall. It should be noted that an additional circumferential grove located at the hole position was also machined. This was needed to improve the adhesion strength of the epoxy filler by allowing a greater sunken surface area onto which it could bind without being removed when the outer tube surface was polished.

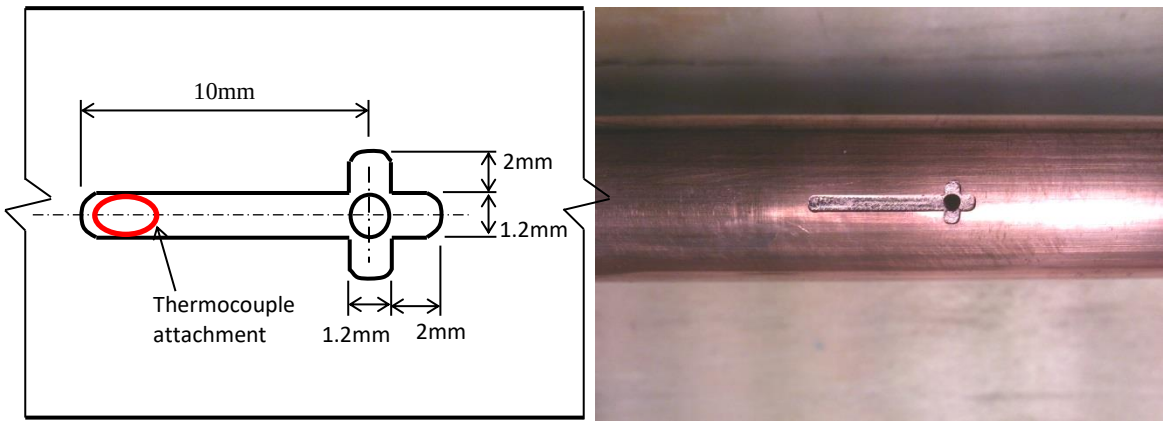

Figure 3-6: (a) Schematic details of a groove on inner tube wall (b) and picture showing the milled product.

The thermocouple attachment was made by soldering the ends of the cobalt- and copper wires onto the groove surface at the point furthest away from the hole through which the thermocouple wire entered the tube. Only 1.5 mm of the constantan- and copper wires' insulation was removed and the exposed portion was soldered. A further 8.5 mm of the outer Teflon coating was also removed to reduce the thickness of the thermocouple and thus making it easier to embed, as shown in Figure 3-5. After the junction was soldered and the thermocouple was laid flat in the groove, a layer of thermal epoxy was applied to fill any voids around the thermocouple wires and to seal the hole in the tube, preventing any water leaks. The epoxy, named TBS (Thermal Bonding System), was manufactured by Electrolube and had a thermal conductivity of 1.1 W/mK. Once the epoxy had dried, the surface was sanded down and polished smooth, as shown in Figure 3-7.

To ensure correct data analysis, it was essential that each measuring point was as close as possible to its intended position relative to the other measuring points. As mentioned earlier, the measuring points were equally spaced at 315 mm from the inlet and outlet and 550 mm apart along the tube length. All measurement points were attached to within 1 mm.

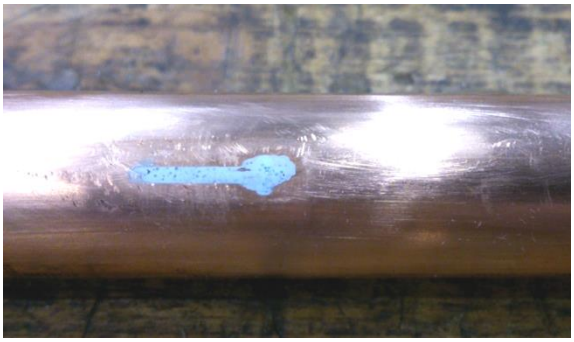

Figure 3-7: An embedded thermocouple.

3.3.2 Outer Tube and Measuring Station Thermocouple Attachments

The thermocouple junctions that were placed on the outer tube and at the inlet and outlet measuring stations were formed by fusing the cobalt and copper wire tips of the thermocouple together (see Figure 3-8). To fuse a thermocouple tip, one end of the thermocouple wire was fixed to a small DC inverter's positive outlet, while the other end (1.5 mm of the cobalt- and copper wires' insulation removed) was brought in contact with the negative port. This created a short circuit which produced enough heat to fuse the cobalt and copper wires together, producing a neat thermocouple junction.

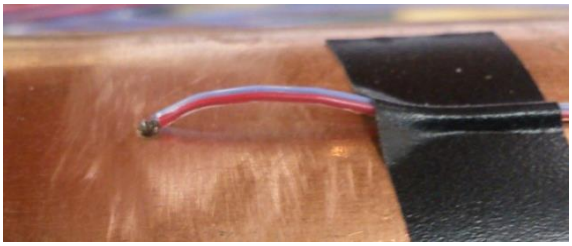

Figure 3-8: An example of a thermocouple with a fused junction.

It was found through testing that it was very important for the thermocouple junction to be fixed comprehensively to the tube surface, as any relative movement affected the calibration factor of the thermocouple channel. To eliminate relative movement, imposed by the copper tube wall due to temperature change, each thermocouple junction was fixed to the tube wall with aluminium tape and a hose clamp acting exactly on the juncture, as shown in Figure 3-9.

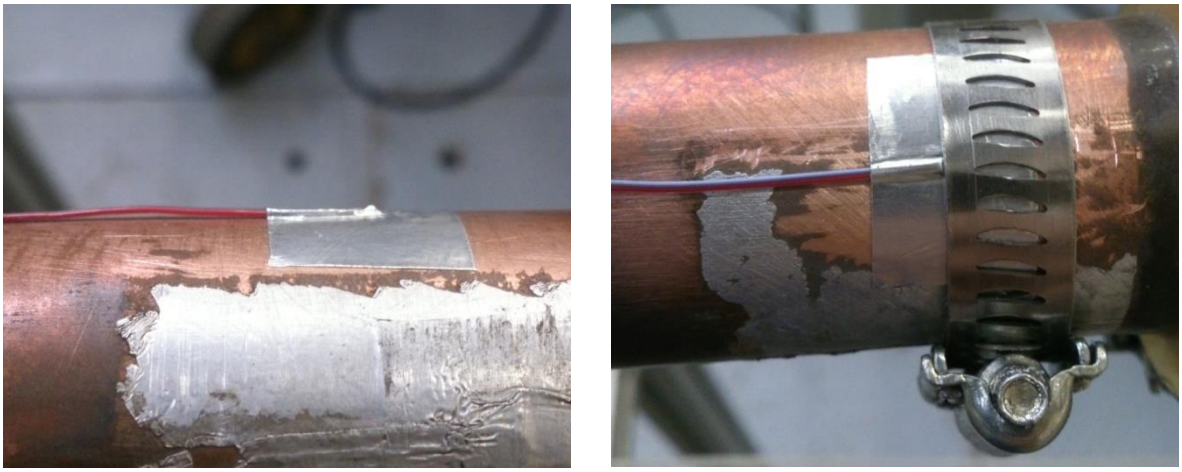

(a) **(b)**

Figure 3-9: (a) A fused-tip thermocouple taped to the outer tube surface with aluminium tape and (b) held in positive contact with a hose clamp.

3.3.3 Concentricity of Tubes

Concentricity was vital for comparable velocity profiles along the length of the heat exchanger. Computed for its own weight as well as the water in it, it was calculated that the inner tube would have sag of less than 3% of its outer diameter if it were supported at distances of 0.80 m. However, it was decided that since the thermocouples were spaced at 550 mm apart, it would be easier to space the supports at similar distances.

To ensure concentricity, the outer tube was assembled around the inner tube by attaching nine pieces of tube end to end, and connecting them with machined Perspex^{TM} acrylic glass fittings (shown in Figure 3-10). The thick-walled acrylic glass fittings were not only used as connector sockets, but also to house spacer pins that kept the inner tube in a desired location relative to the outer tube (refer to Figure 3-11). After fitting each of the acrylic glass sockets onto a tube end, four circumferentially equally spaced holes (0.85 mm diameter) were machined through the acrylic glass and tube walls to allow the fitment of stainless steel spacer pins. The pins were constructed from hypodermic needles with a diameter of 0.80 mm and a regular wall thickness, of which the sharp ends were filed off.

The inner diameter of the acrylic glass fittings was machined precisely to result in a smooth uniform annular outer wall diameter. The fittings were fitted to the copper tubes with epoxy. Different epoxies were tested for their strength and elasticity at prolonged exposure to a temperature of 65°C, which ensured it would withstand the 60°C heated fluid used when conducting tests. A product by Pratley[1] was found to fulfil all the requirements.

[1] Pratley Fixit Car

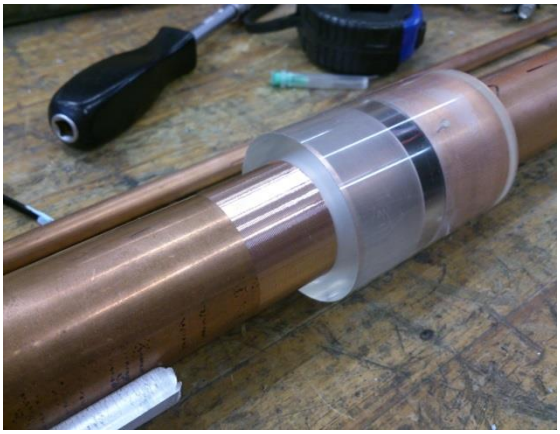

Figure 3-10: Acrylic glass fitting machined to fit the outer tubes.

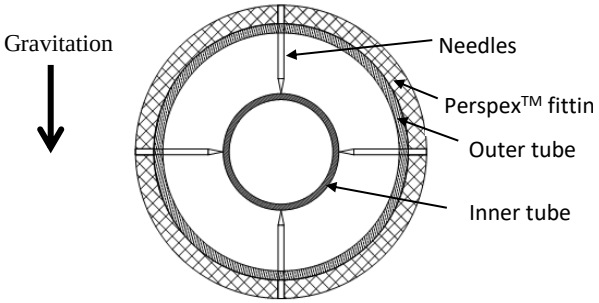

Figure 3-11: Diagram of showing the cross section of an acrylic glass socket with needles to support the inner tube.

For the worst case scenario (which was the 0.483 diameter ratio test section), the spacer pins occupied less than 5.25% of the annular cross-sectional flow area and since there were only eight supports along the 5 m tube length (550 mm apart), it was assumed that the effect of the pins on the flow pattern could be neglected.

Besides the need for the spacer needle pins, it was also important to develop a method with which the inner tube could be placed concentrically centred inside the outer tube during construction. For this purpose, two wooden spacers were machined with outer and inner diameters that exactly matched the size of the annular passage. These spacers were then positioned over the inner tube to where the section of outer tube was to be connected. Each section of outer tube was slid over the inner tube and over the wooden spacers to where it was glued to the Perspex™ fitting.

While the wooden spacers kept the two tubes concentric, the stainless steel needles were inserted into the holes (an example illustrated in Figure 3-12). Once it was ensured that all needles made good contact with the inner tube, the needle-end protruding from the outer tube was removed and grinded flush with the acrylic glass. Epoxy was used to seal the needle and the hole into which it fit. To prevent the needles from being forced outward, a hose clamp was tightened onto the circumference of the acrylic glass fitting, securing all four needles into place and thereby securing the inner tube's radial position relative to the outer tube. After that, the wooden spacers were pulled out and positioned for the next outer tube section. The transparent acrylic glass permitted inspection to see if the inner tube still rested in place on the spacer pins, as shown in Figure 3-13. Figure 3-14 shows a complete connection between two sections of outer tube, clamped down to increase its strength and pressure capacity.

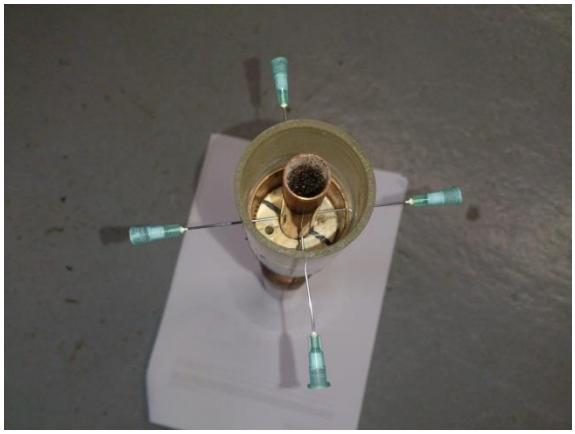

Figure 3-12: Example of how a wooden spacer was used to align the two tubes concentric while stainless needles were positioned.

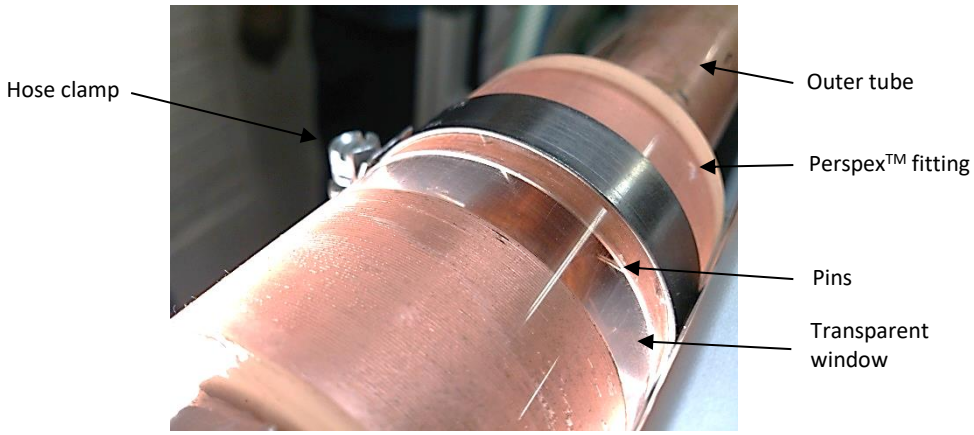

Figure 3-13: Transparent Perspex™ allows inspection of the spacer pins.

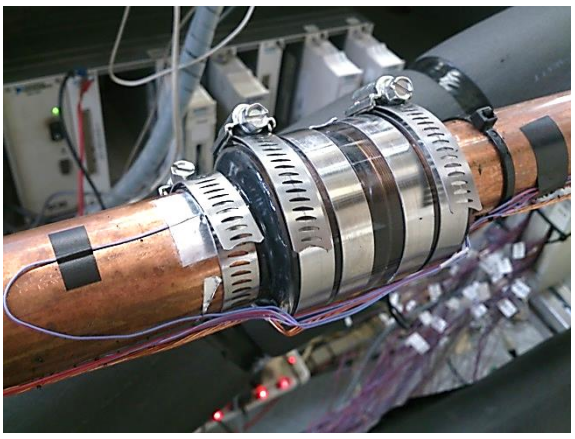

Figure 3-14: A complete connection between outer tube sections with a Perspex™ fitting and clamps to increase strength.

3.3.4 Insulation

Heat transfer between the annulus and the surroundings had to be kept to a minimum if a good energy balance was to be achieved during the experimental tests. The energy balance error, *EB*,

was calculated as the percentage difference between the heat transfer rates of the annulus to the average heat exchange rate of the two flow passages.

$$EB = \frac{|\dot{Q}_o - \bar{Q}|}{\bar{Q}} \times 100 \tag{3-2}$$

where

$$\bar{Q} = \frac{\dot{Q}_i + \dot{Q}_o}{2} \tag{3-3}$$

with $\dot{Q}_i$ being the heat transfer rate measured on the inner tube side and $\dot{Q}_o$ the heat transfer rate on the annulus side. The calculation of the heat transfer rates will be discussed in detail in the next chapter.

Commercial pipe insulation jackets, with a thermal conductivity of 0.036 W/mK as per manufacturer's specification [31], were wrapped around the outer tube and sealed in place with insulation tape, as is represented in Figure 3-2. In the worst-case scenario, with an outer tube temperature of 60°C and ambient at 20°C, it was computed that a 20 mm insulation thickness will allow only 19.98 W/m of heat to transfer to the ambient. This would be less than 0.5% of the anticipated heat transfer between the inner and outer tube at the minimum heat transfer rate tested. However, due to dimensional availability of the insulation material, insulation with a thickness of 25 mm or more was used. All other tubes and pipes leading to and from the test bench were also insulated to keep energy loss to the atmosphere at a minimum. If the pipes connecting the chiller and electric heater to the test section were to have had a large amount of heat transfer to/from the ambient, it would have been challenging to control the inlet temperatures.

3.4 Summary: Experimental Setup

In this chapter a description of the test facility and a discussion on the manufacturing of the experimental test section were given. The test bench allowed for easy switching between test sections, as well as switching of flow directions in the inner tube and annulus. Four concentric tube-in-tube heat exchanger test sections were constructed, each with a different diameter ratio. Care was taken to eliminate factors and workmanship influences that might have significant effects on the fluid mechanics, which in turn might have effects on the heat transfer ability and pressure drop penalties in the annular flow passages.

In the next chapter a detailed account of the experimental procedure will be given.

CHAPTER 4 - CALIBRATION AND EXPERIMENTAL PROCEDURE

4.1 Introduction

In this chapter, a detailed account is given of the procedure followed to calibrate instruments and thermocouples and the methodology used to conduct experiments. Also included is an explanation of how each test section went through phases of testing the quality of workmanship after construction, calibration and finally data capturing. An account is also given of the different test cases, a clarification of steady state requirements and the sequence of operations during data capturing.

4.2 Pressure Test

It was of utmost importance that there were no leaks on the tubes of the heat exchanger. This was essential for two reasons: (1) It was important that the insulation covering the tubes remained dry to maintain its insulating capabilities and (2) if the inner tube leaked into the annulus, the heat transfer calculations would be compromised due to non-representative measured mass flow rates and non-representative data processing methods followed. Therefore, the heat exchanger had to undergo two pressure tests. The first test was conducted on the inner tube only to detect any possible fluid seeping from the holes where the thermocouples protruded through the tube wall. The second pressure test was done after the outer tube had been assembled over the inner tube to see if the annulus had any leaks.

At maximum flow velocity the heat exchanger was exposed to gauge pressure as high as 6 Bar. Any small leak would quickly propagate to a sizeable seepage at this high pressure. Pressure testing was done by connecting the test section onto the test bench and pumping water through it. Flow speeds started at low flow velocities and were gradually increased to 10% above the maximum expected velocity during the experiments. The test was done with both hot and cold water of 60°C and 10°C respectively. All other connections and hoses were also checked for leaks and fixed where necessary. Once the pressure tests were complete, the heat exchanger was covered with insulation.

4.3 Thermocouple Calibration

Thermocouples were calibrated *in situ* after they had been attached to the tube walls. This was deemed more accurate than the method of calibration in a thermal bath before attachment, because the thermocouple's junction might be damaged during the attachment process, altering the thermocouple's resistance and thereby changing the behaviour of the thermocouple. Each of the four test sections required a calibration of the thermocouple channels before conducting experiments on it.

The thermocouples were calibrated during isothermal tests by coupling the heat exchanger to only one water supply (either from the hot water loop or the cold water loop) at both the inner and annular flow passage inlets and connecting the outlets to one shared outlet (illustrated in Figure 4-1). This ensured that water of the same temperature flowed through both the inner tube and the annulus and that no internal heat transfer occurred. To obtain a suitable reference temperature

during the *in situ* calibration runs, two PT100 RTDs (Resistance Temperature Detectors) with an accuracy of 0.1°C were installed, one each at the tube inlet and at the outlet. Once the temperature of the tube inlet and outlet, as measured by each PT100, matched one another (within ± 0.03°C) and differed by less than 0.1°C over a time period of 1 minute, a set of 100 samples were recorded for each thermocouple channel (50 channels in total).

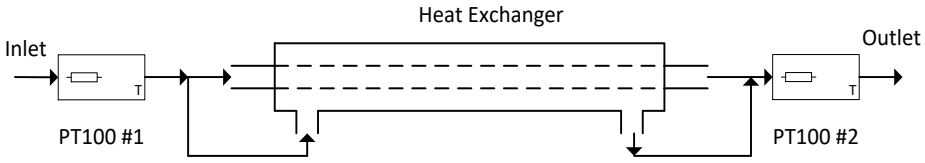

Figure 4-1: Diagram of *in situ* calibration setup.

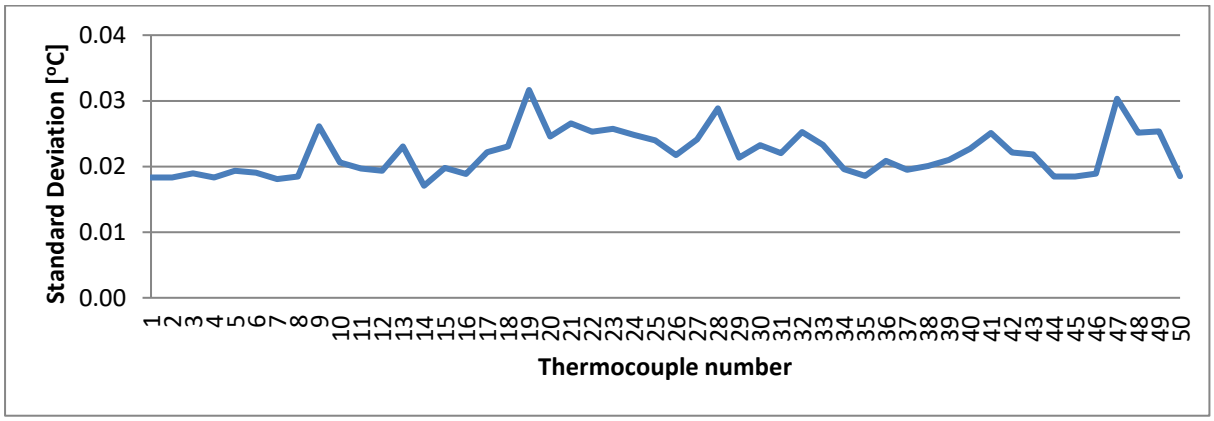

Figure 4-2: Standard deviation of the error in measurement the thermocouples after calibration.

The water temperature was adjusted at increments of 5°C, from 8°C to 63°C. To ensure the effect of forced convective heat transfer was captured during calibration, data for three different flow velocities were recorded at each temperature interval. After having reached the upper temperature value of 63°C, the isothermal test temperature was reduced to 60°C and then decreased at intervals of 5°C, again capturing data at three different flow velocities. This procedure produced a matrix of captured data with which the thermocouples could be calibrated, for both heating and cooling and at three different flow velocities.

A third order polynomial calibration factor was developed for each thermocouple channel by comparing the average measured temperature of each thermocouple channel (based on the 100 sampling points) to the average temperature measurement of the PT100s. Figure 4-2 shows for the 0.409 annular ratio test section the standard deviation of the error in measurement of each thermocouple after calibration has been applied. From such a figure, it can be seen which thermocouple channels produced consistent incorrect readings. For the current thermocouple set, shown in Figure 4-2, the maximum standard deviation was ±0.0317°C, which resulted in a maximum thermocouple error of approximately 0.06°C. Since this was well below the ±0.1°C error accepted in literature [32], all thermocouple channel outputs of this set were used. Thermocouples whose calibrated temperature did not fall within ±0.05°C standard deviation were

disregarded. This procedure was followed for the calibration of all test sections. The full set of calibration results is available in Annexure C.

A major advantage of the *in situ* calibration was the ability to, at random intervals, check whether the calibration was still good, ensuring accurate data recording. If the calibration suddenly changed, it signified that something caused the thermocouples to deviate. An investigation could then be done to determine the cause of the deviation and repairs could be done before continuing with tests. An evaluation of the problem would show whether previous data collected should be discarded, or if it was still usable.

4.4 Pressure Transducer Calibration

Differential pressure transducers, manufactured by Validyne Engineering, were used and had an accuracy of 0.25% of the full scale. To minimise errors, three different diaphragms were used, namely 0 – 14 kPa, 0 – 22 kPa and 0 – 55 kPa. Each diaphragm was calibrated using a static water column to induce pressure and a 50 kPa calibrated differential pressure gauge (0.05% full scale accuracy) to measure true pressure. A series of readings was taken between zero pressure and maximum pressure and a linear calibration coefficient was deduced from the difference between the recorded and true data.

4.5 Experiment Test Cases

The research objectives in Chapter 1.3 included (1) testing the effects of different annular diameter ratios, flow velocities, inlet temperatures and the heat flux directions on the heat transfer coefficient and friction factor and (2) to contribute data to a tube-in-tube heat exchanger database with which new correlations can be formed.

To comply with these objectives, an extensive number of tests had to be performed at different combinations of fluid velocities and temperatures. Each test section was experimentally tested at six different inlet temperatures, three temperatures for a heated annulus and three for a cooled annulus, denoted as C50, C40, C30, H30, H20 and H15, where C50 represents the case of the annulus being cooled from an annular inlet temperature (T_{oi}) of 50°C. Due to hardware limitations the inlet temperature could only be kept constant within a range of $\pm$1.5°C of the desired inlet temperature over the range of tests. Table 4-1 gives a description of the test cases.

At each of these inlet temperatures, the inner tube velocity was varied at five different settings and at each inner tube velocity the outer tube flow was varied through a range of seven different flow speeds. Figure 4-3 illustrates the array of Reynolds numbers tested for each inlet temperature. That totalled up to 1260 different test conditions to be tested. Table 4-2 gives a summary of the test case combinations to be tested.

Table 4-1: Test cases for each test section.

Case	Mode	T_{oi}
C50	Cooled	50°C ± 1.5°C
C40	Cooled	40°C ± 1.5°C
C30	Cooled	30°C ±1.5°C
H30	Heated	30°C ±1.5°C
H20	Heated	20°C ±1.5°C
H15	Heated	15°C ±1.5°C

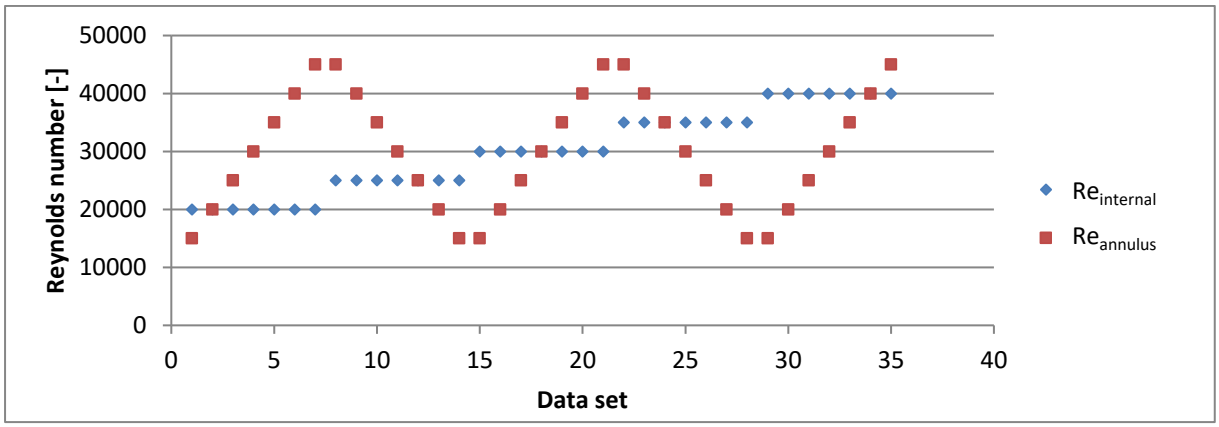

Figure 4-3: Inner tube and annulus Reynolds numbers test array.

Table 4-2: Summary of test cases

Variable	Test points / Range	Number of variable variations
Annular diameter ratio, *a*	0.327, 0.386, 0.409 and 0.483	4
Inlet temperature		
Heated annulus	15, 20 and 30 °C	3
Cooled annulus	30, 40 and 50 °C	3
Tube Reynolds Number		
Re_i	20 000 – 40 000, increments of 5 000	5
Re_o	15 000 – 45 000, increments of 5 000	7
	Total Tests:	**1260**

Some redundancy was acceptable due to the importance of recording usable and accurate data. Some might say that the alteration of the inner tube's Reynolds Number was unnecessary, but it was unknown what type of data analysis future research might involve. If, for instance, a Wilson

plot analysis was to be done, a matrix of data would be needed, similar to which is described in Table 4-2.

Of particular interest in this research was the effect of heat flux direction. Varying the annular inlet temperature was certain to give some variation in this regard, which could be used to identify possible trends or patterns.

4.6 Steady State

At start-up, the setup took some time to exchange heat between the tubes and with the thermal insulation, but steady state was influenced mostly by changing inlet temperatures. Due to the length of the pipes from the hot and cold water reservoirs to the setup (5 – 20 m), some heat exchange to the ambient did occur. Thus, each time the velocity in either the inner or outer tube was changed, a spike in temperature was observed at the inlet measuring stations of the setup. Time was required to allow the temperature change to settle before steady state could be reached. This time duration was, however, not constant, but depended on the water temperature and velocities at that particular moment. It was found that the inlet temperature could only be kept constant (within ± 0.1°C) for about 4 minutes, due to limitations on the water reservoirs' temperature control.

For purposes of this investigation, steady state was deemed to have been reached if the following conditions were satisfied simultaneously over a period of 60 seconds:

- Change in inlet temperature of less than 0.1°C, for both the inner tube and annular cavity.

$$\Delta T_{ii} < 0.1°C$$
$$\Delta T_{oi} < 0.1°C \quad (4\text{-}1)$$

- A change in energy balance error of less than 0.5%.

$$EB < 0.5\% \quad (4\text{-}2)$$

- A change of less than 0.1°C in the differential fluid temperature across each tube, as measured by the measuring stations at the inlets and outlets.

$$\Delta T_i = |T_{ii} - T_{io}| < 0.1°C$$
$$\Delta T_o = |T_{oi} - T_{oo}| < 0.1°C \quad (4\text{-}3)$$

Once these criteria were achieved, it was assumed that the heat transfer rate had reached steady state.

Upon reaching steady state, a data set was recorded at 10Hz over a period of 200 seconds, resulting in 2000 data points for each input channel. In Chapter 5 it will be shown how this data set was filtered to the best 200 consecutive data points. If the steady state conditions failed during the 4 minutes necessary to conduct one test, the data was scrapped and the test was restarted.

4.7 Data Capturing Process

It was important to develop a method of testing that would ensure rapidly reaching steady state, as the sheer number of tests to be conducted left no time to waste. Factors that influenced steady state

were the rate at which the cold and hot reservoirs could cool and heat to a desired temperature and the time the heat exchanger needed to reach thermal equilibrium.

The process followed when testing is contained in Figure 4-4. The diagram explains the steps followed from start-up to reaching steady conditions, to saving a data set. The first step in the test procedure was to set the electric heater and chiller units to the inlet temperatures required, allowing the reservoirs to reach the selected targets.

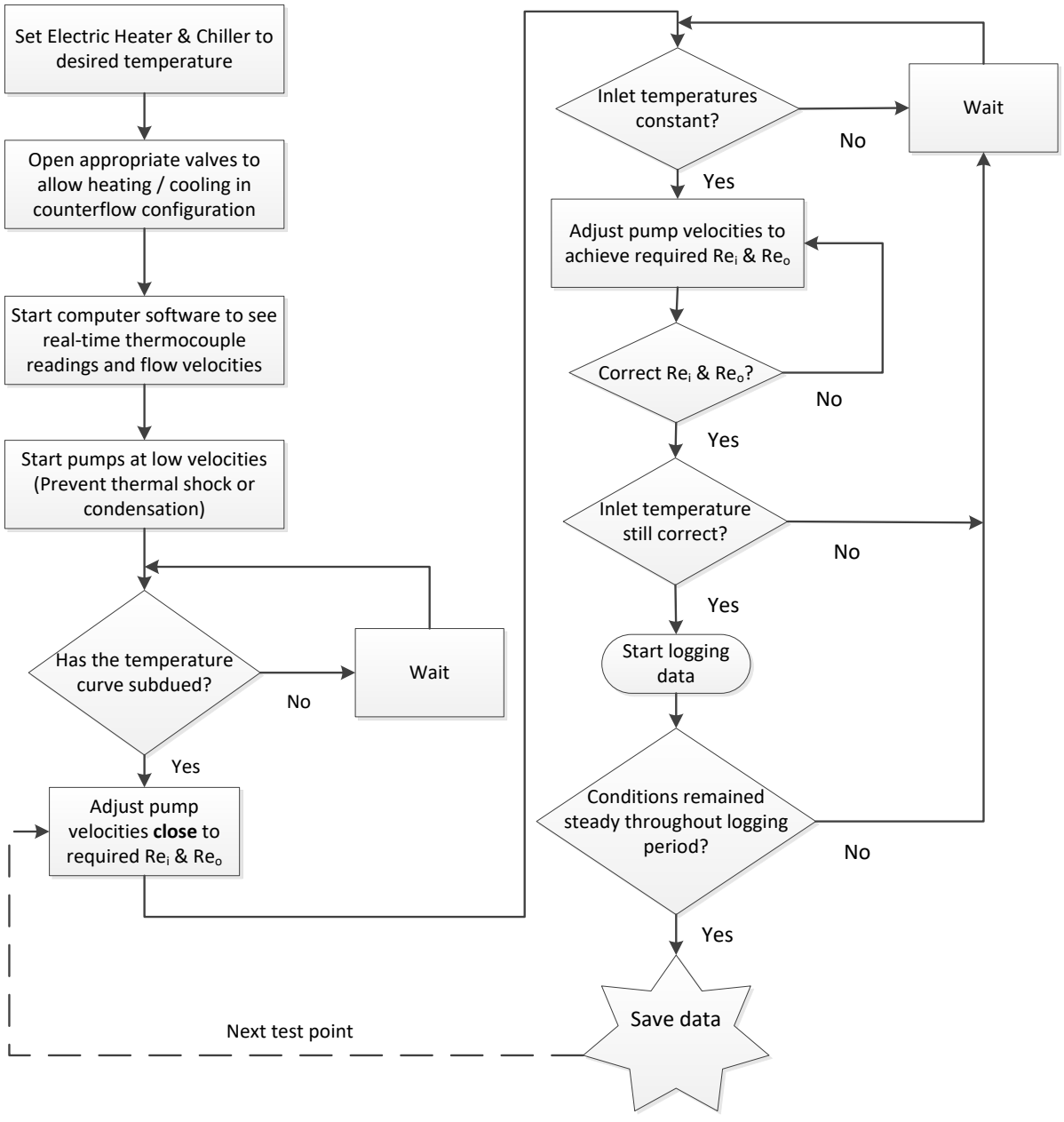

Figure 4-4: Flow chart explaining data capturing process.

With the array of valves installed on the feed to the heat exchanger, it was important to open the correct valves to allow either heating or cooling in a counter flow configuration. Next, the computer

software was started to allow remote control of the pumps and real-time updates on the thermocouple readings and flow rates.

After having started the pumps, the Variable Speed Drives (VSDs) were set to allow pumping at low velocity. Rapid pumping of hot or cold water through the heat exchanger might cause thermal shock on the tube connections, or result in condensation on the outside of the outer tube, saturating the insulation. A plot of the thermocouple readings (in real-time) along the tube displayed on the computer screen made it easy to see when the incoming hot and cold fluids reached the outlet of each flow passage (inner tube and annulus). Once the temperature curve stabilised, the pump velocities for both flow loops were fine-tuned to achieve the required Reynolds numbers. Since the Reynolds number is temperature dependent, it would only be possible to make final pump adjustments once the temperature reached steady state.

After having reached steady temperatures and flow, data capturing could commence. If the conditions remained steady during the data logging period, the data was saved and the fluid velocity adjusted for the next test point.

4.8 Chapter Summary

The construction of the test section were carefully executed with special attention to the influence it might have on the experimental results. After completion, the heat exchangers had to be tested for leaks. When satisfied with the quality of workmanship, *in situ* calibration was done and a review of thermocouple availability was completed. Differential pressure transducers were calibrated using a static water column to induce pressure. The vast amount of test cases were explained and detailed. The conditions for steady state were stipulated and some constraints were mentioned. Lastly, an explanation was given of how data capturing was sequenced to enable optimal time management.

The next chapter explains the procedure followed to analyse and reduce the data.

CHAPTER 5 - DATA ANALYSIS

5.1 Introduction

This chapter describes the methodology followed to analyse the data collected. A detailed description is given of the procedure to calculate the mean and local heat transfer coefficients. A breakdown of the uncertainty analysis is also given. The relation between the NTU (Number of Transfer Units) and the effectiveness of a heat exchanger is explained. The NTU-effectiveness will be used to determine if the heat exchangers' length was optimal.

5.2 Data Reduction

As described in Chapter 4.5, a vast number of tests were conducted. To save time, the data reduction and analysis was streamlined as much as possible. Figure 5-1 shows, in short, the methodology followed to reduce and analyse the data. The figure explains how the data was recorded and saved for each test. After that the calibration factors were applied and the data was reduced to useable data. Analysis was then performed to compute the average and local heat transfer coefficient and friction factor, as well as the uncertainties involved. The results could then be compared for different tests, inlet temperatures and annular ratios and comments could be made. In the sections that follow a description is given of each step in the analysis process. The steps to summarise results for comparison are self-explanatory and will not be commented on.

5.2.1 Record Data

For each test point, at predetermined combinations of inlet temperatures, flow velocities and a particular annular diameter ratio, a total of 2000 data points were logged for each input channel once steady state had been reached. The recorded data was then stored as a text file with a descriptive name allowing easy identification.

5.2.2 Apply Calibration and Reduce

Raw thermocouple and pressure transducer data had to be conditioned by using the calibration curves obtained earlier, before it could be used. For this purpose, Labview (version 9.0.1) was used to reduce the original recorded raw data file to usable data.

The "zero-pressure" reference values for the pressure transducers were recorded at the beginning of each test day during stationary fluid conditions. The reference values had to be subtracted from the recorded pressure measurements first, before applying any calibration corrections. For thermocouple measurements this was not necessary and calibration corrections could be applied directly.

After calibration corrections were applied to the raw data, the data-series from the remaining channels was cropped by isolating the best 200 consecutive data points. This was done by evaluating data according to the given steady state conditions and selecting the set of points with the smallest deviation in inlet temperatures, energy balance and temperature difference measured across each flow passage. The calibrated and reduced data series was then saved to a text file for retrieval when needed.

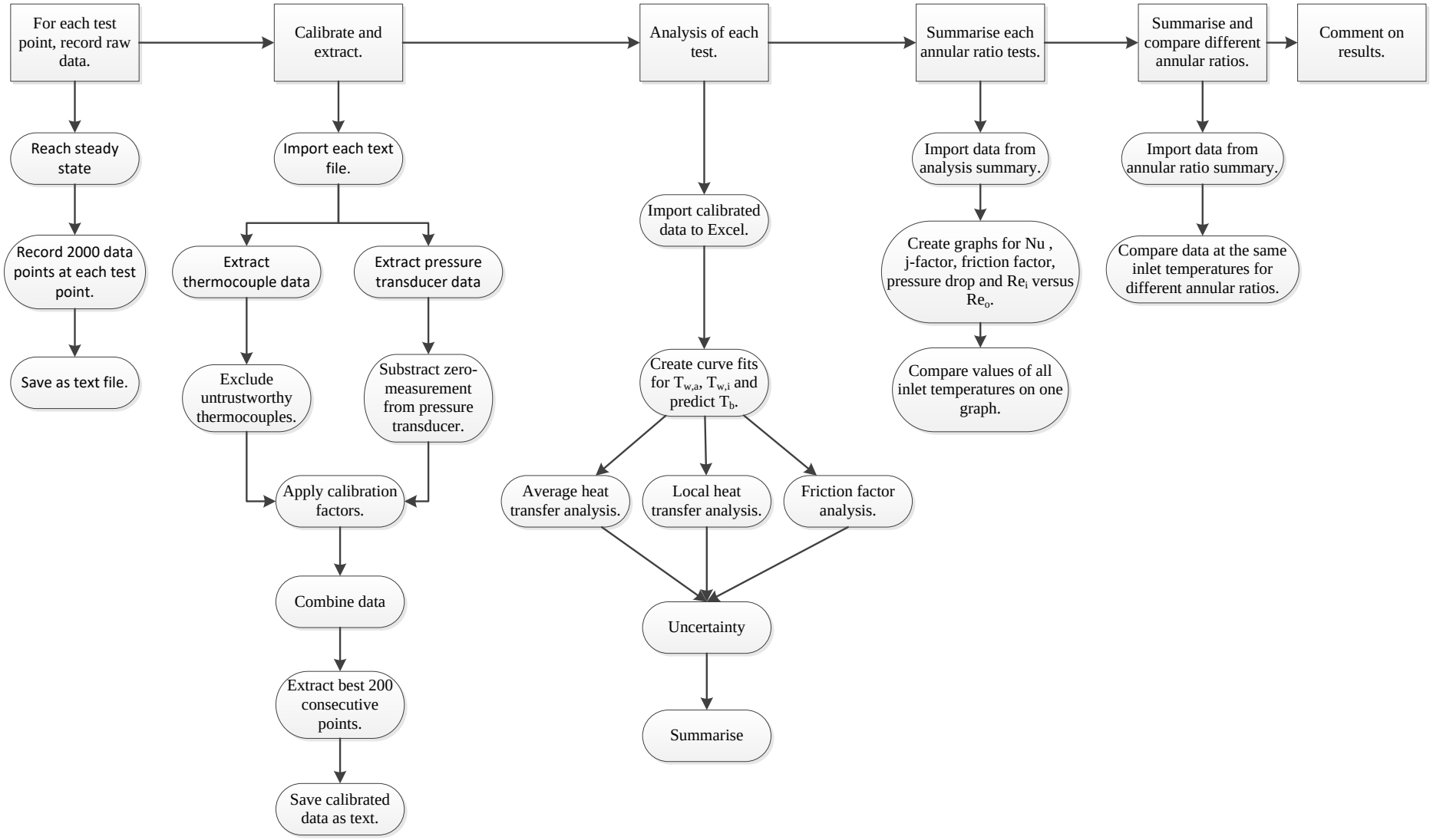

Figure 5-1: Data reduction process.

5.2.3 Analysis of each test

In this section the data analysis process is explained by referring to measured values obtained during an arbitrary chosen test case. The example test case under consideration is for a cooled annulus with a 0.386 annular diameter ratio where the inlet temperatures of the annular passage and inner tube are approximately 50°C and 10°C respectively. The flow rates selected for documenting the process in this chapter are such that the Reynolds numbers are 35,000 in the both annulus and inner tube.

Assumptions that were made for analysis purposes:

- Axial heat conduction through the inner tube wall was negligible compared to radial conduction.[2]
- Heat transfer between the outer tube and atmosphere was negligible.[3]
- Hypothetically, fully developed thermal flow existed in the 0.315 m – 4.75 m section of the heat exchanger, allowing local heat transfer analysis in this region.

After the calibration corrections were applied and the best set of data was extracted, the data was imported into a spread sheet for analysis.

5.2.3.1 Local wall and bulk fluid temperatures

Measured temperature values include inlet and outlet fluid temperatures as well as inner tube and outer tube wall temperatures at discrete locations along the length of the heat exchanger. However, in order to obtain local heat transfer coefficients, local annular bulk fluid temperatures and local wall temperatures at any point along the length of the heat exchanger were needed, and not just at the discrete measuring locations. In the following section the methods used to achieve this, is described.

Consider Figure 5-2 and Figure 5-3 that show the thermocouple measurements on the inner and outer walls of the annulus respectively as obtained from the two thermocouples installed at each measuring station. The average of the two thermocouple measurements at each location is also indicated. It can be seen that for the case under consideration, the wall measurements obtained from the two thermocouples per station were in good agreement. By considering the overall trend of the wall temperatures, outliers can easily be identified and excluded from the data analysis if needed.

By considering the axial temperature profile of the inner tube wall shown in Figure 5-2, it is easy to place a curve fit through the local measured average wall temperatures which will allow one to calculate the derived local wall temperature at any axial location. This is indeed the method that was used in this study and is discussed shortly.

Since the annular bulk fluid temperature was only measured at the inlet and outlet, a method was needed with which the local bulk fluid temperature along the length of the heat exchanger could be obtained. This was done by considering the axial temperature profile measured on the outer adiabatic wall of the annulus.

[2] Axial conduction in the inner tube found to be less than 0.01% than the total heat transfer rate for all cases.
[3] Maximum heat loss of 0.51% through the outer tube insulation measured over total heat exchanger length.

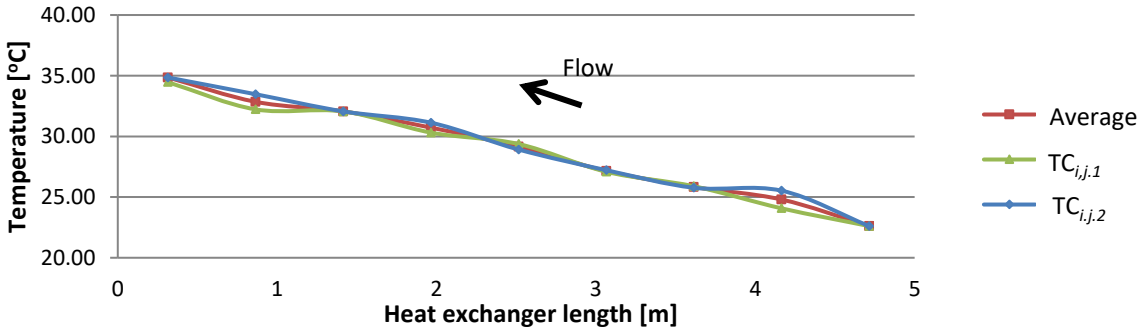

Figure 5-2: Thermocouple measurements of the inner tube wall temperature.

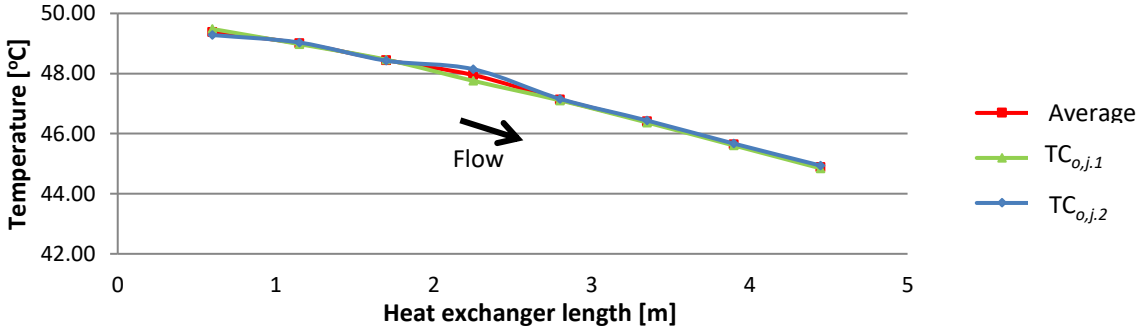

Figure 5-3: Thermocouple measurements of the outer tube wall temperatures.

Consider Figure 5-4 showing the averaged local temperature readings obtained for the inner tube wall (T_{iw}), the outer tube wall (T_{ow}), the annulus bulk fluid inlet (T_{oi}) and the outlet (T_{oo}); as well as the inner tube inlet (T_{ii}) and outlet (T_{io}). The arrows indicate the flow directions in the annulus and in the inner tube. It can be seen from Figure 5-4, that both of the wall temperatures profiles followed an approximate linear trend.

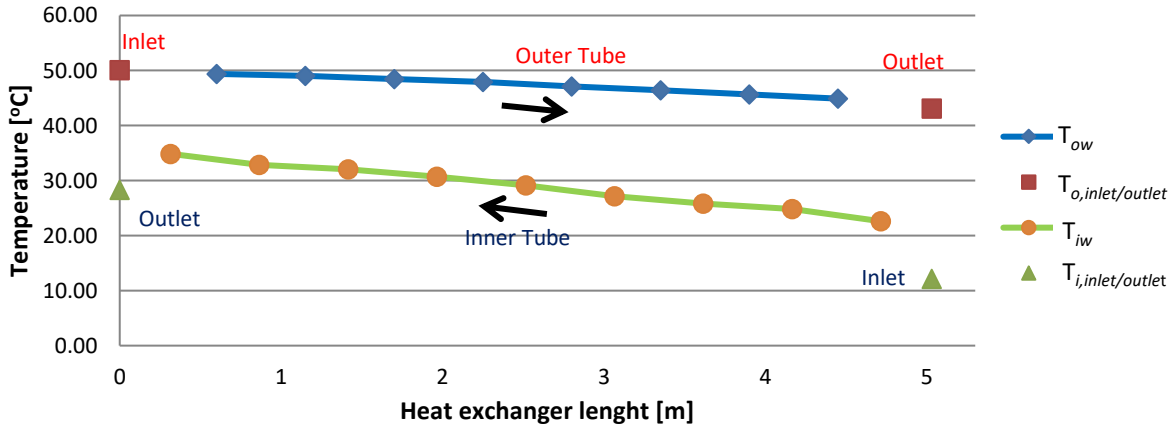

Figure 5-4: Inner and outer tube wall temperatures and inlet and outlet bulk fluid temperatures.

As the inner tube fluid was cooler than the fluid in the annulus, heat was transferred from the annulus to the inner tube (cooled annulus). The outer tube wall temperature was directly dependent on the annular bulk fluid, as it was thermally insulated on the outside and the assumption was made

that it could only exchange heat with the fluid. As the temperature of the bulk fluid changed along the length of the section, the outer tube temperature thus had to follow it. Therefore, a measured temperature change on the outer tube wall had to indicate a change in bulk fluid temperature at that point. It was consequently assumed that, once fully developed flow was achieved, the bulk fluid temperature would have the same profile as the outer tube wall temperature along the tube length.

Using the method of least squares fitting [33], an exponential curve was fitted through the measured outer wall temperature points. The logic was that, once fitted through the measured inlet and outlet bulk temperature points, this curve would predict the local bulk temperature, seeing that the outer wall temperature changes with the bulk temperature. However, it was discovered that the outer wall temperature curve did not fit perfectly onto both the inlet and outlet bulk temperatures.

The reason for the misfit could be attributed to the thermal developing region at the entrance of the heat exchanger. According to theory [2], a developing region has a higher local heat transfer rate due to a thinner thermal boundary layer. Therefore a hypothetical assumption was made that there existed a higher local heat transfer coefficient in the annular inlet section, up to the point of fully developed thermal flow, resulting in a higher heat flux and different bulk temperature than previously assumed. The temperature profile across the length of the tube would thus be according to Figure 5-5 (exaggerated to show effect). It was hypothetically assumed that once thermally developed flow has been achieved, the temperature curve would be almost linear. This hypothetical assumption is tested and discussed in Section 6.4.4.

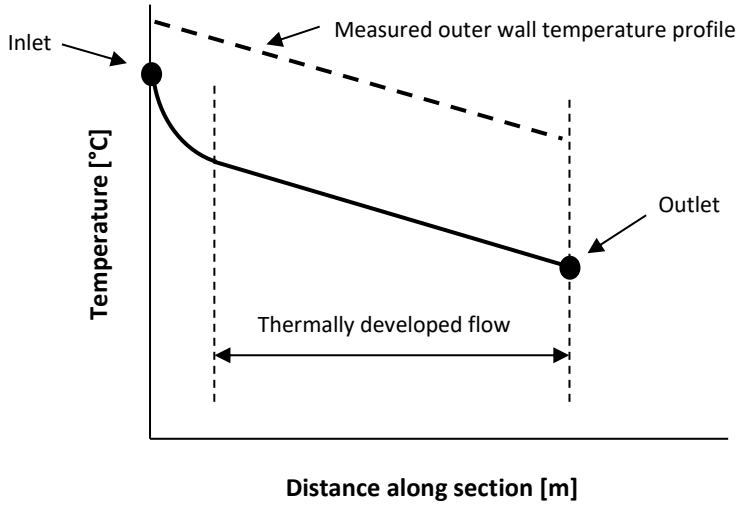

Figure 5-5: Assumed annular bulk fluid temperature curve along the length of the heat exchanger.

Without the ability of the test setup to measure the thermally developing region's temperature change, it was opted to adhere to the previous assumption of fully thermal developed flow for the tube section under consideration. In order to avoid the entrance effects, the curve shape obtained from the outer tube wall surface was fitted through the measured outlet bulk fluid temperature point and not through the inlet bulk fluid temperature value. This will inadvertently lead to small errors in the predicted bulk fluid temperature at the entrance of the tube section, of which the magnitude depends largely on the annular flow velocity. To eliminate this effect in the entrance region, only

part of the test section would be considered in the local analysis, as would be explained in a following section.

Figure 5-6 gives an illustration of a curve fit used to predict the local annular bulk fluid temperature. It was found that the local axial temperature is correlated best when using an exponential curve fit of the following form:

$$T_{local,predicted}(x) = \alpha e^{\beta x} \tag{5-1}$$

where α and β are calculated by method of least squares fitting from the measured temperatures and x is the axial distance from the annulus inlet. Other curve fit types that were considered include linear fit, third order polynomial fit and a sixth order polynomial fit. For the data set under consideration, the exponential curve in Figure 5-6 has a goodness of fit value, R^2, of 0.9865.

As explained, the local bulk temperatures were predicted by fitting the temperature profile of the outer wall onto the exit bulk fluid temperature, resulting in the predicted fluid bulk temperature differing from the measured value at the entrance. The predicted value will differ from the true value until thermal developed flow has been reached.

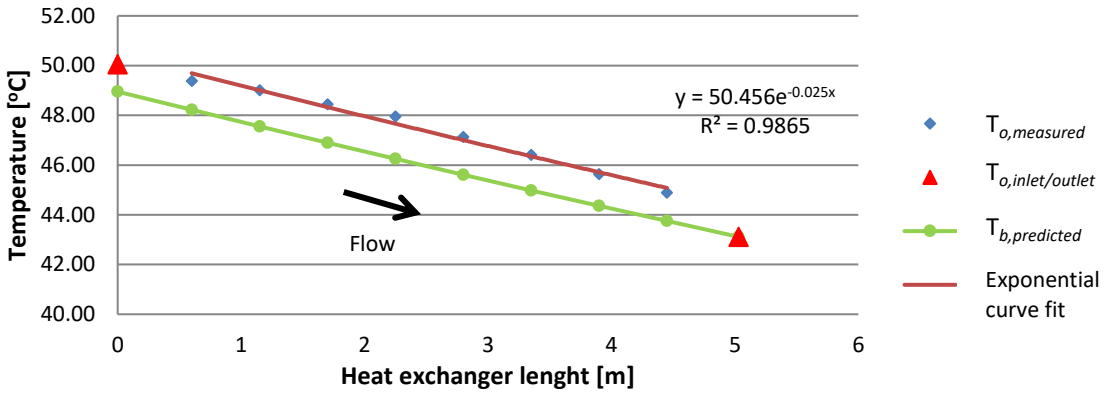

Figure 5-6: Curve fitted through the outer tube measured temperatures used to predict local annular bulk fluid temperatures.

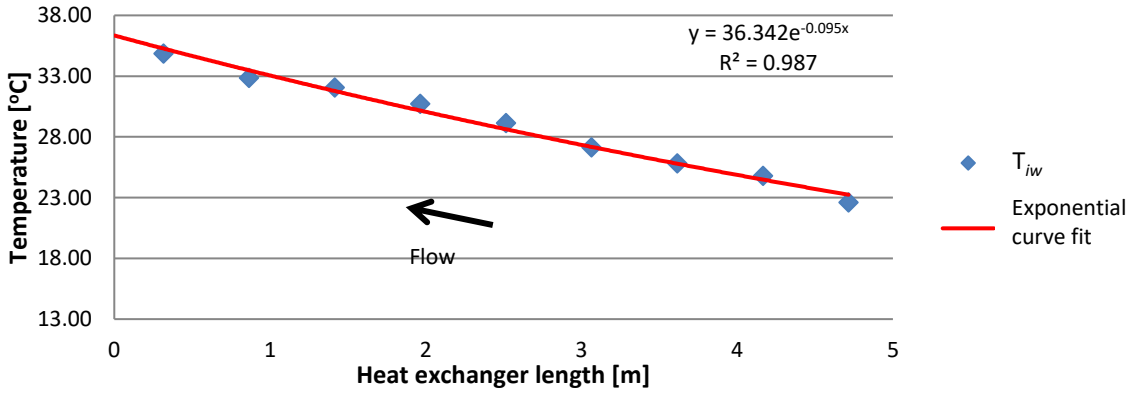

Figure 5-7: Inner tube wall temperatures with an exponential curve fit.

The method of least squares fitting was also applied to fit an exponential curve through the measured inner wall temperature data points as depicted in Figure 5-7. Here, a goodness of fit value, R^2, of 0.987 was achieved.

5.2.3.2 Average heat transfer coefficients

The average heat transfer coefficient, $\overline{h}$, is an important performance indicator of a heat exchanger. To determine the average heat transfer coefficient, the entire test section is considered as one control volume (CV).

The average heat transfer coefficient between the inner tube and annulus is computed from:

$$\bar{h} = \frac{\dot{Q}}{A_s \Delta T_{LMTD}} \tag{5-2}$$

where $\dot{Q}$ is the heat transfer rate, A_s is the heat transfer surface area and ΔT_{LMTD} is the logarithmic mean temperature difference. The surface area is calculated as:

$$A_s = \pi L_{hx} D_1 \tag{5-3}$$

while the logarithmic mean temperature difference for the annulus is calculated as:

$$\Delta T_{LMTD} = \frac{(\overline{T}_{iw} - T_{oi}) - (\overline{T}_{iw} - T_{oo})}{ln[(\overline{T}_{iw} - T_{oi})/(\overline{T}_{iw} - T_{oo})]} \tag{5-4}$$

where T_{oi} and T_{oo} are the measured annular bulk fluid inlet and outlet temperatures respectively. The inner wall temperature is treated as being constant along the entire length, but evaluated as the effective average, $\overline{T}_{iw}$, of the local temperatures discussed in the previous section. It is computed by summation of all usable thermocouple measurements on the inner tube, divided by the number of thermocouples:

$$\overline{T}_{iw} = \frac{(\sum T_{iw,j})}{n} \tag{5-5}$$

In theory, the heat transfer rate from the fluid in the inner tube to the inner tube wall, $\dot{Q}_i$, should be the same as the heat exchange rate from the inner tube wall to the annular fluid, $\dot{Q}_o$, minus losses to ambient. As mentioned previously, to express the relative magnitude of the losses and measurement inaccuracies, the energy balance error, *EB*, is calculated as the percentage difference between the heat transfer rate of the annulus to the average heat exchange rate of the two flow passages. Equations (3-2) and (3-3) used to calculate the *EB* is repeated here and renumbered as equations (5-6) and (5-7).

$$EB = \frac{|\dot{Q}_o - \bar{Q}|}{\bar{Q}} \times 100 \tag{5-6}$$

where

$$\bar{Q} = \frac{\dot{Q}_i + \dot{Q}_o}{2} \tag{5-7}$$

The heat transfer rate between the annular fluid and the inner tube wall is expressed as:

$$\dot{Q}_o = \dot{m}_o c_{p,o}(\bar{T}_{oi} - \bar{T}_{oo}) \tag{5-8}$$

where $\dot{m}_o$ was the annular mass flow rate measured by the appropriate Coriolis flow meter and c_p the specific heat (The method and temperature at which the specific heat and other fluid properties were calculated will be discussed later in this section). Alternatively, to increase accuracy since the temperature difference between the inner tube inlet and outlet was greater than that of the annulus, the heat transferred could also be calculated by:

$$\dot{Q}_i = \dot{m}_i c_{p,i}(\bar{T}_{ii} - \bar{T}_{io}) \tag{5-9}$$

where $\bar{T}_{ii}$ and $\bar{T}_{io}$ are the arithmetic average temperature of the thermocouples at inner tube inlet and outlet respectively.

The average dimensionless Nusselt number was computed for the heat transfer in the annulus using the calculated average convective heat transfer coefficient, the thermal conductivity of the bulk fluid, k, and the hydraulic diameter D_h of the annular passage, implementing the following equation:

$$\overline{\mathrm{Nu}}_{Dh} = \frac{\bar{h} D_h}{k} \tag{5-10}$$

where the hydraulic diameter was computed as the difference between the inner diameter of the outer tube D_o and outer diameter of the inner tube D_1, given as:

$$D_h = D_o - D_1 \tag{5-11}$$

The Colburn j-factor, which is commonly used in friction factor analogies, is expressed as:

$$j = \frac{\mathrm{Nu}_{Dh}}{\mathrm{Re}_{Dh}\mathrm{Pr}^{1/3}} \tag{5-12}$$

where the Reynolds number is calculated as:

$$\mathrm{Re}_{Dh} = \frac{\dot{m}_o D_h}{\mu_o A_o} \tag{5-13}$$

with μ_o being the annular fluid viscosity and A_o being the annular flow passage cross sectional area.

All fluid properties used in this study, including the viscosity, density, specific heat, conductivity and Prandtl number, were calculated using the method of Popiel and Wojtkowiak [34] at the

average annular bulk fluid temperature $\bar{T}_b$, which was calculated as the average of the annulus inlet $\bar{T}_{oi}$ and outlet $\bar{T}_{oo}$ temperatures:

$$\bar{T}_b = \frac{(\bar{T}_{oi} + \bar{T}_{oo})}{2} \tag{5-14}$$

Using the arithmetic average was acceptable since for all cases the bulk fluid temperatures had almost linear axial temperature profiles as a result of the high mass flow rates in both the inner and annular flow passages.

5.2.3.3 Hypothetical local heat transfer coefficients

To determine the hypothetical local heat transfer coefficients based on the hypothesis that the flow became thermally fully developed, the test section was divided into the eight control volumes having axial length of 550 mm each, starting at 0.315 m from the inlet to 4.750 m from the inlet, as shown in Figure 3-3. By only considering local heat transfer from 0.315 m onwards along the tube should eliminate the effects of the developing entry region. The same methodology used to determine the average heat transfer coefficient was then applied to each of the control volumes to determine the local average heat transfer coefficient for that portion of the heat exchanger, referred to in this dissertation as the local heat transfer coefficients. The inner and outer tube wall temperatures and local bulk temperature for each control volume were computed using the curve fit functions of the form given in Eq.(5-1).

5.2.3.4 Friction factor

The overall friction factor for annular flow was computed using the measured pressure drop, Δp, over the test section, as recorded by the differential pressure transducers, using the following equation:

$$f = \frac{2D_h \Delta p}{\rho_o L_{dp} {V_o}^2} \tag{5-15}$$

where L_{dp} is the pressure drop length and V_o is the average annular fluid velocity. All fluid properties were again calculated at the mean bulk temperature using the method of Popiel and Wojtkowiak [34]. The average velocity was calculated from the measured mass flow rate with

$$V_o = \frac{\dot{m}_o}{\rho_o A_o} \tag{5-16}$$

As proposed by Kakac [35], a property variation might be considered to allow for variations due to large differences between the fluid bulk temperature and the tube wall surface. To compensate for this variation, the friction factor correlation for turbulent liquid flow in ducts should be:

$$\frac{f}{f_{cp}} = \frac{1}{6}\left(7 - \frac{\mu_b}{\mu_w}\right) \quad for\ heating\ liquids \tag{5-17}$$

$$\frac{f}{f_{cp}} = \left(\frac{\mu_b}{\mu_w}\right)^{0.24} \quad for\ \text{cooling}\ liquids \tag{5-18}$$

where f_{cp} refers to the constant property solution, μ_b is the viscosity evaluated at bulk fluid temperature and μ_w is the viscosity evaluated at the wall temperature.

5.3 Uncertainties

Every measurand has an inherent error associated with the measurement. The magnitude of this error is quantified by the uncertainty, which identifies an interval around the measured value in which the true value is expected to lie [36]. This section gives an overview on the fluid property and measuring equipment's uncertainties. More information on how each parameter's uncertainty was computed is available in Appendix A.

5.3.1 Fluid and Tube Property uncertainties

The uncertainties of the temperature dependent properties, calculated using the method of Popiel and Wojtkowiak [34], was given by the authors and is summarised in Table 5-1 below:

Table 5-1: Uncertainties of temperature-dependent fluid properties.

Entity	Range	Uncertainty
Conductivity, k	0°C – 150°C	2.00%
Density, ρ	0°C – 150°C	0.002% – 0.004%
Prandtl number, Pr	0°C – 150°C	2.30%
Specific heat, c_p	0°C – 150°C	0.06%
Viscosity, μ	0°C – 150°C	1.00%

5.3.2 Measuring Equipment uncertainties

The method of Kline and McClintlock [36] was used to determine the uncertainties of the measuring equipment (shown in Table 5-2), which included the thermocouple stations, Coriolis flow meters and pressure transducers. According to this method the precision is determined by taking the standard deviation of a data set and multiplying it by two for a 95% confidence interval. The bias was provided by each equipment's original manufacturer. The method is discussed in more detail in Appendix A.

To reduce the uncertainty (random error) in the measurement of temperature at a certain point, more than one thermocouple was used: the entry and exit ports of the inner tube and annulus each had 4 thermocouples, while the inner tube and annular walls each had 2 thermocouples at a measuring station. The precision for each of these measuring stations was thus calculated by

$$\delta x_{i,random} = 2 \times \frac{\sigma_{avg}}{\sqrt{N}} \tag{5-19}$$

where N is the number of thermocouples at a station and σ_{avg} is the standard deviation of the averaged data set of N number of data sets for the measuring station. The results for the inlet/outlet ports and tube walls uncertainty measurements are shown in Table 5-2.

Table 5-2: Uncertainty of measurement equipment.

Instrument	Range	Bias	Precision	Uncertainty
Thermocouple stations				
Inlet / Outlet port	-200°C – 350°C	0.1°C	0.01°C	0.10°C
Inner / Outer tube wall	-200°C – 350°C	0.1°C	0.08°C	0.12°C
Coriolis flow meters				
CMF025	0 – 0.607 kg/s	0.10% full scale	Flow rate dependent	
CMF050	0 – 1.833 kg/s	0.10% full scale	Flow rate dependent	
CMF100	0.694 – 5.55 kg/s	0.10% full scale	Flow rate dependent	
Pressure transducers				
	0 – 14 kPa	0.25% full scale	0.013 kPa	0.048 kPa
	0 – 22 kPa	0.25% full scale	0.031 kPa	0.086 kPa
	0 – 55 kPa	0.25% full scale	0.107 kPa	0.245 kPa

The measurement of the tube diameters had an uncertainty of 0.02 mm and for the tube length measurements the uncertainty was 1 mm.

5.3.3 Summary of calculation uncertainties

In the illustration of the data reduction process in Figure 5-1 it was explained that in the analysis of each test the average and local heat transfer coefficients, friction factor and uncertainties were calculated. Table 5-3 gives as example a summary of the uncertainties in the analysis for two test cases: 1) cooled 0.386 annular diameter ratio at T_{oi} of 15°, Re_{Dh} of 45 000, Re_i 40 000 and 2) heated 0.386 annular diameter ratio at T_{oi} of 50°, Re_{Dh} of 45 000, Re_i 40 000. The table shows the individual contributions to the uncertainty of the friction factor, j-factor and average Nu_{Dh} and thus allows a sensitivity analysis to determine which parameters had the greatest influence on results.

Table 5-3: Uncertainties involved in the calculation of the friction factor, j-factor and Nu_{Dh} for the tests of a 0.386 annular diameter ratio with Re_{Dh} at 45 000, Re_i at 40 000 and T_{oi} at 50°C and 15°C.

Property	50°C	15°C	Property	50°C	15°C
T_{ii}	0.10°C	0.10°C	$A_{s,o}$	0.02%	0.02%
T_{io}	0.10°C	0.10°C	D_i	0.17%	0.17%
T_{oi}	0.10°C	0.10°C	D_h	0.14%	0.14%
T_{oo}	0.10°C	0.10°C	$\dot{Q}_i$	0.87%	0.51%
$\bar{T}_{iw}$	0.13°C	0.13°C	$\dot{Q}_o$	2.31%	3.91%
$\bar{T}_b$	0.07°C	0.07°C	h	1.21%	1.14%

ΔT_i	0.14°C	0.14°C	Re_i	1.02%	1.02%
ΔT_o	0.14°C	0.14°C	Re_{Dh}	1.03%	1.03%
ΔT_{LMTD}	0.10°C	0.11°C	V	0.19%	0.19%
$\dot{m}_i$	0.11%	0.12%	f	0.55%	0.24%
$\dot{m}_o$	0.12%	0.11%	j	2.18%	2.09%
L_{hx}	0.02%	0.02%	Nu_{Dh}	1.76%	1.66%
$A_{s,i}$	0.02%	0.02%			

Table 5-4 gives the average uncertainties for the Nu_{Dh}, j-factor and friction factor for each annular inlet temperature test case (averaged over all the Re_{Dh} and Re_i permutations for a given T_{oi}). The inlet temperature had some influence on the uncertainty. For the Nu_{Dh} uncertainties were higher for the H30 and C30 cases, probably due to the fact that the smaller difference between annular fluid and inner tube wall temperatures resulted in an average heat transfer with higher uncertainty. For the j-factor it seems that the uncertainties decreases as the annular inlet temperature increased. This might be linked to the fact that the j-factor is calculated by dividing Nu_{Dh} with Pr, thus reducing the effect of the Pr (which has a relative high uncertainty of 2.3%). The friction factor uncertainties did not seem to be affected by the inlet temperature case.

Table 5-4: Uncertainties for Nu_{Dh}, j-factor and friction factor, averaged for annular inlet temperature cases.

	Nu_{Dh} Uncertainty				***j*-factor Uncertainty**				**Friction Factor Uncertainty**			
	0.327	**0.386**	**0.409**	**0.483**	**0.327**	**0.386**	**0.409**	**0.483**	**0.327**	**0.386**	**0.409**	**0.483**
H15	1.6%	1.8%	1.8%	2.5%	2.1%	2.2%	2.2%	2.8%	0.7%	0.6%	1.5%	1.5%
H20	1.7%	1.9%	1.9%	2.3%	2.1%	2.3%	2.3%	2.6%	0.8%	0.5%	1.9%	1.0%
H30	2.0%	2.2%	2.4%	2.8%	2.3%	2.6%	2.7%	3.1%	1.8%	0.7%	1.3%	2.0%
C30	2.8%	2.7%	3.0%	3.2%	3.1%	3.0%	3.3%	3.4%	1.0%	0.5%	1.2%	1.8%
C40	2.2%	2.2%	2.3%	2.9%	2.5%	2.5%	2.6%	3.2%	0.9%	0.5%	0.5%	2.8%
C50	1.9%	1.9%	2.0%	2.4%	2.3%	2.3%	2.4%	2.7%	1.2%	0.6%	0.4%	2.4%
Average	2.0%	2.1%	2.2%	2.7%	2.4%	2.5%	2.6%	3.0%	1.1%	0.6%	1.1%	1.9%

Table 5-5 reports the average uncertainties for each test section as well as the overall average uncertainty in the Nu_{Dh}, j-factor and friction factor. The 0.327 test section had the lowest uncertainties while the 0.483 had the highest uncertainties. It can be deduced from the table that the uncertainty increases with the hydraulic diameter of the test section. The overall uncertainty for the Nu_{Dh} was 2.3%, while the j-factor had an uncertainty of 2.6%. Although the friction factor had an average uncertainty of only 1.2%, it is the opinion of the author that in some instances the equipment was faulty.

Table 5-5: The average uncertainties for Nu_{Dh}, *j*-factor and friction factor.

	0.327	0.386	0.409	0.483	Average
D_h (mm)	17.00	22.98	20.20	26.18	
Nu_{Dh} Uncertainty	2.0%	2.1%	2.2%	2.7%	2.3%
***j*-factor Uncertainty**	2.4%	2.5%	2.6%	3.0%	2.6%
Friction Factor Uncertainty	1.1%	0.6%	1.1%	1.9%	1.2%

Understanding and knowing the uncertainties for the calculated values will assist the reader in interpreting the results in the next chapter.

5.4 Chapter summary

In this chapter the analysis and data reduction method was explained. The process followed to calculate the average Nusselt number for comparison purposes is now clear. The method of deriving functions for local wall and bulk temperatures to enable the calculation of local heat transfer has been discussed. Light was cast on the friction factor calculation for an annulus from measured pressure drop. After that, a discussion followed on the different types of uncertainty encountered and the means to calculate each. The reader has been made aware of the random errors in thermocouples as well as the uncertainty induced in analysis. Tables were given of the uncertainties in the calculation of temperature dependent fluid properties, the measurement equipment used and values of the Nu_{Dh}, *j*-factor and friction factor.

CHAPTER 6 - RESULTS

6.1 Introduction

This chapter contains the results of the data processed as described in Chapter 5. To eliminate redundancy, this chapter focuses on the results of the 0.386 annular ratio test section. The chapter starts with a comparison of the calculated average heat transfer rate and friction coefficient to existing predictions and then moves to an investigation into the influence of the annular inlet temperature, local heat transfer rates, heated annulus versus cooled annulus and the influence of the inner tube Reynolds number. Additional results for the 0.483, 0.409 and 0.327 test sections are available in Appendix B. However, the influence of the annular diameter ratio is shown at the end of the chapter by comparing the results for the average heat transfer rate, Colburn *j*-factor and friction factor of the different test sections to one another.

6.2 Comparison to Existing Correlations

Although the effect of different inner tube Reynolds numbers (Re_i) on the heat transfer and friction factor coefficients was not in the scope of the study, testing was done over a range of Re_i values to produce an array of data that will allow future research using other types of data analysis such as the Wilson plot method. For this section the effect of the Re_i was disregarded by averaging the results over the range of Re_i values for each consecutive Re_{Dh} number considered. An observation on the effect of the inner tube Reynolds number will follow later in the chapter.

6.2.1 Average Heat Transfer Compared to Existing Correlations

For each inlet temperature case the average heat transfer coefficient over the test section (represented by the Nu_{Dh}) was calculated and plotted against the range of Re_{Dh} using the analysis method described in Chapter 5.2. Figure 6-1 depicts Nu_{Dh} against Re_{Dh} for the 0.386 test section at an inlet temperature of 50°C. Error bars indicate the uncertainty for each calculated value. As expected, the Nu_{Dh} increases with an increase in Re_{Dh}. The uncertainty of the average Nu_{Dh} varies over the Re_{Dh} range between 1.7% and 2.2%.

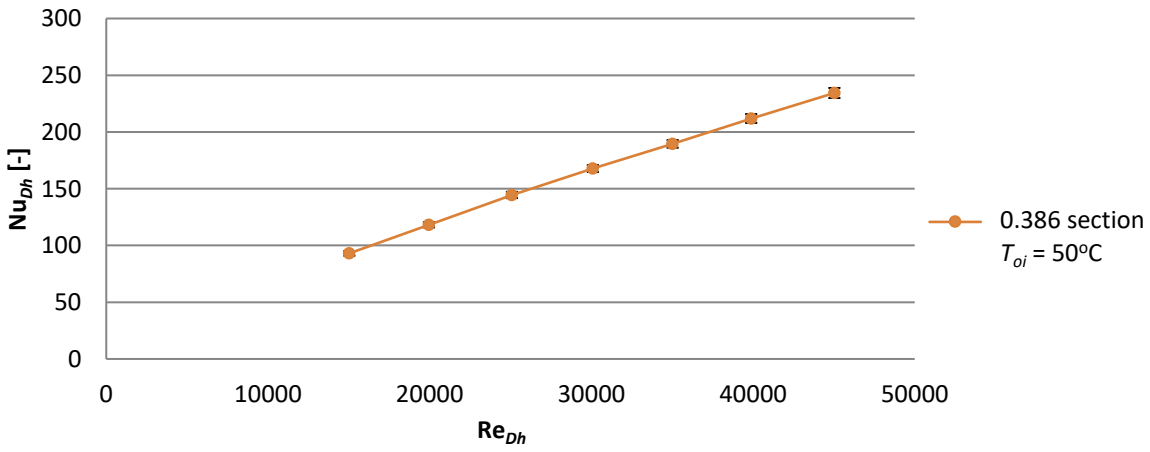

Figure 6-1: Average Nusselt number over range of annular Reynolds numbers for the 0.386 test section at a 50°C inlet temperature (C50) with error bars indicating the uncertainties.

The calculated heat transfer coefficients were compared with predictions from some of the existing correlations (as given in Table 2-2) using the same temperature and mass flow inputs. Refer to Figure 6-2 and Table 6-1. The correlation of Lu and Wang over-predicted the experimental values, as well as those of Dirker & Meyer, Gnielinski, Swamee *et al* and Dittus & Boelter, by more than 50% and was subsequintly left out of Figure 6-2. All the afore-mentioned correlations underpredicted the experimental values. All these correlations, except for Dittus & Boelter, contained a ratio between properties dependent on the annular bulk temperature T_b and inner tube wall temperature T_{wi}.

In Figure 6-2 a comparison of the results are given for the annular inlet temperature cases of T_{oi} at (a) 50°C (C50) and (b) 15°C (H15) for the 0.386 section. Reviewing graph (a) the cooling case at 50°C, it was noted that the experimental Nu_{Dh} was in proximity to the predictions of Dirker & Meyer and Gnielinski, with an average variation of 13.5% and 10.3% respectively, but differed by 21.2% and 28.7% respectively from the predictions of Dittus & Boelter and Swamee *et al*. It was noted that the predictions of Swamee *et al.* and Dittus & Boelter clustered and that of Dirker & Meyer and Gnielinski clustered. Studying the heated annulus case, graph (b), with annular inlet at 15°C showed that the experimental values correlated best with predictions from Dirker & Meyer, Gnielinski and Dittus & Boelter, where each correlation under predicted by 17.4%, 9.8% and 18.0%.

The differences between the calculated Nu_{Dh} and the predictions from existing correlations (as given in Table 2-2) are shown in Table 6-1. The predictions of Dirker & Meyer and Gnielinski seem to be in good correlation with the experimental data. Predictions from Dittus & Boelter are more suitable for heated cases than for cooled cases. Although the correlations of Dirker & Meyer and Gnielinski made predictions on average within 15.8% and 10.2% of the measured values, there was no single correlation that was able to consistently correctly predict the Nusselt number for both cooled and heated annuli over the considered range of Re_{Dh} and T_{oi}.

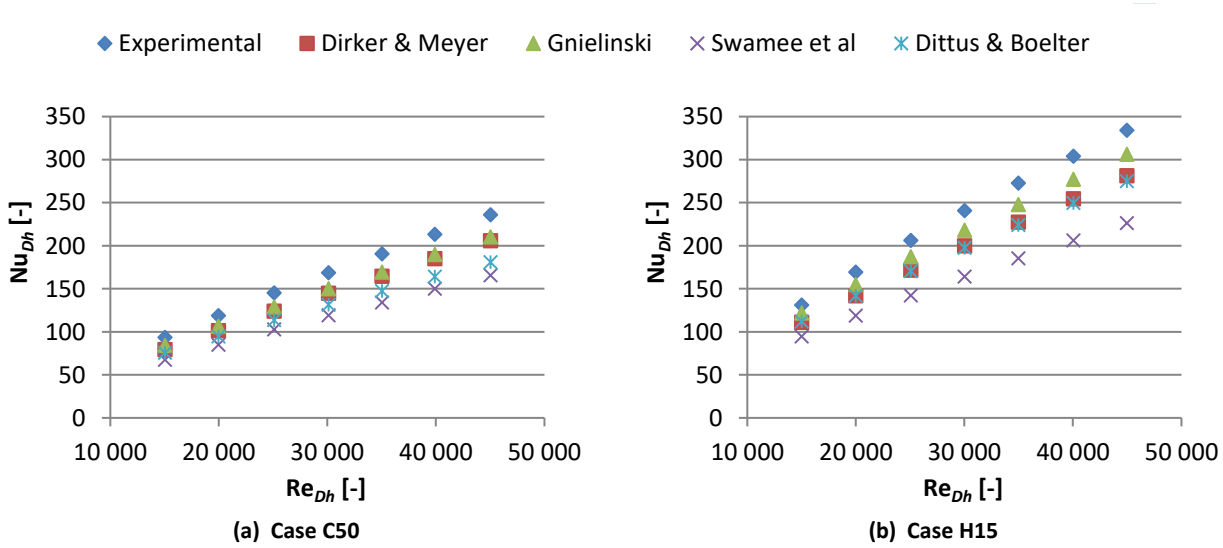

Figure 6-2: Comparison of computed Nusselt number and existing correlations against Re_{Dh} for (a) cooling of the annulus with T_{oi} at 50°C and (b) heating with T_{oi} at 15°C.

Table 6-1: Difference between Nusselt numbers computed from measurements and correlations, for the 0.386 test section with T_{oi} for all six cases.

T_{oi}	Dirker & Meyer	Gnielinski	Lu & Wang	Swamee et al	Dittus & Boelter
50°C (C50)	13.5%	10.3%	-68.7%	28.7%	21.2%
40°C (C40)	15.7%	11.0%	-65.3%	30.5%	24.2%
30°C (C30)	17.5%	11.5%	-62.5%	32.0%	27.0%
30°C (H30)	14.7%	9.6%	-57.5%	29.6%	16.0%
20°C (H20)	16.0%	9.2%	-55.9%	30.7%	16.9%
15°C (H15)	17.3%	9.8%	-53.7%	31.8%	18.0%

6.2.2 Experimental Friction Factors Compared to Existing Correlations

In similar fashion the experimental friction factors were compared to existing correlations presented in Table 2-3. Figure 6-3 illustrates afore-mentioned comparison for annular inlet temperature cases of T_{oi} at (a) 50°C (C50) and (b) 15°C (H15) for the 0.386 section. For both the cooled and heated cases the experimental obtained friction factors were higher than any prediction. Table 6-2 illustrates the percentage that each prediction differs from the experimental results. It is noted that in both cases the predictions of Gnielinski and Jones & Lang and that of Blasius and Kenade *et al*. group together. The predictions of Gnielinski and Jones & Lang was on average 14.0% and 13.4% lower than the experimental values.

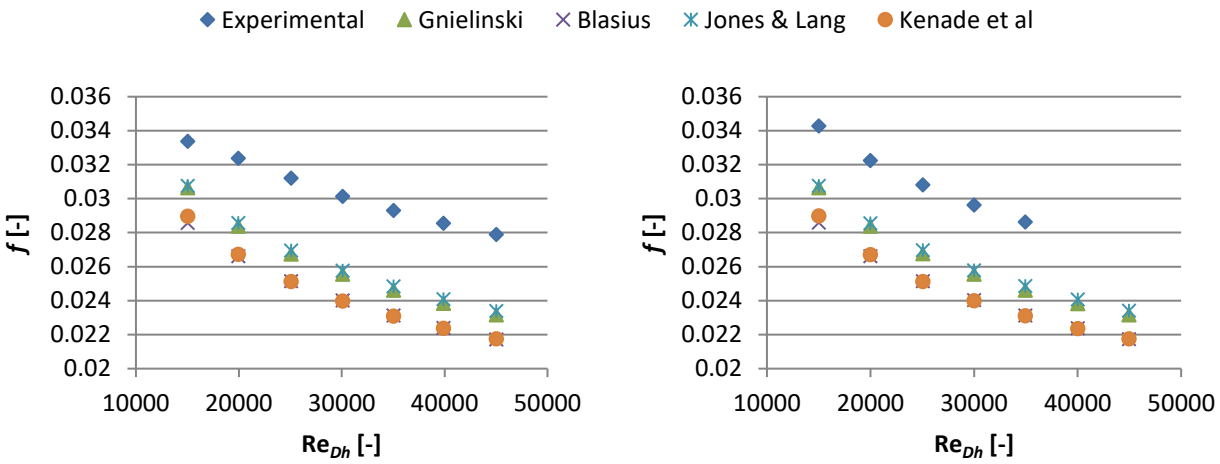

Figure 6-3: Comparison of experimental friction factor and existing correlations against Re_{Dh} for (a) cooling of the annulus with T_{oi} at 50°C and (b) heating with T_{oi} at 15°C.

Table 6-2: Difference between friction factors computed from measurements and correlations, for the 0.386 test section with T_{oi} for all six cases.

T_{oi}	Gnielinski	Blasius	Jones & Lang	Kenade et al
50°C (C50)	14.2%	19.6%	13.5%	19.4%
40°C (C40)	15.0%	20.3%	14.4%	20.1%
30°C (C30)	15.7%	20.9%	15.0%	20.8%
30°C (H30)	12.7%	18.2%	12.1%	18.0%
20°C (H20)	13.7%	19.1%	13.1%	18.9%
15°C (H15)	12.7%	18.1%	12.1%	17.9%

6.3 Influence of the Inlet Temperature

As described in Chapter 4.7, each test section was tested at six different annulus inlet temperatures and an array of inner tube and annular Reynolds numbers. Due to mentioned hardware limitations the inlet temperature could only be kept constant within a range of ±1.5°C of the desired inlet temperature over the range of tests.

Below follows a study of the Nusselt number, Colburn *j*-factor and friction factor measured over Re_{Dh} ranging from 15 000 to 45 000, at the six different inlet temperature cases.

6.3.1 Nusselt number

Figure 6-4 shows the experimentally obtained Nu_{Dh} while varying the Re_{Dh} at the different inlet temperature cases. The figure shows that the heated annuli cases generally had higher Nu_{Dh} values compared to the cooled cases. The Nu_{Dh} increased with an increase in the Re_{Dh} while an increase in the annular fluid inlet temperature resulted in a decrease in Nu_{Dh}. The cases H15 and C50 had an average difference in Nu_{Dh} of 30.8%. The cases H30 and C30 both had annular inlet temperatures of 30°C, but the heated annulus had on average higher Nusselt numbers, differing by 0.28% from the heated case. A more in-depth investigation into the impact of heating or cooling the annulus will follow later in the chapter.

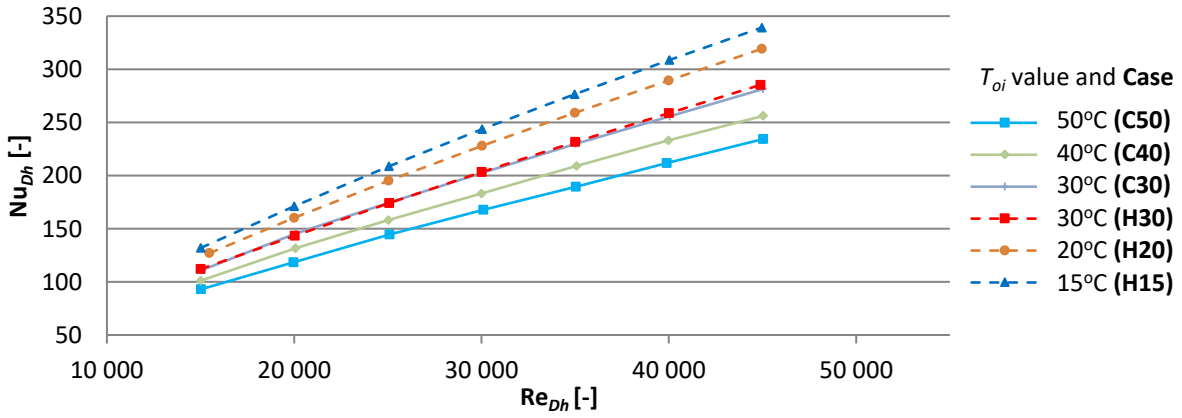

Figure 6-4: Nusselt number versus Re_{Dh} for the six inlet temperature cases in the 0.386 test section.

6.3.2 Colburn *j*-factor

The Colburn *j*-factor is often used to reduce / remove the effects of the temperature dependency of the fluid properties in the heat transfer results. Figure 6-5 illustrates that the *j*-factor decreased with an increase in Re_{Dh}. This is similar in nature to general friction factor behaviour, and will be discussed in Section 6.3.3. As the inlet temperature was increased, the *j*-factor also decreased. The difference between the cases of H15 and C50 was 13.1% on average, with heated annuli having a higher value. Considering H30 and C30, both at inlet temperatures of about 30°C, it was observed that the heated annulus had on average a 2.6% higher value. Since the *j*-factor is dependent on the Nu_{Dh} and Pr, it can be expected that it will also decrease with an increase in the inlet temperature.

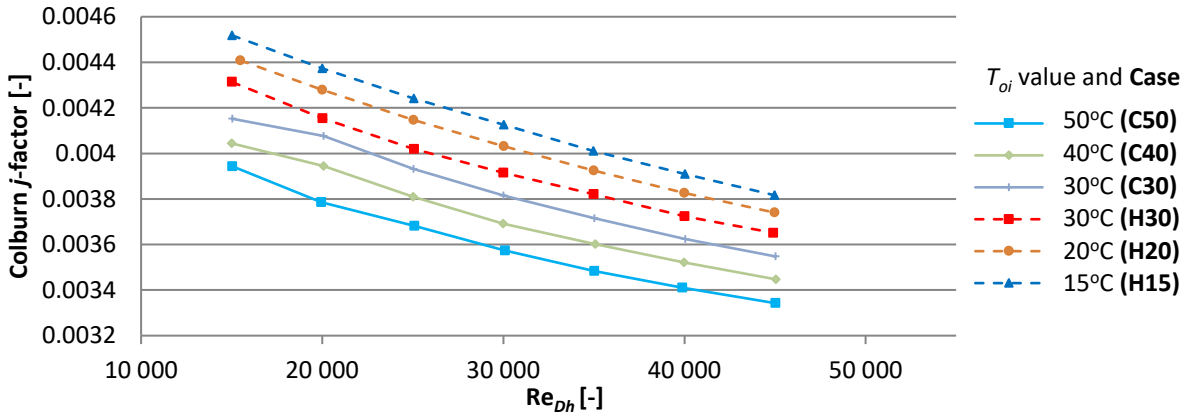

Figure 6-5: Colburn *j*-factor versus Re_{Dh} for the six inlet temperature cases in the 0.386 test section.

As mentioned before, the *j*-factor was computed by dividing the Nu_{Dh} by the Re_{Dh} and the Pr to the exponent *p*, which was given as $p = 1/3$ (Eq. (5-12)). It was considered that there might exist a value of the exponent *p* for which all the *j*-factor values for different annular inlet temperatures shown in Figure 6-5 fall onto a single line. This value can be called the adjusted *j*-factor. Figure 6-6 illustrates an adjusted *j*-factor with exponent $p = 0.542$.

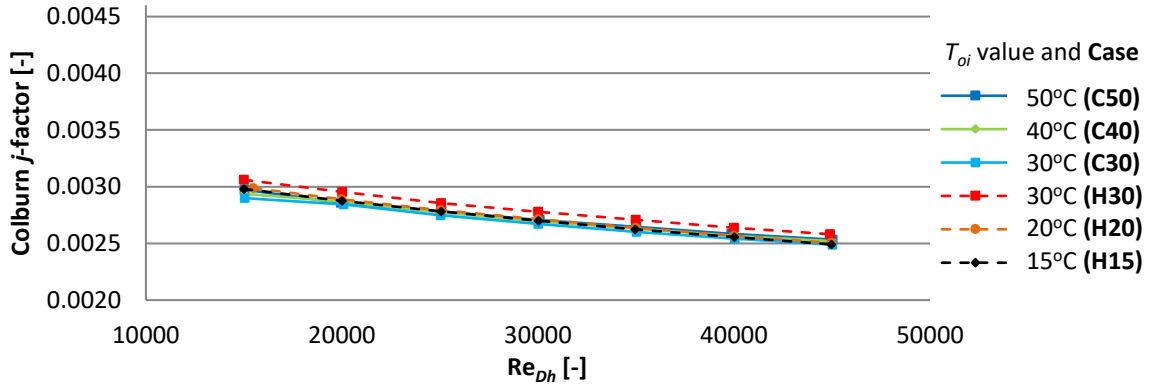

Figure 6-6: The adjusted Colburn j-factor versus Re_{Dh} for the six inlet temperature cases in the 0.386 test section.

Table 6-3 shows a comparison between the *j*-factor and adjusted *j*-factor and gives an indication of how the values differ with change in inlet temperature. It is seen that with the exponent of $p = 0.33$

the *j*-factor differ on average by 7.8%, where with the adjusted *j*-factor with p = 0.542 the values differ by only 0.03% on average.

Table 6-3: Comparison of the *j*-factor to the adjusted *j*-factor.

T_{oi}	*j*-factor with p = 0.33	Difference from C50 case	Adjusted *j*-factor with p = 0.542	Difference from C50 case
50°C (C50)	0.00360	0.0%	0.00273	0.0%
40°C (C40)	0.00372	-3.3%	0.00271	0.5%
30°C (C30)	0.00384	-6.5%	0.00268	1.5%
30°C (H30)	0.00394	-9.4%	0.00280	-2.6%
20°C (H20)	0.00405	-12.4%	0.00273	0.0%
15°C (H15)	0.00414	-15.0%	0.00272	0.4%
Average		7.8%		0.03%

6.3.3 Friction Factor

Acquiring accurate data for the pressure drop deemed very difficult due to the low differential measured values, especially at low Re_{Dh} cases where the pressure drop ranged between 3 – 6 kPa. This is seen in Figure 6-7, where for Re_{Dh} values below 25 000 the friction factor trends appear less predictable. It was noted that at higher Re_{Dh} values, the friction factor did not vary as such with inlet temperature, but was rather dependent on whether it was a heated or cooled application. At a Re_{Dh} value of 45 000 there was a 2.3% difference between heated and cooled measurements, with cooled annuli (warmer fluid temperature, but relatively colder inner tube wall temperature) having a larger friction factor. It is suspected that the colder inner tube results in higher surface friction and pressure drop across the test section length, contributing to the larger friction factor. Considering Eq. (5-15), it is seen that in the calculation of the friction factor, the fluid velocity squared appears in the divisor, which explains why at higher Re_{Dh} the velocity becomes the dominant determinant in the calculation.

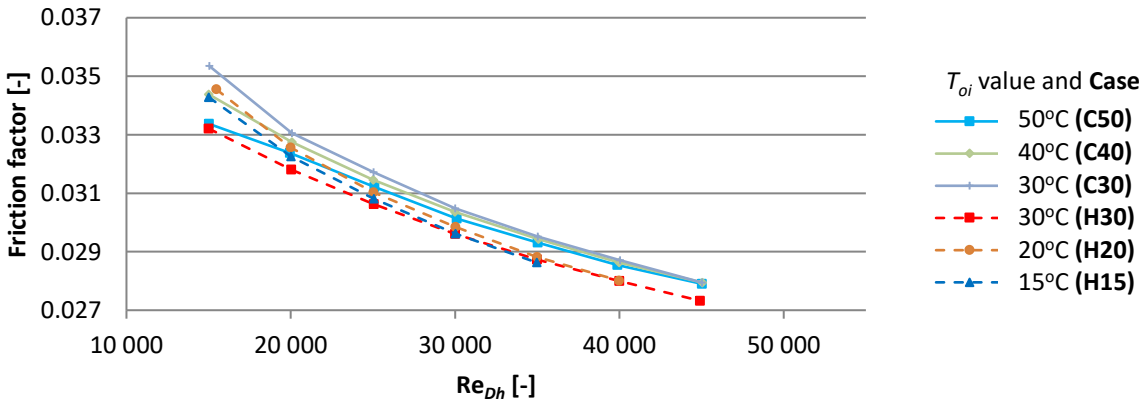

Figure 6-7: Friction factor versus Re_{Dh} for the six inlet temperature cases in the 0.386 test section.

6.4 Hypothetical Local Heat Transfer Coefficients

The local heat transfer coefficients were computed, as described in Chapter 5.2.3, by dividing the test section into equal length control volumes (CVs). By considering each control volume as a small test section, with known inlet and outlet conditions, the average Nusselt number computed for each particular control volume was estimated to be the local Nusselt number for that part of the test section. The small test sections considered resulted in high uncertainties due to the very small temperature changes, sometimes as high as 52%.

This section first attempts to draw a comparison between the experimental results and existing correlations. The analysis of the local Nusselt number then extends to the condition of constant Re_{Dh} across the test section length. To ensure the test sections was designed to be in the optimal length region for effective heat transfer, a NTU-effectiveness analysis is done.The effect of annular inlet temperature on the local heat transfer coefficinet is shown. Lastly, a reflection is given on the viability of the hypothetical local heat transfer coefficients.

6.4.1 Comparison with existing correlations

The experimentally obtained local Nusselt number values were compared with the predictions of some of the existing correlations in Table 2-2 by applying the inlet and outlet temperature of each control volume to the correlations. Note that this comparison disregarded the fact that the Re_{Dh} would reduce slightly along the length of the test section (each subsequent CV) as a result of temperature dependent fluid properties. The Re_{Dh} in this instance was calculated using the average bulk temperature for the heat exchanger as a whole. The situation where the sectional results are considered at constant Re_{Dh} over all the CVs will be discussed in the next section. The comparison is shown in Figure 6-8. The correlation of Lu and Wang was again disregarded as it over-predicted by more than double the value of the other predictions. The Re_{Dh} averaged over the entire section was at 35 000 and the inlet temperature was at 50°C.

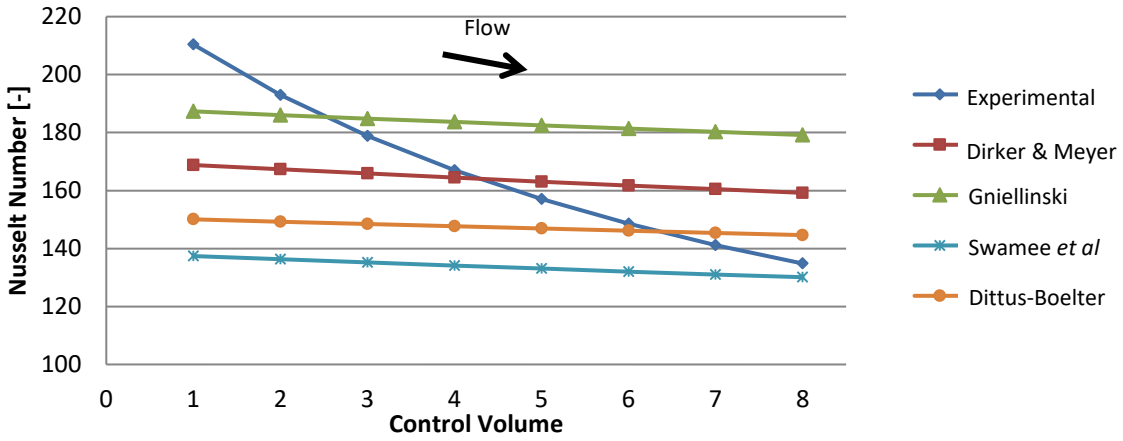

Figure 6-8: Comparison of calculated hypothetical local heat transfer coefficient values for each CV of the annulus against predictions of existing correlations. (*a* of 0.386, average Re_{Dh} = 35 000, C50)

It is seen from Figure 6-8 that all the existing correlations predicted different magnitudes, but a similar trend along the length of the test section. An important observation is that the local Nusselt number (average Nusselt number for the small individual control volumes) reduces along the length of the test section, for the experimental results and the predictions. This leads the author to believe

that the heat transfer coefficient is not constant along the length of a heat exchanger, but higher at the inlet. This notion will be investigated and discussed in more depth as the section progresses. It is observed that no single correlation can predict the experimental obtained local Nusselt number properly.

6.4.2 Constant Reynolds numbers

It is possible that the observed reduction in local Nusselt number along the test section (as witnessed in Figure 6-8) was partly due to the effect of a reducing Re_{Dh} being neglected. In order to consider the local Nusselt number at a constant Re_{Dh} over each CV of the test section, it was necessary to interpolate the local Nusselt number data at a desired Re_{Dh} value. For this purpose, the "TREND()" function was used in Microsoft Excel which produced interpolated results with a minimum goodness of fit value, R^2, of 0.978.

Figure 6-9 illustrates the local Nusselt number at different values of constant Re_{Dh} for the control volumes in the 0.386 test section at inlet temperatures of (a) 50°C (C50) and (b) 15°C (H15). The charts have been scaled similar to allow comparison. As expected, higher Re_{Dh} values resulted in higher local Nusselt numbers. It was noted that the Nusselt number was higher at the entrance of the test section, reducing along the length, with the slope tending to flatten out at the exit. This might opt some readers to question whether the heat exchanger length had not been optimal length?

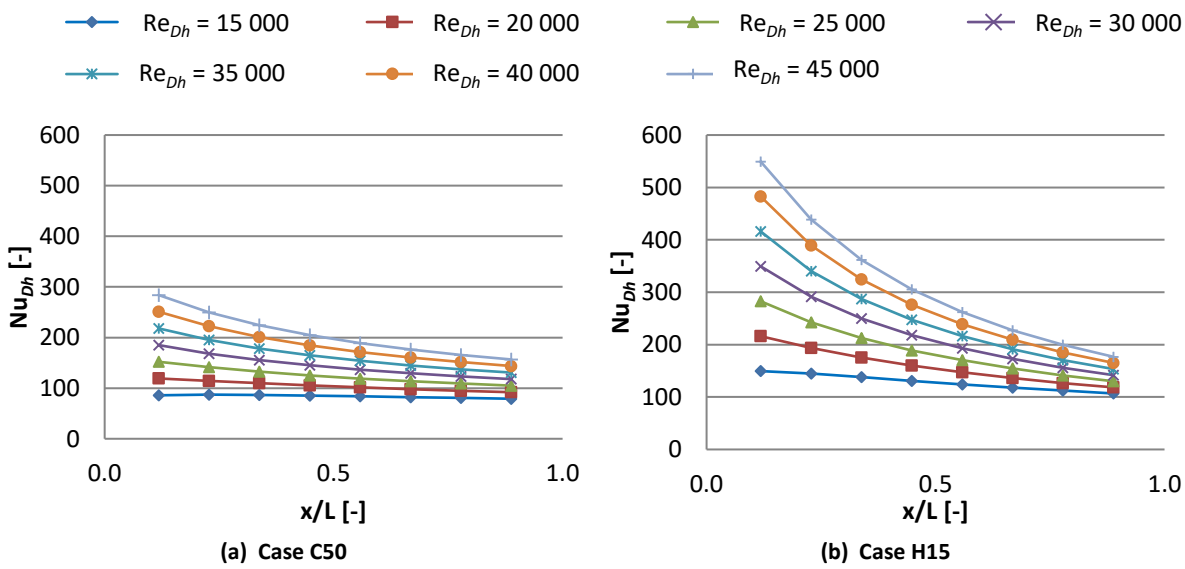

Figure 6-9: Hypothetical local Nusselt numbers along the length of the test section for different annular Reynolds numbers at inlet temperatures of (a) 50°C and (b) 15°C.

By determining the NTU-effectiveness relation for the test sections used in this study it is possible to estimate if the test section lengths were optimal. A detailed description of the NTU and effectiveness analysis method and results for the 0.386 test section is given in Appendix C. Overall, the heated annulus conditions had higher NTU values with a maximum of 1.631 for the case H30 at a maximum effectiveness of 0.791. This signifies that the heat exchanger length was within optimal region and could still be longer than 5.03 m.

6.4.3 Effect of annular inlet temperature

The dependency of the local heat transfer coefficient on annular inlet temperature is illustrated in Figure 6-10 by plotting the local Nusselt numbers along the heat exchanger length at a constant Re_{Dh} value of 45 000, at the different inlet temperature cases. Comparing the curves, it seems as if the values for the C30 case were too low, as it should have been positioned roughly between the values of C40 and H20, instead of in the region of C50.

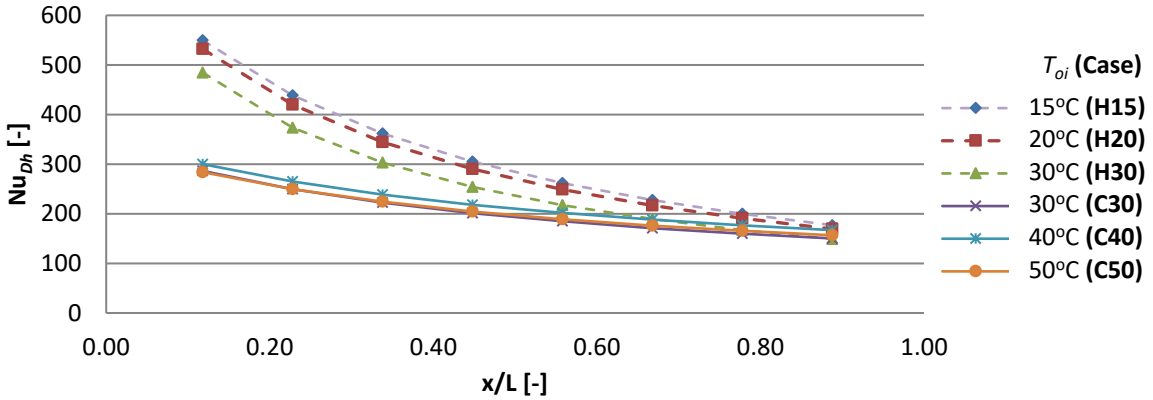

Figure 6-10: Hypothetical local Nusselt number along the length of the 0.386 test section at constant Re_{Dh} of 45 000 at different inlet temperature cases.

By comparing Figure 6-9 (a) and (b) and considering Figure 6-10, it is clear that much larger heat transfer coefficients existed at the entrance of the test section of a heated annulus compared to a cooled annulus. Both heated and cooled annuli had about the same Nusselt numbers at the exit of the heat exchanger. For instance, consider the Reynolds number value of 45 000 given in Figure 6-10. For cases C30 and H30 respectively the inlet local Nusselt numbers were 286 and 485, while the Nusselt numbers towards the outlet dropped to 150 and 149. This means that for the C30 case, there was a 47% reduction in the local heat transfer coefficient, while for the H30 case there was a 69 % reduction. The same tendencies were observed for all test sections.

6.4.4 Reflection on the calculation method of Local Heat Transfer

According to Incroperia and DeWitt [37], the heat transfer coefficient will decay rapidly as the thermal boundary layer develops, reaching a constant value once fully developed conditions are reached. But according to them fully developed thermal conditions can only be reached if there is either a uniform surface heat flux or a uniform surface temperature, neither of which is true for this case. Hence fully developed thermal flow with constant fluid properties will not exist, resulting in a local heat transfer coefficient dependent on the position *x* along the heat exchanger. This indicates a flaw in the assumption made in Section 5.2.3: "Hypothetically, fully developed thermal flow existed in the 0.315 m – 4.75 m section of the heat exchanger, allowing local heat transfer analysis in this region." This hypothesis proved to be incorrect, as results indicated fully developed thermal flow never exists along the length of the heat exchanger.

6.5 Direction of Heat Transfer

When studying Figure 6-4 it was noted that there was a slight difference in values for the cases of C30 and H30, although both cases had an annular inlet temperature of approximately 30°C. This raised the question whether the direction of heat transfer coefficient (and thus the characteristics of

the radial temperature gradient at the diabatic wall) had an influence on heat transfer coefficient, or whether the results obtained were due to small temperature control errors in the experiments. This section will consider the annular inlet temperature and average bulk temperature to determine if either of these could be responsible for the difference in heat transfer coefficient between the C30 and H30 cases. Next, the average Nusselt number for all four different test sections will be compared to determine if there is a fixed pattern coupled to the heat transfer direction.

6.5.1 Annular Inlet and Bulk Temperatures

Although the intended inlet temperature was 30°C, it was not always possible to reach the exact temperature due to equipment limitations. Figure 6-11 shows the annular inlet temperatures for the H30 and C30 cases for the 0.386 test section over the range of Re_{Dh} values. The figure illustrates that for the 0.386 test section the heated tests had on average a higher inlet temperature of 30.60°C when compared to the cooled tests at 29.74°C, each having a scatter with a standard deviation of 0.41°C and 0.53°C respectively.

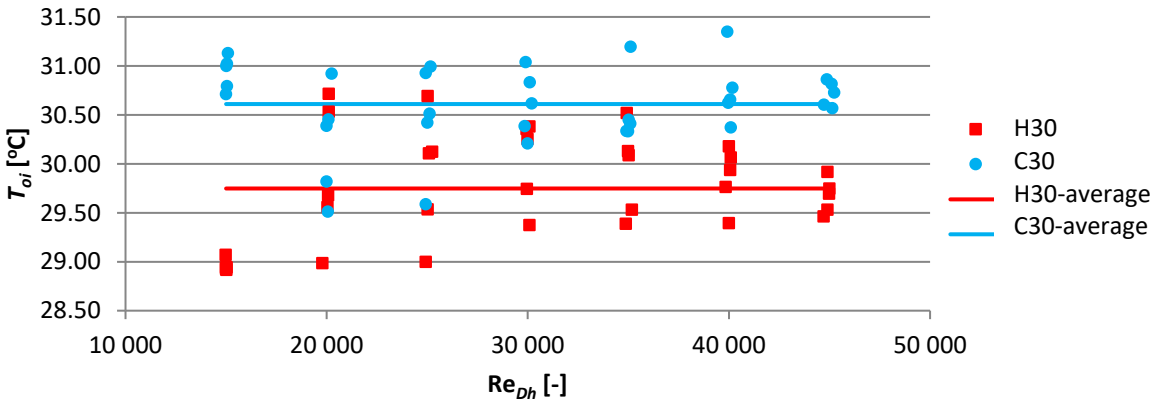

Figure 6-11: Annular inlet temperature for the H30 and C30 tests on the 0.386 test section.

Comparing the average annular bulk temperatures (by taking into account the measured exit fluid temperature) in Figure 6-12 showed that the heated annuli had a consistent higher bulk temperature of 31.63°C on average compared to the cooled annuli at 28.90°C.

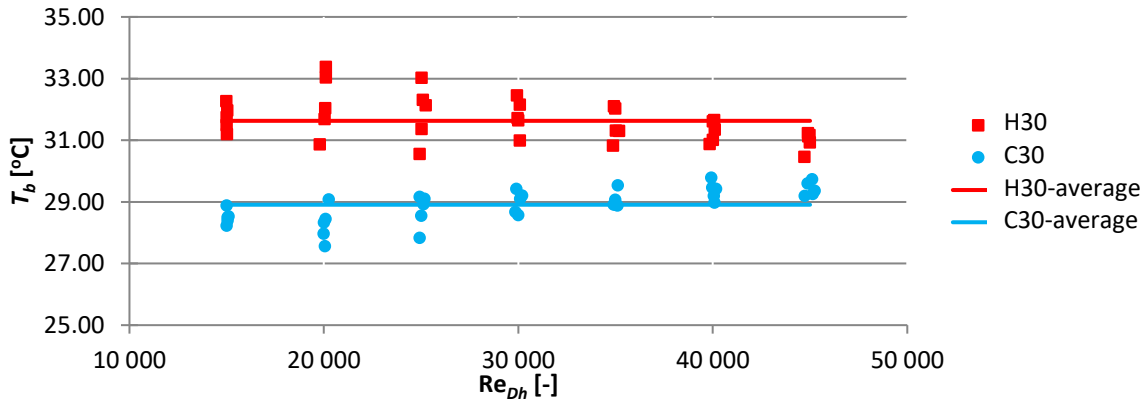

Figure 6-12: Annular bulk temperature for the H30 and C30 tests on the 0.386 test section.

Comparing the findings of Figure 6-11 and Figure 6-12 indicates that the C30 case had on average higher annular inlet temperatures and a lower average bulk temperature than the H30 case (which makes sense since the fluid was cooled for the C30 case). Consider Figure 6-13 which shows how, for constant Re_{Dh}, the Nu_{Dh} varies with annular bulk temperature. As the bulk temperature increases, the Nu_{Dh} decreases. The average Nusselt number is more sensitive to cooler bulk temperatures due to temperature dependent properties (especially the Prandtl number). The lower the bulk temperature of a fluid, the higher the Prandtl number and Nu_{Dh}. For example in this instance the fluid bulk temperatures of 28.9°C and 31.6°C has Prandtl numbers of 53.25 and 50.17, which differs by 5.7%. This might explain the results in Figure 6-4 where the cooled C30 case had larger Nusselt numbers than the H30 case.

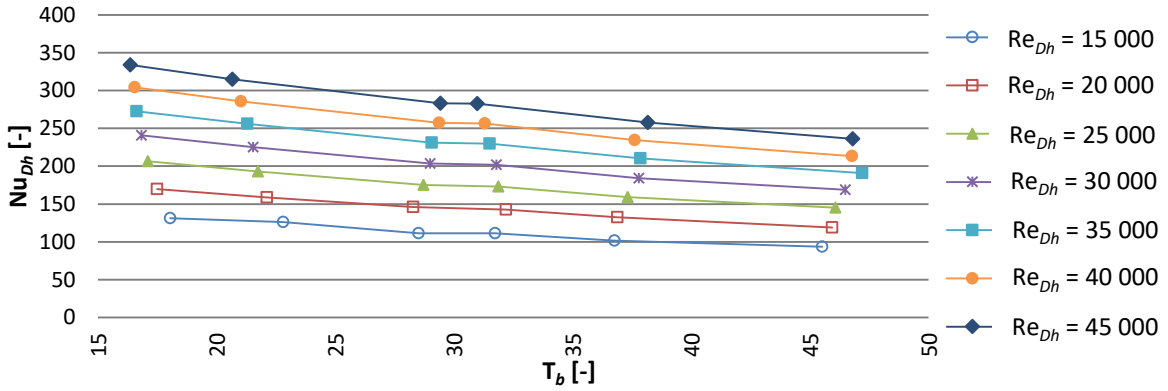

Figure 6-13: Variation of Nu_{Dh} with annular bulk fluid temperature for the 0.386 test section at different Re_{Dh}.

6.5.2 Average Nusselt numbers for each test section

A deeper investigation was launched to determine a trend across all annular test sections on when the calculated average Nusselt number would be greater for the cooled annulus compared to a heated annulus when both have a T_{oi} of 30°C. From Section 5.2.3.2, which describes the analysis of the average heat transfer coefficient, it was clear that the annular inlet temperature, average annular bulk temperature and average inner wall temperature all had an influence on the calculated Nusselt number.

The influence of heat transfer direction was examined by taking the difference in measured temperatures and resulting Nusselt number between the C30 and H30 case for each test section. Figure 6-14 shows a comparison of these differences for each of the four test sections, in terms of the following axis scales:

Annular inlet temperature: $\Delta\bar{T}_{oi} = (\bar{T}_{oi,C30} - \bar{T}_{oi,H30}) \times 10$

Average annular bulk temperature: $\Delta\bar{T}_{b,a} = \bar{T}_{b,a,C30} - \bar{T}_{b,a,H30}$

Average inner wall temperature: $\Delta\bar{T}_{w,i} = (\bar{T}_{w,i,C30} - \bar{T}_{w,i,H30}) / 10$

Nusselt number: $\Delta\overline{Nu} = (\overline{Nu}_{,C30} - \overline{Nu}_{,H30})/\overline{Nu}_{,C30} \times 100$

The values for the annular inlet temperature and average inner wall temperature were scaled to allow a better visual comparison. Each temperature was averaged over the range of Re_{Dh} in each test case.

By examining Figure 6-14 it can be seen that the 0.483 case was the only case which had a larger $\bar{T}_{oi}$ for the H30 case than for the C30 case (giving a negative $\Delta\bar{T}_{oi}$ value). The difference in $\bar{T}_{w,i}$ and $\bar{T}_{b,a}$ were negative for all test cases (larger values for H30). Looking at the difference in the calculated average Nusselt number shows a similar trend to the differences in $\bar{T}_{oi}$, where only the 0.483 case was negative. This finding tends to allow the assumption that for these experiments the heat transfer direction did not have an influence on the heat transfer coefficient, instead the test case with the marginally larger $\bar{T}_{oi}$ resulted in a larger average Nusselt number.

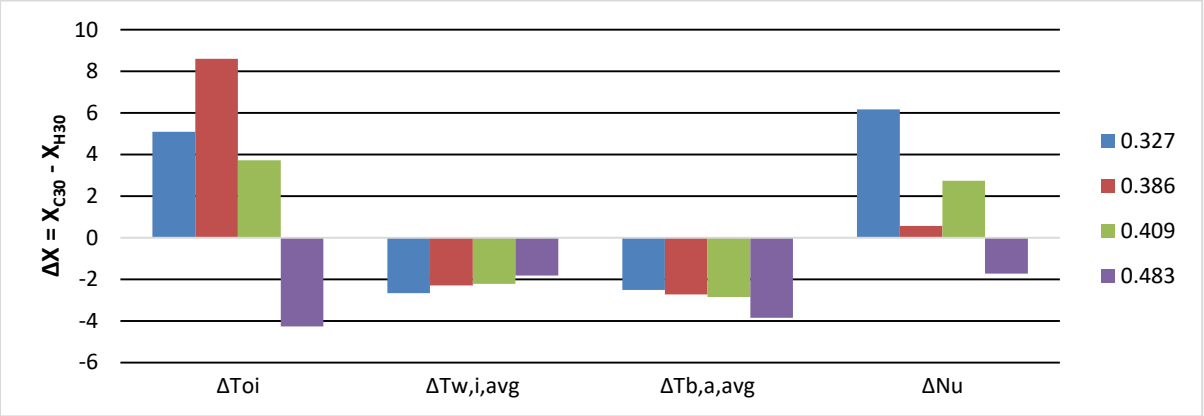

Figure 6-14: Comparison of the differences in temperatures and Nusselt number between the C30 and H30 cases for across all annular ratios tested.

6.6 Inner tube Reynolds number influence

Up to now all the results were averaged over the five variants of Re_i for the applicable Re_{Dh} value. This section presents a more in-depth look at the effect of different Re_i on the outcome.

Figure 6-15 shows the effect of incorporating the individual Re_i on the average Nusselt number results for the 0.386 test section with an annular inlet of 50°C (C50). Figure 6-15 (a) illustrates the whole test set for the case C50, having a Re_{Dh} range of 15 000 to 45 000 and Re_i ranging from 20 000 to 40 000. The figure's scale is too small to make any conclusions and for that reason Figure 6-15 (b) is included to show more detail regarding the spread of the data from approximately Reynolds number values between 40 000 and 45 000.

The Nu_{Dh} results shown had an average uncertainty of 1.75%, which is shown in Figure 6-15 (b) as error bars. It is clear that the test runs at different Re_i produced a scatter of data, but the scatter was still well within the uncertainty margin. It is the opinion of the author that the scatter can be attributed to the inability to have exact repetition on the inlet temperatures and Re_{Dh}.

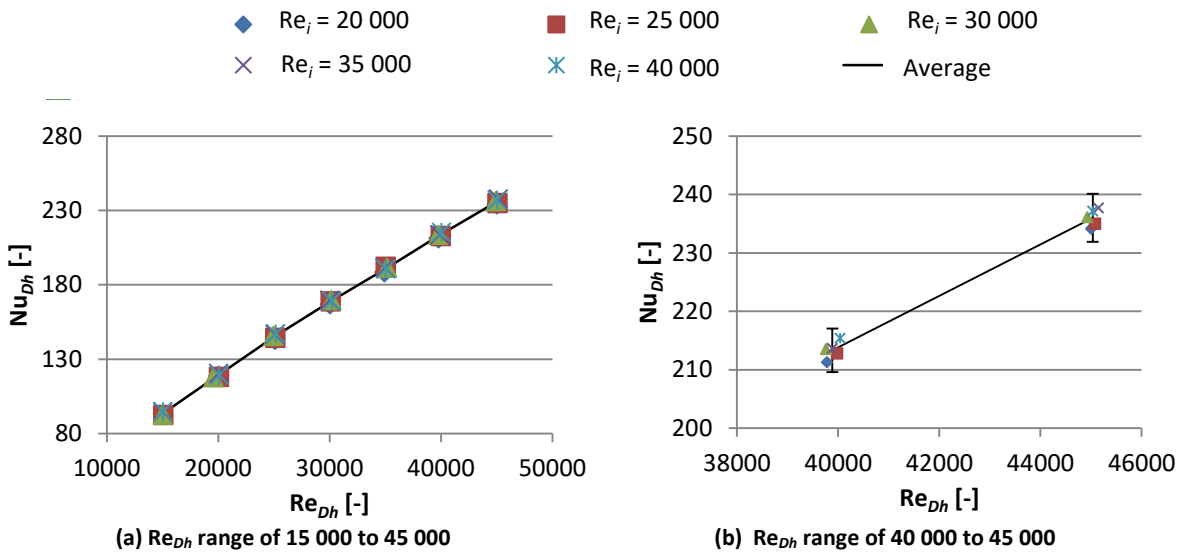

Figure 6-15: Nusselt number against Re$_{Dh}$ for 0.386 test section at 50°C inlet temperature, showing effect of different Re$_i$.

Considering the effect of different Re$_i$ on local Nusselt number results, Figure 6-16 illustrates the test set for the 0.386 test section for case C50 at a Re$_{Dh}$ value of 45 000 (as before, $x/L = 0$ represent the inlet). It is deduced that the rate at which Nu$_{local}$ changes along the annular length is dependent on the Re_i (via the inner wall temperature). As the Re$_i$ increases, the local development rate decreases. It is seen that the Re$_i$ of 20 000 had the highest Nusselt number at the entrance of the test section, but the lowest value at the end of the section. This resulted in a very similar average Nusselt number across the length of the test section for the different Re$_i$.

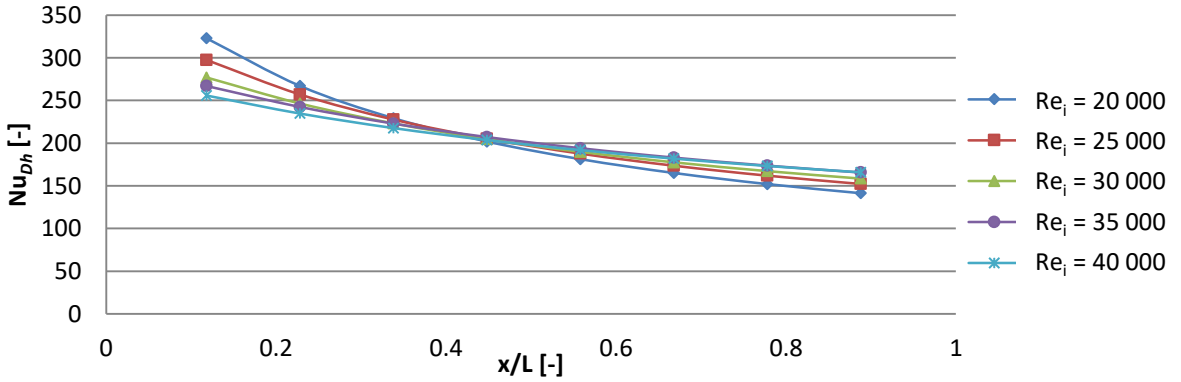

Figure 6-16: Local Nusselt number along the length of the 0.386 test section (50°C inlet temperature, a Re$_{Dh}$ = 45 000) at different Re$_i$.

This seems to imply that the rate at which Nusselt number develop is not only dependent on inlet temperatures for the inner tube and annulus, Re$_{Dh}$ and annular diameter ratio, but also on Re$_i$ (which indirectly affects the steady state wall temperature on the inner annular wall) and possibly flow passage length. Based on the available data it is unclear what the reasons are for this phenomenon. It was noticed that as the Re$_i$ increased the rate at which Nusselt number develop flattened out more. It can thus be possible that if a high enough Re$_i$ is reached that the curve would be almost completely horizontal.

6.7 Annular Diameter Ratio influence

Works by some researchers have suggested that the annular diameter ratio has an influence on the heat transfer coefficient and the friction factor of a test section (Chapter 2.2). This section will compare and discuss the results for Nusselt number, Colburn *j*-factor and friction factor over the annular diameter range tested, namely 0.327, 0.386, 0.409 and 0.483. Each of the figures in this section depicts the effect of different inlet temperature cases, Re_{Dh} and annular diameter ratios on the results.

The 0.409 test section was the first test section on which tests were conducted. Due to unfamiliar conditions, equipment and procedures, the author believes that the results from this test section might not be as reliable as that of the others.

6.7.1 Nusselt number

The effect of the annular diameter ratio, *a*, on the average Nusselt number is displayed in Figure 6-17 by trending the percentage change in Nu_{Dh} from the test section with *a* of 0.327 to the other three test sections. The H20 case for *a* of 0.409 was an outlier which varied between -11% to -36% and was subsequently left out to make the rest of the graph more legible. The reason for the large difference in the values for this particular case is unknown, but comparing its data with the rest of the data, it seems as if the data for the 0.409 section is out of proportion. It is noticed that except for the H20 case, there was less than 8% difference in the recorded Nusselt number over the *a* range (average uncertainty 2.3%).

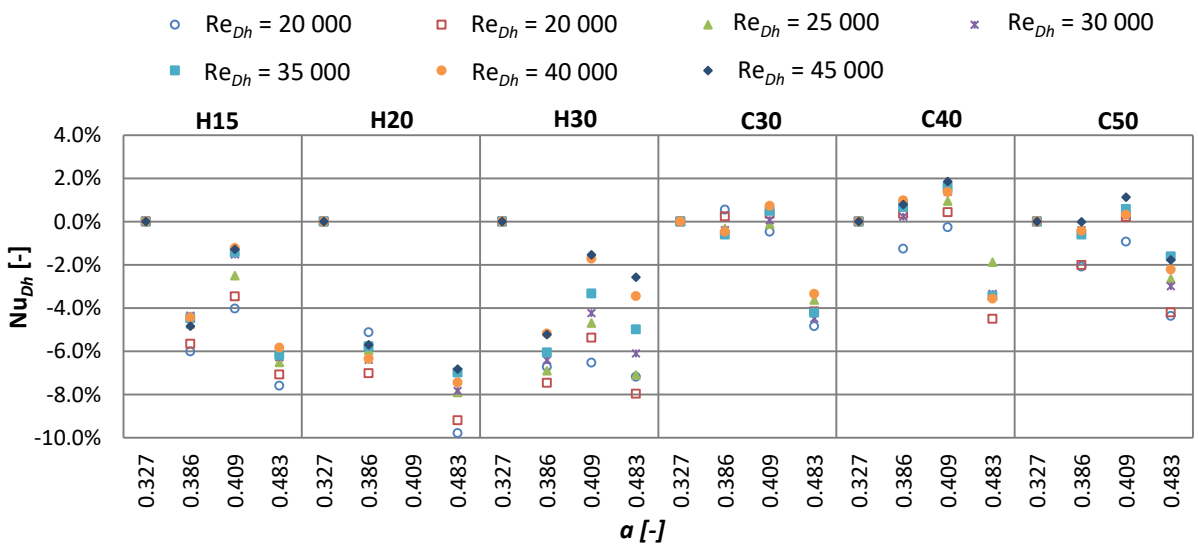

Figure 6-17: Nusselt number % variation for different *a* compared to 0.327 value.

If the 0.409 section is not considered, it is noted that the results indicates a decrease in Nu_{Dh} as the *a* increases. The difference in Nu_{Dh} compared to the 0.327 section was more for a Re_{Dh} of 15 000 than for 45 000. For the H15 case the Nu_{Dh} reduces by up to 7.6% as the *a* increases from 0.327 to 0.483 (at Re_{Dh} of 15 000), which increases to 9.8% for the H20 case. For the C50 case the Nu_{Dh} reduces by 4.4% considering the 0.483 section (which is beyond the uncertainty band of 2.3%). At Re_{Dh} of 35 000 to 45 000 the influence of the change in Nu_{Dh} is maximum 7.4% for H20 case. It

seems that the *a* does have a small influence on the Nu_{Dh}, leading to a decrease as the *a* increases. For heated annuli the effect is greater than for cooled annuli.

6.7.2 Colburn *j*-factor

As mentioned, the Colburn *j*-factor is a function of the Nusselt number, Reynolds number and Prandtl number, calculated at the bulk annular temperature.

Figure 6-18 illustrates the *j*-factor results for a range of inlet temperature cases and Re_{Dh} over different *a*. It is seen that the influence of the *a* on the *j*-factor increases as the Re_{Dh} decrease. As with the Nu_{Dh} an increase in *a* seem to influence the *j*-factor more at cooler annular inlet temperatures. If the values for the 0.409 section was to be disregarded, there seem to be an increase in difference from the 0.327 section as the *a* increased. But considering Table 5-5 it is noted that the 0.483 section has an average calculation uncertainty of 3.0%, compared to uncertainties of 2.4%, 2.5% and 2.6% for the 0.327, 0.386 and 0.409 sections. The maximum variation in the *j*-factor was a reduction of 8.1% for case H30 and *a* of 0.483.

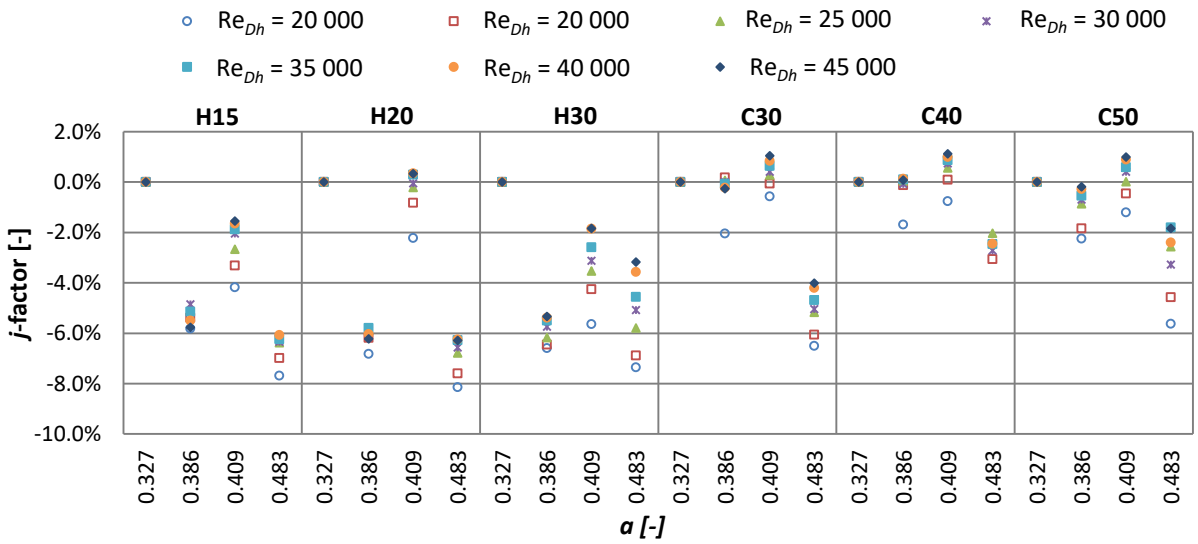

Figure 6-18: Colburn *j*-factors % variation for different *a* compared to 0.327 value.

In Section 6.3.2 an adjusted *j*-factor was introduced where the exponent *p* was changed from 0.33 to 0.542. This resulted in Figure 6-6 where the curves of different inlet temperatures almost fell onto a single line, indicating that the inlet temperature had little effect. Recreating Figure 6-18 with the adjusted *j*-factor however resulted in a very similar figure (shown in Figure 6-19) with only a small reduction in the differences as result of different annular ratios on the values.

Considering Figure 6-18 and Figure 6-19, it can be concluded that there seem to be a trend where the Colburn *j*-factor is influenced by the annular diameter ratio of the test section, having smaller values as *a* increases (increased difference from 0.327 section).

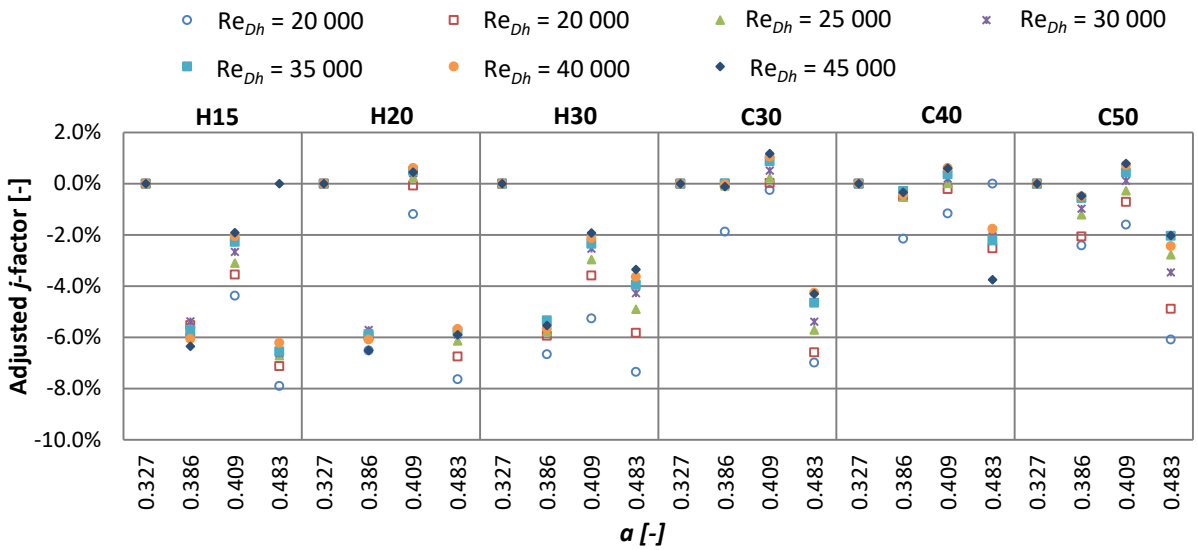

Figure 6-19: Adjusted Colburn j-factors % variation for different *a* compared to 0.327 value.

6.7.3 Friction factor

The friction factor proved more difficult to measure accurately and it is suspected that it was influenced by a variance in calibration of the different pressure transducers used. The author does not feel comfortable with the results for the friction factor and would not base any concrete conclusions on these results.

In Figure 6-20 it is clear that the friction factor for the annular diameter ratio of 0.409 had a much larger band between different Re_{Dh} than for the other annular diameter ratios, especially for inlet temperature cases H20, C40 and C50 (up to 540% difference). Heated cases also exhibited a large spread with differences of more than 100%.

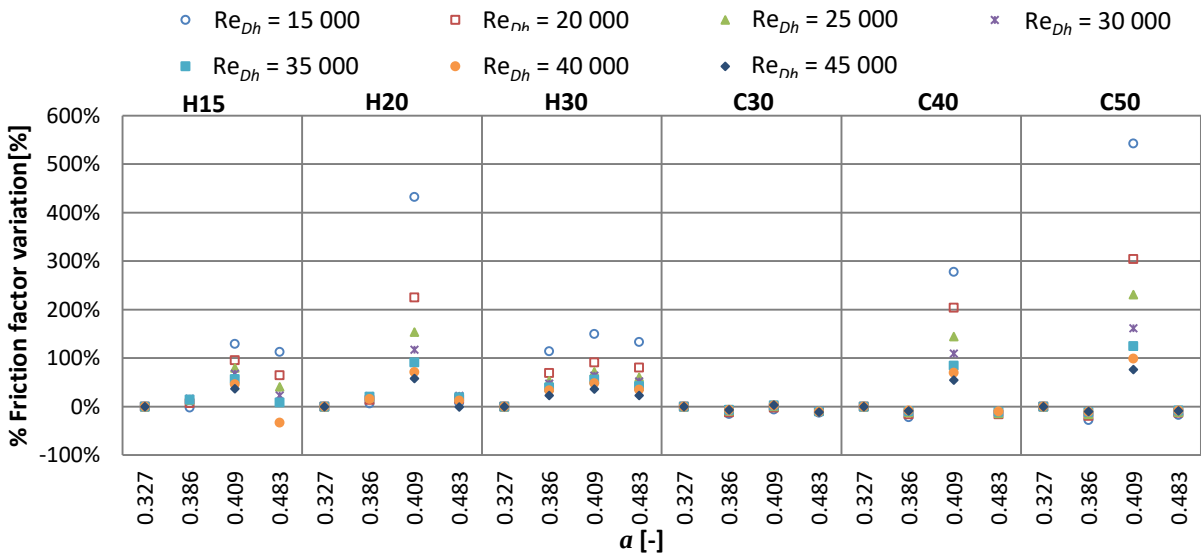

Figure 6-20: Friction factor % variation for different *a* compared to 0.327 value.

In order to get a better visual on the effect of different *a*, Figure 6-21 considers only the cooling cases and disregards the outliers for the 0.409 test cases. It is difficult to determine with certainty whether there is a pattern in the effect of different inlet temperatures and annular diameter ratios on the friction factor. It could be argued that the friction factor was not affected by the annular diameter ratio, but rather decreasing as the Re_{Dh} increased.

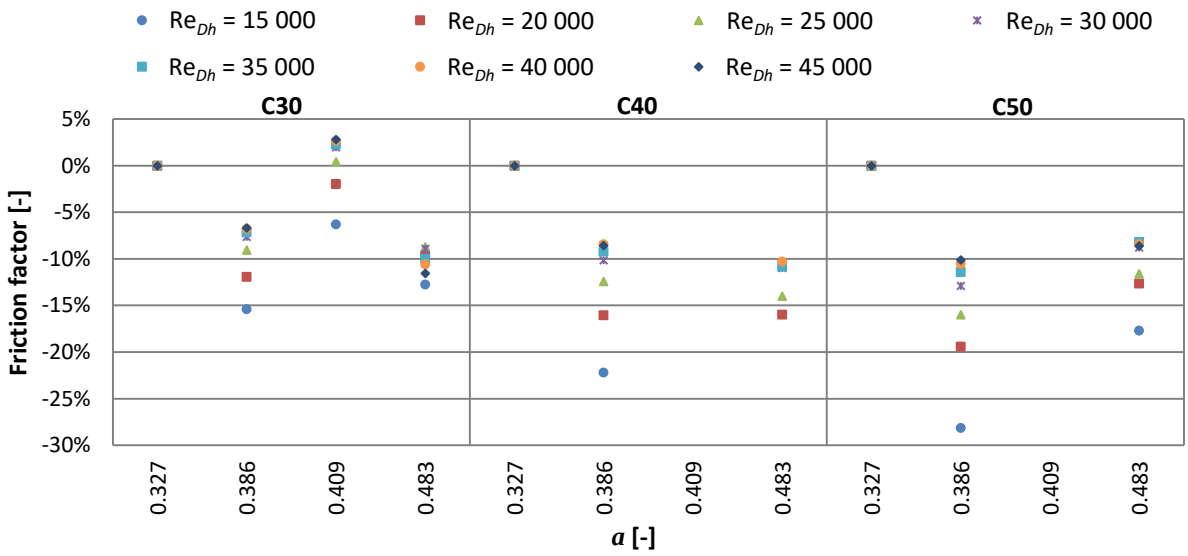

Figure 6-21: Friction factor % variation for different *a* compared to 0.327 value, cleaned up.

6.8 Results Summary

The average Nusselt number over the length of the test section compared well with existing correlations, falling on average within 15.8% and 10.2% from predictions by Dirker & Meyer and Gnielinski, but there was no single correlation that could predict the Nusselt number accurately at any given Re_{Dh}. The existing correlations also seemed sensitive to the direction of heat transfer.

Different annular fluid inlet temperatures did have an influence on the average heat transfer coefficient, with lower inlet temperatures having larger Nusselt numbers and *j*-factors. At high Re_{Dh} the inlet temperature did not seem to have an effect on the friction factor, but the direction of heat transfer did have an influence resulting in higher friction factors for cooled annuli.

Local Nusselt number analysis proved that larger heat transfer coefficients existed at the entrance of the test section compared to the exit. The heated annulus had much larger Nusselt numbers at the entrance of the section than the cooled annulus, even though both had about similar Nusselt numbers at the exit. The decay of heat transfer along the length of the heat exchanger suggests however that the assumption of fully developed flow was false and that in fact the local heat transfer was a function of the distance along the heat exchanger.

The effect of the heat transfer direction was considered by comparing results for heated and cooled annuli cases, both with annular inlet temperature of 30°C. It was found that the heat transfer direction did not have a significant effect on the average heat transfer coefficient. Differences in the heat transfer coefficient in the heated and cooled cases could be attributed to small differences

in the annular fluid inlet temperature. Analysing the local Nusselt numbers did prove that there is a difference in the magnitude of heat transferred across the length of the heat exchanger. Cooler fluid temperature case (the heated cases in this study) tended to have higher heat transfer coefficients close to the entrance of the test section. Thus, it seems that if a short test section was to be considered, it would be advantageous to operate it as a heated annulus if the application allows for it.

The inner tube Reynolds number has some effect on the average Nusselt number, but these effects fall within the experimental uncertainty and can be discarded. For local Nusselt number analysis the Re_i has an influence on the rate at which Nusselt number develop, which was dependent on the distance from the test section entrance. It was noticed that as the Re_i increased the rate at which Nusselt number develop flattened out more, which leads one to think that it can thus be possible that if a high enough Re_i is reached that the curve would be almost completely horizontal.

It was found that the annular diameter ratio did not appear to have a clear impact on the average Nusselt number, especially in the Re_{Dh} range of 35 000 to 45 000. The difference in Nu_{Dh} between the annular diameter ratios differed with each annular inlet temperature case, making it difficult to identify any trends. The biggest difference was 9.8% smaller at the H20 case, but this fell within 5.2% for the cooled cases.

The Colburn *j*-factor had variances of up to 8.1% smaller when different annular diameter ratios were compared, which was within the limits of the uncertainty. Comparing the values for the adjusted *j*-factor produced a very similar figure with slightly lower differences between the different annular diameter ratios. It can be argued that there seems to be a trend where the Colburn *j*-factor is influenced by the annular diameter ratio of the test section, having smaller values as *a* increases (increased difference from 0.327 section).

Due to difficulty of pressure drop measurement, the friction factor results were not clear cut, but it could be concluded that the annular diameter ratio had very little effect, if any, on the friction factor calculated for the annulus.

CHAPTER 7 - SUMMARY AND CONCLUSIONS

7.1 Conclusions

Four test sections were successfully constructed and used to conduct experiments where the effect of the inlet temperature, direction of heat transfer, fluid velocity and different annular diameter could be tested. Novel construction methods allowed the capture of accurate data, which had reasonable agreement with predictions from literature.

Analysis of the data gave insight to the effect of above-mentioned variables and it was concluded that the heat transfer direction and annular diameter ratio has minute effects on average heat transfer coefficient. Local analysis proofed that the heat transfer coefficient did not remain constant throughout the length of the heat exchanger, suggesting that fully thermal developed flow was not reached. This indicated that the hypothesis assumption that fully developed thermal flow existed in parts of the heat exchanger was incorrect.

Next follows a summary of the important findings and contributions from this study.

7.2 Summary of findings

- Experimentally produced results could be validated with existing correlations, verifying the accuracy and usefulness of the data collected.
- The combined effect of the thermocouple being embedded into the inner tube wall and the *in-situ* calibration has increased the ability to capture accurate temperature data for flow in a smooth concentric annulus.
- Lower annular fluid inlet temperatures resulted in larger Nusselt numbers and *j*-factors. At lower Re_{Dh} cooler inlet temperatures resulted in higher friction factors, but at high Re_{Dh} the inlet temperature did not seem to have an effect on the friction factor.
- Local analysis proved that the heat transfer coefficient decays along the length of the heat exchanger, suggesting fully developed thermal flow was not reached, proving the hypothesis that fully developed thermal flow existed was incorrect. Furthermore it showed that the heated annulus had much larger Nusselt numbers at the entrance of the section than the cooled annulus, even though both had about similar Nusselt numbers at the exit. This reflects the larger average Nusselt numbers reported earlier for the heated annuli cases compared to the cooled annuli cases.
- The direction of heat transfer was found not to have an effect on the average heat transfer coefficient. Instead the test case with the marginally larger annular inlet temperature resulted in a larger average Nusselt number.
- The Reynolds number in the inner tube has a minute effect on the average Nusselt number, but it seems the rate at which local Nusselt number develop along the test section length is not only dependent on inlet temperatures for the inner tube and annulus, Re_{Dh} and annular diameter ratio, but also on Re_i and possibly tube length.
- It seems that the annular diameter ratio does have an influence on the Nu_{Dh}, leading to a decrease in the Nu_{Dh} as the *a* increases. For heated annuli the effect was greater than for cooled

annuli, having an average of 7.8% and 3.1% decrease consecutively in Nu_{Dh} as a increased from 0.327 to 0.486.

- The j-factor showed no variance greater than its calculation uncertainty band with a change in the annular diameter ratio. But a similar trend as to the Nu_{Dh} was witnessed with maximum difference of 8% smaller. Examining the change in the adjusted j-factor again proofed similar results, but with slightly smaller changes.
- It seemed that the friction factor was not influenced by the annular diameter ratio, but rather by the flow velocities.

7.3 Summary of contributions

- A methodology was developed to construct long tube-in-tube heat exchanger test sections in a way that minimised the geometric effects on the fluid mechanics and heat transfer properties of the annular flow.
- A method was developed to obtain more reliable local wall temperature measurements on the outer tube and inner tube of the heat exchanger.
- The effects of different flow velocities, the inlet temperatures of the fluid in the annuli and the heat flux directions on the heat transfer and friction factor were tested.
- An extensive data-set was produced that will allow for more in-depth analysis and possible future heat transfer correlation development.
- Results were obtained that indicate that heat transfer direction and annular diameter ratio has relatively small effects on average heat transfer coefficient.
- It is shown that heat transfer coefficient do not remain constant throughout the length of the heat exchanger for the thermal boundary condition considered in this study (not fully uniform heat flux, nor fully uniform wall temperature). This is an indication that fully developed thermal flow was not reached.

BIBLIOGRAPHY

1. Hansen, H., *Heat Transfer in Counterflow, Parallel Flow and Cross Flow*. 1976, New York: McGraw-Hill.
2. Cengel, Y.A., *Heat and Mass Transfer: A Practical Approach*. 3rd ed. 2006, New York: McGraw-Hill.
3. Sieder, E.N. and G.E. Tate, *Heat Transfer and Pressure Drop of Liquids in Tubes.* Industrial and Chemical Engineering, 1936. 28: p. 1429-1436.
4. Dirker, J. and J.P. Meyer, *Convective Heat Transfer Coefficients in Concentric Annuli.* Heat Transfer Engineering, 2005. 26(2): p. 38-44.
5. Davis, E.S., *Heat transfer and pressure drop in annuli.* Transactions of ACME, 1943. Oct: p. 755-760.
6. Foust, A.S. and G.A. Christian, *Non_Boiling Heat Transfer Coefficients in Annuli.* American Institute of Chemical Engineers, 1940. 36: p. 541.
7. Dittus, F.W. and L.M.K. Boelter, *Heat Transfer in Automobile Radiators of the Tubular Type.* University of California Publications in Engineering, 1930. 2(13): p. 443-461.
8. VanZyl, W.R., J. Dirker, and J.P. Meyer, *Single-Phase Convective Heat Transfer and Pressure Drop Coefficients in Concentric Annuli.* Heat Transfer Engineering, 2013. 34(13): p. 1112-1123.
9. Briggs, D.E. and E.H. Young, *Modified Wilson Plot Technique for Obtaining Heat Transfer Correlations for Shell and Tube Heat Exchangers.* Chemical Engineering Progress Symposium, 1969. 65: p. 35-45.
10. Swamee, P.K., N. Aggarwal, and V. Aggarwal, *Optimum design of double pipe heat exchanger.* International Journal of Heat and Mass Transfer, 2008. 51(9-10): p. 2260-2266.
11. Lu, G. and J. Wang, *Experimental investigation on heat transfer characteristics of water flow in a narrow annulus.* Applied Thermal Engineering, 2008. 28(1): p. 8-13.
12. Kim, W.K., H. Martin, and V. Gnielinski, *Pressure drop and heat transfer in shell-and-tube heat exhangers without baffles Part I. The graetz-nusselt problem in a cylindrical shell containing a bundle of seven tubes.* Chemical Engineering and Processing: Process Intensification, 1993. 32(2): p. 99-110.
13. Gnielinski, V., *Heat Transfer Coefficients for Turbulent Flow in Concentric Annular Ducts.* Heat Transfer Engineering, 2009. 30(6): p. 431-436.
14. Monrad, C.C. and J.F. Pelton, *Heat Transfer by Convection in Annular Spaces.* American Institute of Chemical Engineers, 1942. 38: p. 593-611.
15. Wiegard, J.H., E.L. McMillen, and R.E. Larson, *Annular Heat Transfer Coefficients for Turbulen Flow.* American Institute of Chemical Engineers, 1945. 41: p. 147-153.
16. Kays, L.M. and E.Y. Leung, *Heat Transfer in Annular Passages - Hydrodynamically Developed Turbulent Flow with Arbitrarily Prescribed Heat Flux.* International Journal of Heat and Mass Transfer, 1963. 6: p. 537-557.
17. Petukhov, B.S. and L.I. Roizen, *General Relationships for Heat Transfer in Turbulent Flow of a Gas in Tubes of Annular Section.* High Temperature, 1964. 2: p. 65-68.
18. Stein, R.P. and W. Begell, *Heat Transfer to Water in Turbulent Flow in Internally Heated Annuli.* American Institute of Chemical Engineers, 1958. 4(2): p. 127-131.
19. Crookston, R.B., R.R. Rothfus, and R.I. Kermode, *Turbulent Heat Transfer In Annuli With Small Cores.* International Journal of Heat and Mass Transfer, 1968. 11: p. 415-426.
20. Hager, W.H., *Blasius: A life in research and education.* Experiments in Fluids, 2003. 34: p. 566-571.
21. Quarby, A., *An Experimental Study of Turbulant Flow through Concentric Annuli.* International Journal of Mechanical Engineering Science, 1967. 9: p. 205-221.
22. Rothfus, R.R., et al., *Isothermal Skin Friction in Flow throh Annular Sections.* Industrial and Chemical Engineering, 1955. Engineering Design and Process Development(913-918).
23. Lee, Y. and H. Barrow, Proc. Inst. Mech. Engrs., 1964. 178: p. 1.
24. Brighton, J.A. and J.D. Jones, Trans. Am. Soc. mech. Engrs, 1964. 86: p. 835.

25. Jonsson, V.K. and E.M. Sparrow, *Experiments on turbulent-flow phenomena in eccentric annular ducts.* Fluid Mechanics, 1966. 25(1): p. 65-85.
26. Jones, O.C. and J.C.M. Leung, *An Improvement in the Calculation of Turbulent Friction in Smooth Concentric Annuli.* Journal of Fluids Engineering, 1981. 103: p. 615-623.
27. Meter, D.M. and R.B. Bird, *Turbulent Newtonian Flow in Annuli.* AIChE Hournal, 1961. 7: p. 41-45.
28. Rothfus, R.R., C.C. Monrad, and V.E. Senecal, *Velocity Distribution and Fluid Friction in Smooth Concentric Annuli.* Ind. Eng. Chem., 1950. 42: p. 2511-2520.
29. Kaneda, M., et al., *The characteristics of turbulent flow and convection in concentric circular annuli.* International Journal of Heat and Mass Transfer, 2003. 46: p. 5045-5057.
30. Rayle, R.E., *Influence of orifice geometry on static pressure measurements.* ASME, 1959. Paper No. 59-A-234.
31. Armacell. *AP Armaflex® & AP Armaflex W Tube Insulation*. www.armacell.us 2011 7 May 2013].
32. A.C.E.O.T., *Manual on the use of thermocouples in temperature measurement*. 4 ed. 1993: ASTM International.
33. Weisstein, E.W. *Least Squares Fitting--Exponential*. 6 November 2013 [cited 2013 3 September]; Available from: http://mathworld.wolfram.com/LeastSquaresFittingExponential.html.
34. Popiel, C.O. and J. Wojtkowiak, *Simple Formulas for Thermophysical Properties of Liquid Water for Heat Transfer Calculations (from 0°C to 150°C).* Heat Transfer Engineering, 1998. 19(3): p. 87-101.
35. Kakac, S., *The Effect of Temperature-Dependent Fluid Properties on Convective Heat Transfer*, in *Handbook of Single-Phase Convective Heat Transfer*. 1987, John Wiley & Sons.
36. Kline, S. and F. McClintock, *Describing uncertainties in single-sample experiments.* Mechanical Engineering, 1953. 75: p. 2-8.
37. Frank P. Incropera, D.P.D., *Introduction to Heat Transfer*. Third ed. 1996, New York: Wiley.
38. Dunn, P.F., *Measurement and Data Analysis for Engineering Science*. 2nd ed. 2010: CRC Press.

APPENDIX A – UNCERTAINTY ANALYSIS

The contribution of individual sources of error to the overall uncertainty was tracked to understand which equipment, temperature properties or parts of equations had the biggest influence on the uncertainty of the calculated heat transfer coefficient and friction factor. This appendix gives an in-depth methodology used to determine the relevant uncertainties.

Uncertainty Theory

Experimental or measurement uncertainties are inherent in data acquisition and calibration. Numerical uncertainties can also exist in the analysis stage, according to Dunn [38]. Errors that arise in the measurement process can be categorised into bias (systematic) and random (precision) errors. These are shown in Figure A-1 and are discussed below.

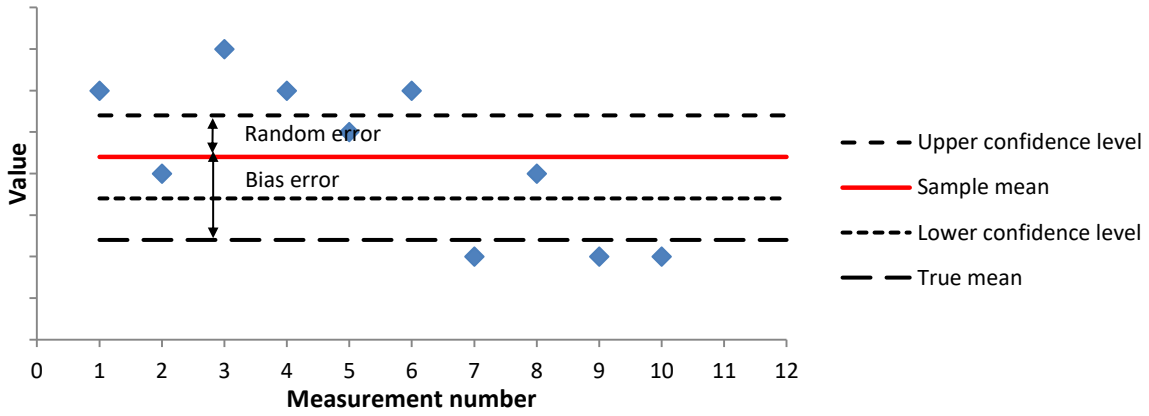

Figure A-1: Description of error types.

Bias errors can be defined as the difference between the true mean value and the sample mean value (accuracy) and lacks any statistical information. Bias errors can usually be minimized through calibration. On the other hand, experiments have *random* errors resulting from a large number of very small, uncontrollable effects that are independent of one another and individually influence the measured value. These errors result in scatter in data produced under fixed conditions and is an indication of the repeatability, or precision, of the measurement. The random error is defined as the difference between the confidence level, either upper or lower, and the sample mean value. Random errors cannot be minimized by calibration, but can be reduced by repeated measurements and the careful control of conditions.

A result, according to Dunn [38], is defined as a variable that is not measured but which is a function of measured variables, called *measurands*. Each measurand consists of the measured value, the measuring equipment's *bias* and the *random uncertainty* in the measurement. According to method of Kline and McClintlock [36], the combination of the bias and random error results in the uncertainty δx_i of the measurement, described as:

$$\delta x_i = \delta x_{i,bias} + \delta x_{i,random}$$

The result of a measurand can thus be mathematically described as:

$$x_i = x_i(measured) \pm \delta x_i(95\%\, confidence)$$

where the actual value will lie somewhere between $x_i - \delta x_i$ and $x_i + \delta x_i$ with a 95% confidence level. The measured value x_i will either be the measurement in a single sample or the mean of the data set for a multi-sample experiment.

When considering a multi-variable parameter, it is important to understand that the uncertainty of the parameter is due to the propagation of the uncertainties of each of its dependent variables. By applying the method described by Kline and McClintock [36], the combined uncertainty range (δR) of a parameter $f(x_1, x_2, \dots, x_n)$ is based on the uncertainties of each of its dependent variables $(x_1, x_2, \dots, x_n)$ and is computed by

$$\delta R = \left\{ \sum_{i=0}^{n} \left(\frac{\partial R}{\partial x_i} \delta x_i \right)^2 \right\}^{0.5}$$

It is important that all uncertainties must have the same units as the variable under investigation. By following this method the individual contribution from each error source is calculated. This enables one to conduct a sensitivity analysis when needed.

Quantifying Uncertainty

In this section the mathematical model used to determine the uncertainty contribution of each parameter used in the analysis of the heat transfer is given. The uncertainties can be grouped into single variable results, dependent only on the bias of the measuring equipment and the random error, and multi-variable results where the total uncertainty is dependent on the propagation of individual parameter and calculation errors.

Single Variable Results

Single variable results are dependent only on the uncertainty for the measurement and include the equipment bias and measurement uncertainty (precision). The results for the thermocouples, Coriolis flow meters, pressure transducers and the dimensions of components are single variable results.

According to the method of Kline and McClintock [36], the precision of single variable results were obtained by taking the standard deviation of a 200 point data set and multiplied by two to fall within a 95% confidence interval. More information on the method of calculating the uncertainty of each measuring device follows below.

***Thermocouples*:**
To reduce the uncertainty (random error) in the measurement of temperature at a certain point, more than one thermocouple was used: the entry and exit ports of the inner tube and annulus each had 4 thermocouples, while the inner tube and annular walls each had 2 thermocouples at a measuring station. The precision for each of these measuring stations was thus calculated by

$$\delta x_{i,random} = 2 \times \frac{\sigma_{avg}}{\sqrt{N}}$$

where N is the number of thermocouples at a station and σ_{avg} is the standard deviation of the averaged data set of N number of data sets for the measuring station. The results for the inlet/outlet port and tube wall uncertainty measurements are shown in Table A-2.

***Coriolis flow meters**:*

The uncertainties for the Coriolis flow meters had a bias and precision provided by the original manufacturer, given in the equation below. All the flow meters had a bias of 0.1% full range, but the precision was to be calculated as shown below, where the zero stability is available in Table A-1.

$$\delta Flow\ meter = \pm\left[\left(\frac{zero\ stability}{flow\ rate\ [kg/h]}\right) \times 100\right] \%\ of\ rate$$

Table A-1: Zero stability value as provided by manufacturer.

Model	Zero Stability
CMF025	0.027
CMF050	0.163
CMF100	0.680

As the precision of the flow meters was flow dependent, the uncertainty could not be calculated and tabulated here. It was, however, noted that the precision error would be a minimum at maximum flow rate.

Pressure transducers:

The three pressure transducers each had a bias of 0.25% full scale and the precision was determined from recorded data using the method proposed by Dunn. Results are shown in Table A-2.

Dimension errors:

The measurement of the tube diameters had an uncertainty of 0.02 mm and for the tube length measurements the uncertainty was 1 mm.

Table A-2: Uncertainty of measurement equipment.

Instrument	Range	Bias	Precision	Uncertainty
Thermocouple stations				
Inlet / Outlet port	-200°C – 350°C	0.1°C	0.0069°C	0.11°C
Inner / Outer tube wall	-200°C – 350°C	0.1°C		

Coriolis flow meters				
CMF025	0 – 0.607 kg/s	0.10% full scale	Flow rate dependent	
CMF050	0 – 1.833 kg/s	0.10% full scale	Flow rate dependent	
CMF100	0.694 – 5.55 kg/s	0.10% full scale	Flow rate dependent	
Pressure transducers				
	0 – 14 kPa	0.25% full scale	0.013 kPa	0.048 kPa
	0 – 22 kPa	0.25% full scale	0.031 kPa	0.086 kPa
	0 – 55 kPa	0.25% full scale	0.107 kPa	0.245 kPa

Multi Variable Results

Multi variable results are present when there are more than one source of uncertainty. The result is then influenced by different sources of uncertainty, each with a different factor of intensity. Multi variable results include calculated results where the uncertainty is dependent on the individual uncertainties of each measured parameter as well as the inherent uncertainty in the calculation itself.

Temperature dependent properties:

Temperature dependent properties where computed by using the method of Popiel and Wojtkowiak [34]. The authors stated the uncertainties for each property as a percentage error of the value obtained and is given in Table A-3. The uncertainty contribution of each property was computed as follows:

$$\delta C_p = (\%error) C_p$$
$$\delta \rho = (\%error) \rho$$
$$\delta k = (\%error) k$$
$$\delta \mu = (\%error) \mu$$
$$\delta \mathrm{Pr} = (\%error) \mathrm{Pr}$$

Table A-3: Uncertainties of temperature-dependent fluid properties.

Entity	Range	Uncertainty
Conductivity, k	0°C – 150°C	2.00%
Density, ρ	0°C – 150°C	0.002% – 0.004%
Prandtl number, Pr	0°C – 150°C	2.30%
Specific heat, c_p	0°C – 150°C	0.06%
Viscosity, μ	0°C – 150°C	1.00%

Hydraulic diameter:

The uncertainty of the hydraulic diameter was computed by applying the formula:

$$(\delta R)\ of\ D_h = D_0 - D_1$$

$$\delta D_h = \{(\delta D_0)^2 + (-\delta D_1)^2\}^{\frac{1}{2}}$$

It was stated that the measurement uncertainty for diameters was 0.02 mm, resulting in

$$\delta D_h = \{0.02^2 + 0.02^2\}^{\frac{1}{2}} = 0.0283\ mm = 0.0000283\ m$$

Area calculation uncertainty:

The uncertainty for the heat transfer area of the inner wall of the inner tube was computed by:

$$(\delta R)\ of\ A_{w,i} = \pi L_{hx} D_i$$

$$\delta A_{w,i} = \{(\pi L_{hx}\delta D_i)^2 + (\pi D_i \delta L_{hx}\}^{\frac{1}{2}}$$

For the outer wall heat transfer area of the inner tube the calculated uncertainty was

$$(\delta R)\ of\ A_{wo} = \pi L_{hx} D_1$$

$$\delta A_{w,o} = \{(\pi L_{hx}\delta D_1)^2 + (\pi D_1 \delta L_{hx}\}^{\frac{1}{2}}$$

The contribution of the uncertainty in the cross sectional area calculation for the inner tube was

$$(\delta R)\ of\ A_{c,i} = \frac{\pi}{4} D_i^2$$

$$\delta A_{c,i} = \frac{\pi}{2} D_i \delta D_i = \frac{\pi}{2} D_i \times 0.02\ mm$$

Uncertainty in the calculation of the annular section's cross sectional area was

$$(\delta R)\ of\ A_{c,o} = \frac{\pi}{4}(D_o^2 - D_1^2)$$

$$\delta A_{c,o} = \left\{\left(\frac{\pi}{2} D_o \delta D_o\right)^2 + \left(-\frac{\pi}{2} D_1 \delta D_1\right)^2\right\}^{\frac{1}{2}}$$

Bulk temperature results:

The resulting uncertainty in the bulk temperature, which was the average of the inlet and outlet temperatures, was calculated by:

$$(\delta R)\ of\ \bar{T}_b = \frac{(T_{oi} + T_{oo})}{2}$$

$$\delta \bar{T}_b = \left\{\left(\frac{1 + T_{oo}}{2}\delta T_{oi}\right)^2 + \left(\frac{1 + T_{oi}}{2}\delta T_{oo}\right)^2\right\}^{\frac{1}{2}}$$

Local temperature results:

In the local heat transfer analysis curve fits were used to determine the value of the annular wall temperatures at any point along the tube. The measured error connected to a calculated temperature was computed by taking the standard deviation of the curve fit to the measured values and dividing it by the square root of the number of measuring points, as shown:

$$\delta T_{local} = \frac{\sigma}{\sqrt{n}}$$

The standard deviation of the curve fit to the measured values was given by the Microsoft Excel function "Linest".

Logarithmic mean temperature difference:

The logarithmic mean temperature difference for the annulus was calculated as

$$\Delta T_{LMTD} = \frac{(\overline{T}_{iw} - T_{oi}) - (\overline{T}_{iw} - T_{oo})}{ln\left[\frac{(\overline{T}_{iw} - T_{oi})}{(\overline{T}_{iw} - T_{oo})}\right]} = \frac{(T_{oo} - T_{oi})}{ln\left[\frac{(\overline{T}_{iw} - T_{oi})}{(\overline{T}_{iw} - T_{oo})}\right]}$$

For this the uncertainty was dependent on the inlet and outlet temperatures of the annulus, the average inner tube wall temperatures and the individual uncertainties of the mentioned temperatures. The uncertainty was calculated by:

$$\delta\Delta T_{LMTD} = \left[\begin{array}{l} \left(\left\{\frac{1}{ln\left[\frac{(\overline{T}_{iw}-T_{oi})}{(\overline{T}_{iw}-T_{oo})}\right]} - \frac{(T_{oo}-T_{oi})\frac{(\overline{T}_{iw}-T_{oo})}{(\overline{T}_{iw}-T_{oi})}\frac{(\overline{T}_{iw}-T_{oi})}{(\overline{T}_{iw}-T_{oo})^2}}{\left(ln\left[\frac{(\overline{T}_{iw}-T_{oi})}{(\overline{T}_{iw}-T_{oo})}\right]\right)^2}\right\}\delta T_{oo}\right)^2 \\ + \left(\left\{\frac{-1}{ln\left[\frac{(\overline{T}_{iw}-T_{oi})}{(\overline{T}_{iw}-T_{oo})}\right]} + \frac{(T_{oo}-T_{oi})\frac{(\overline{T}_{iw}-T_{oo})}{(\overline{T}_{iw}-T_{oi})(\overline{T}_{iw}-T_{oo})}}{\left(ln\left[\frac{(\overline{T}_{iw}-T_{oi})}{(\overline{T}_{iw}-T_{oo})}\right]\right)^2}\right\}\delta T_{oi}\right)^2 \\ + \left(\left\{\frac{(T_{oo}-T_{oi})\frac{(\overline{T}_{iw}-T_{oo})}{(\overline{T}_{iw}-T_{oi})}\frac{(T_{oi}-T_{oo})}{(\overline{T}_{iw}-T_{oo})^2}}{ln\left[\frac{(\overline{T}_{iw}-T_{oi})}{(\overline{T}_{iw}-T_{oo})}\right]^2}\right\}\delta\overline{T}_{iw}\right)^2 \end{array}\right]^{\frac{1}{2}}$$

Reynolds number:

The uncertainty calculations for the calculation of the inner tube and annular Reynolds numbers where of similar form with the variables varying between those for the inner tube and the ones for the annular section:

$$(\delta R)\ of\ \mathrm{Re}_{Dh} = \frac{\dot{m}_o D_h}{\mu_o A_o}\ \ and\ \ (\delta R)\ of\ \mathrm{Re}_i = \frac{\dot{m}_i D_i}{\mu_i A_i}$$

$$\delta\mathrm{Re}_{Dh} = \left\{\left(\frac{\delta\dot{m}_o\, D_h}{\mu_o A_o}\right)^2 + \left(\frac{\dot{m}_o\, \delta D_h}{\mu_o A_o}\right)^2 + \left(-\frac{\dot{m}_o\, D_h\, \delta A_o}{\mu_o A_o^2}\right)^2 + \left(-\frac{\dot{m}_o\, D_h\, \delta\mu_o}{\mu_o^2 A_o}\right)^2\right\}^{\frac{1}{2}}$$

$$\delta\mathrm{Re}_i = \left\{\left(\frac{\delta\dot{m}_i\, D_i}{\mu_i A_i}\right)^2 + \left(\frac{\dot{m}_i\, \delta D_i}{\mu_i A_i}\right)^2 + \left(-\frac{\dot{m}_i\, D_i\, \delta A_i}{\mu_i A_i^2}\right)^2 + \left(-\frac{\dot{m}_i\, D_i\, \delta\mu_i}{\mu_i^2 A_i}\right)^2\right\}^{\frac{1}{2}}$$

Heat transfer rate:

The heat transfer rate from the inner tube fluid to the inner tube wall was computed as

$$\dot{Q}_i = \dot{m}_i c_{p,i}(T_{ii} - T_{io}) = \dot{m}_i C_{p,i}\Delta T_i$$

The uncertainty in the (δR) form was computed by:

$$\delta \dot{Q}_i = \left\{ \left(\delta \dot{m}_\iota C_{p,i} \Delta T_i \right)^2 + \left(\dot{m}_i \delta C_{p,i} \Delta T_i \right)^2 + \left(\dot{m}_\iota C_{p,i} \delta \Delta T_i \right)^2 \right\}^{\frac{1}{2}}$$

The uncertainty for the heat transfer rate from the inner tube wall to the annulus fluid was calculated in the (δR) form by:

$$\delta \dot{Q}_o = \left\{ \left(\delta \dot{m}_o C_{p,o} \Delta T_o \right)^2 + \left(\dot{m}_i \delta C_{p,i} \Delta T_o \right)^2 + \left(\dot{m}_\iota C_{p,i} \delta \Delta T_o \right)^2 \right\}^{\frac{1}{2}}$$

Energy balance:

The energy balance had an implied uncertainty calculated with

$$(\delta R)\ of\ EB = \frac{\left| \dot{Q}_o - \bar{Q} \right|}{\bar{Q}}$$

$$\delta EB = \left\{ \left(\frac{1 - \bar{Q}}{\bar{Q}} \delta Q_o \right)^2 + \left(\frac{\bar{Q} \dot{Q}_o + \dot{Q}_o}{\bar{Q}^2} \delta \bar{Q} \right)^2 \right\}^{\frac{1}{2}}$$

where the average heat transfer had an uncertainty contribution given by:

$$\bar{Q} = \frac{\dot{Q}_i + \dot{Q}_o}{2}$$

$$\delta \bar{Q} = \left\{ \left(\frac{1 + \dot{Q}_o}{2} \delta \dot{Q}_i \right)^2 + \left(\frac{1 + \dot{Q}_\iota}{2} \delta \dot{Q}_o \right)^2 \right\}^{\frac{1}{2}}$$

Heat transfer coefficient:

The average heat transfer coefficient between the inner tube and annulus had an uncertainty calculated by:

$$\bar{h_\iota} = \frac{\dot{Q}_\iota}{A_{w,i}(\bar{T}_{b,i} - \bar{T}_{w,i})} = \frac{\dot{Q}_\iota}{A_{w,i} \Delta T}$$

$$\delta \bar{h_\iota} = \left\{ \left(\frac{\delta \dot{Q}_i}{A_{w,i} \Delta T} \right)^2 + \left(-\frac{\dot{Q}_\iota}{A_{w,i}^2 \Delta T} \delta A_{w,i} \right)^2 + \left(-\frac{\dot{Q}_i}{A_{w,i} \Delta T^2} \delta \Delta T \right)^2 \right\}^{\frac{1}{2}}$$

Nusselt number, j-factor and friction factor:

The uncertainty in the dimensionless Nusselt number for the annular section was computed using:

$$(\delta R)\ of\ Nu_{Dh} = \frac{h_o D_h}{k_o}$$

$$\delta Nu_{Dh} = \left\{ \left(\frac{\delta h_o D_h}{k_o} \right)^2 + \left(\frac{h_o \delta D_h}{k_o} \right)^2 + \left(-\frac{h_o D_h}{k_o^2} \delta k_o \right)^2 \right\}^{\frac{1}{2}}$$

The uncertainty in the calculation of the j-factor was calculated by:

$$(\delta R)\ of\ j = \frac{\mathrm{Nu}_{Dh}}{\mathrm{Re}_{Dh} \mathrm{Pr}_o^{\frac{1}{3}}}$$

$$\delta j = \left\{ \left(\frac{\delta \mathrm{Nu}_{Dh}}{\mathrm{Re}_{Dh}\mathrm{Pr_o}^{\frac{1}{3}}} \right)^2 + \left(-\frac{\mathrm{Nu}_{Dh}\delta \mathrm{Re}_{Dh}}{(\mathrm{Re}_{Dh})^2\mathrm{Pr_o}^{\frac{1}{3}}} \right)^2 + \left(-\frac{\mathrm{Nu}_{Dh}\delta \mathrm{Pr}_o}{3\mathrm{Re}_{Dh}(\mathrm{Pr}_o^{\frac{4}{3}})} \right)^2 \right\}^{\frac{1}{2}}$$

The friction factor uncertainty was calculated from:

$$(\delta R)\ of\ f = \frac{2D_h \Delta p}{\rho_o L_{dp} {V_o}^2}$$

$$\delta f = \left\{ \left(\frac{2D_h \delta \Delta p}{\rho_o L_{dp} {V_o}^2} \right)^2 + \left(\frac{2\,\delta D_h\ \Delta p}{\rho_o L_{dp} {V_o}^2} \right)^2 + \left(-\frac{2D_h \Delta p\ \delta \rho_o}{{\rho_o}^2 L_{dp} {V_o}^2} \right)^2 + \left(-\frac{2D_h \Delta p\ \delta L_{dp}}{\rho_o {L_{dp}}^2 {V_o}^2} \right)^2 + \left(-\frac{2D_h \Delta p\ \delta V_o}{\rho_o L_{dp} {V_o}^3} \right)^2 \right\}^{\frac{1}{2}}$$

where the uncertainty of the velocity used in the calculation was determined by:

$$(\delta R)\ of\ V_o = \frac{\dot{m}_o}{\rho_o A_o}$$

$$\delta V_o = \left\{ \left(\frac{\delta \dot{m}_o}{\rho_o A_o} \right)^2 + \left(-\frac{\dot{m}_o\ \delta \rho_o}{\rho_o^2 A_o} \right)^2 + \left(-\frac{\dot{m}_o\ \delta A_o}{\rho_o A_o^2} \right)^2 \right\}^{\frac{1}{2}}$$

Conclusion

Each measurand, calculation and result has an inherent uncertainty associated with it. It is important to quantify these uncertainties to enable the analysis of data and determine the true significance of results. This chapter described the different modes of uncertainty encountered and the methods used to quantify each.

APPENDIX B – ADDITIONAL RESULTS

The results and discussion thereof in Chapter 6 focussed on the 0.386 annular diameter ratio to avoid cluttering and redundancy. This annexure contains a summary of results for all four annular diameter test sections, including figures showing:

- Average Nusselt number across the Re_{Dh} range at the different inlet temperature cases.
- Colburn *j*-factor across the Re_{Dh} range at the different inlet temperature cases.
- Friction factor across the Re_{Dh} range at the different inlet temperature cases.
- Local Nusselt number along the length of all four test sections for different annular Reynolds numbers at inlet temperature cases C50 and H15.
- Variation of Nu_{Dh} with T_b for all four test sections at different Re_{Dh}.

No discussion is given for the results as the necessary discussions was done in Chapter 6.

Table B-1: Average Nusselt number versus Re_{Dh} for the six inlet temperature cases in the 0.327, 0.386, 0.409 and 0.483 test sections.

a	
0.327	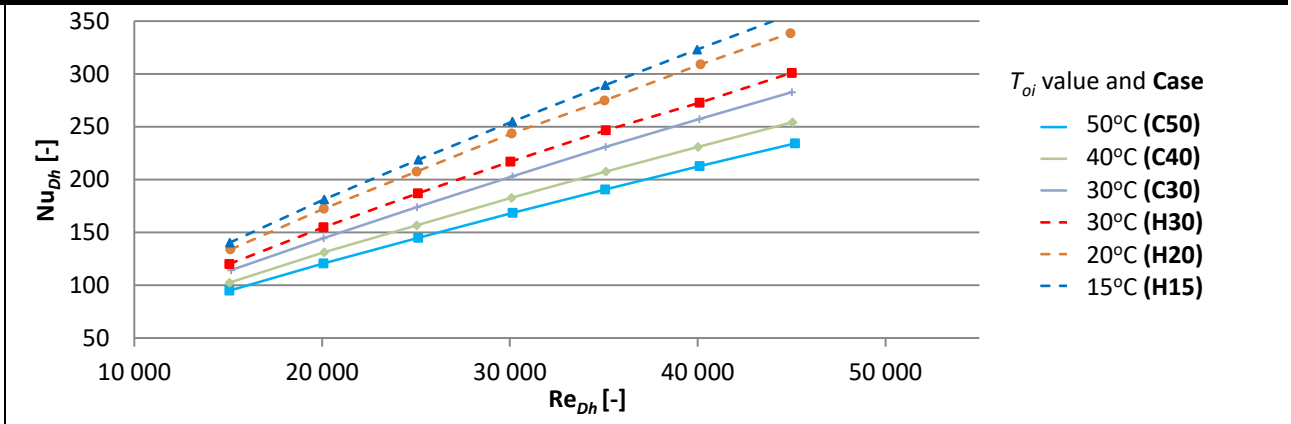
0.386	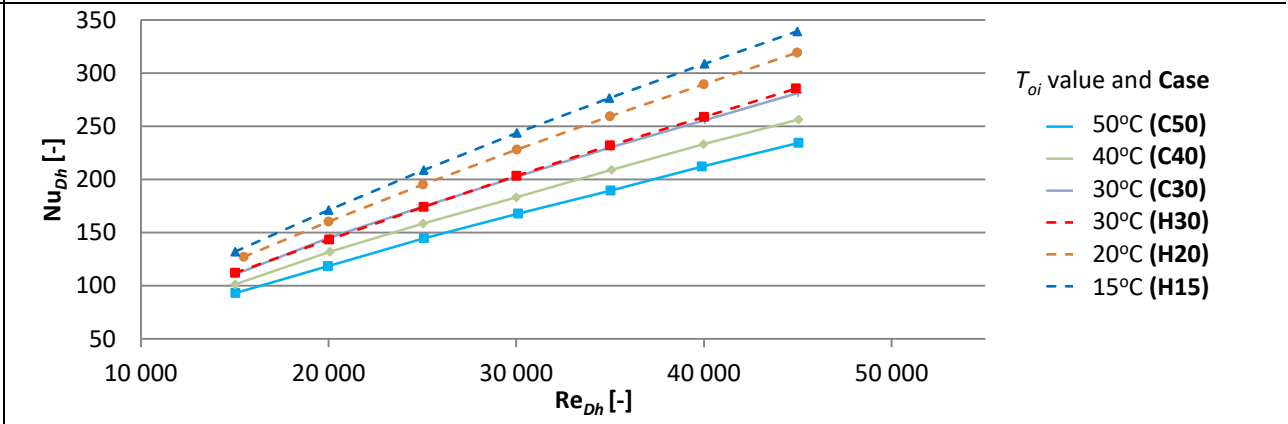
0.409	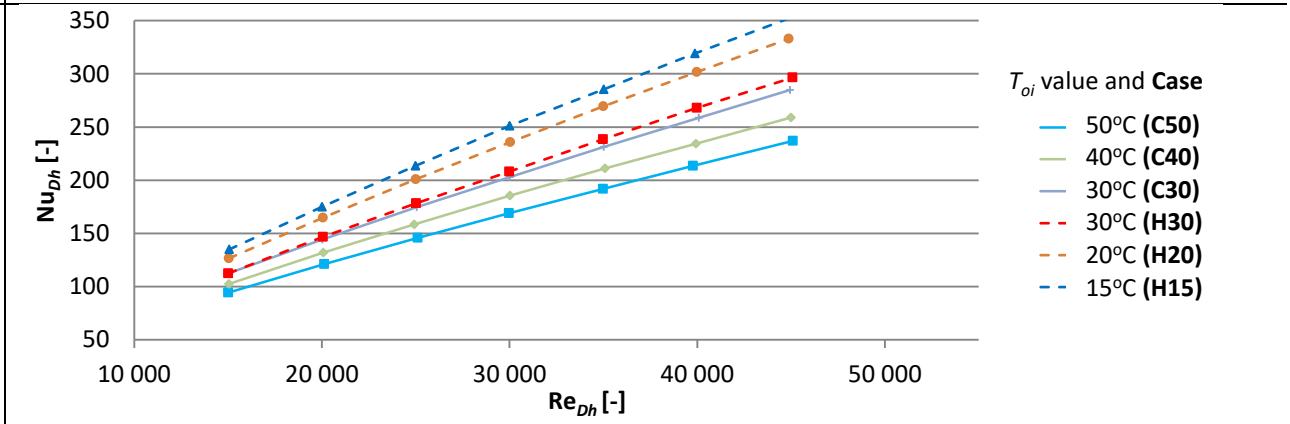
0.483	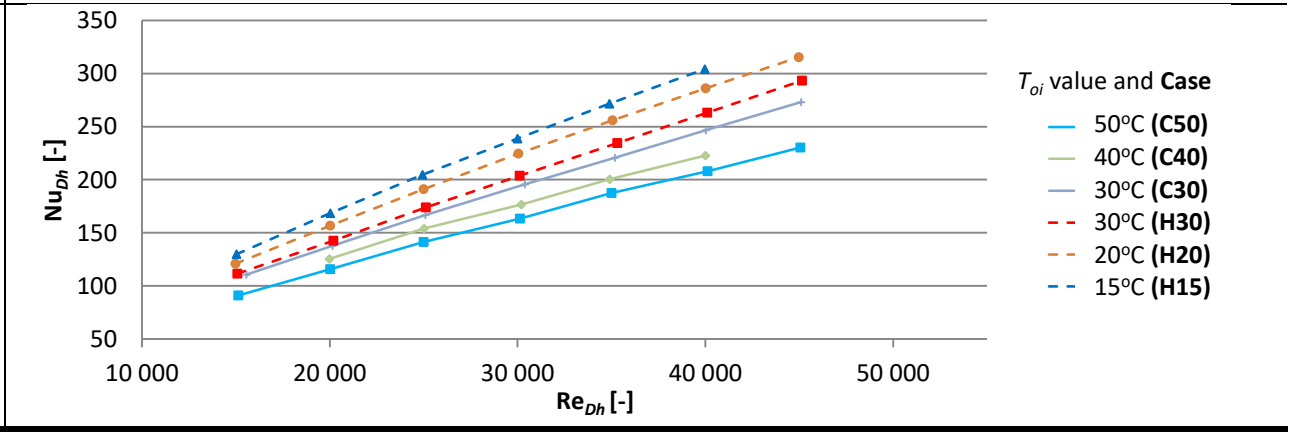

Table B-2: Colburn j-factor versus Re_{Dh} for the six inlet temperature cases in the 0.327, 0.386, 0.409 and 0.483 test sections.

a	
0.327	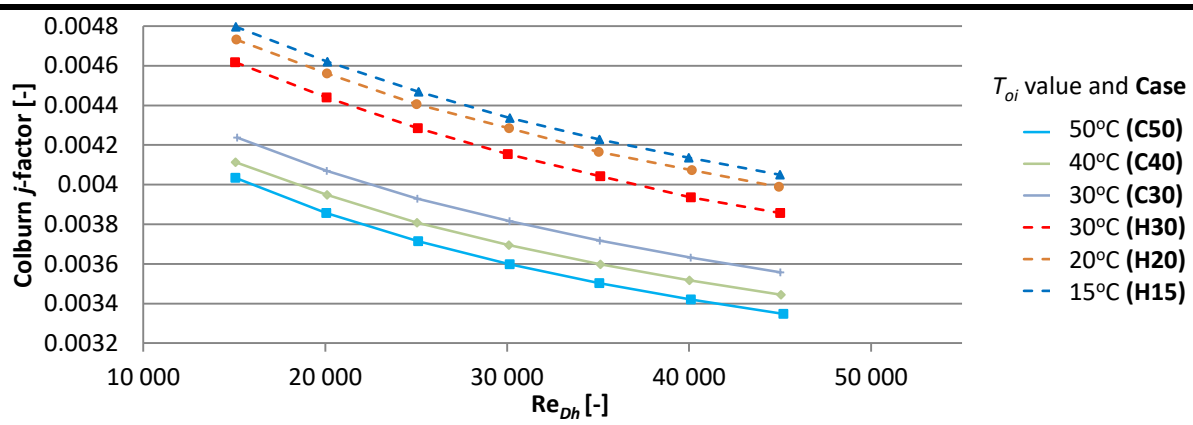
0.386	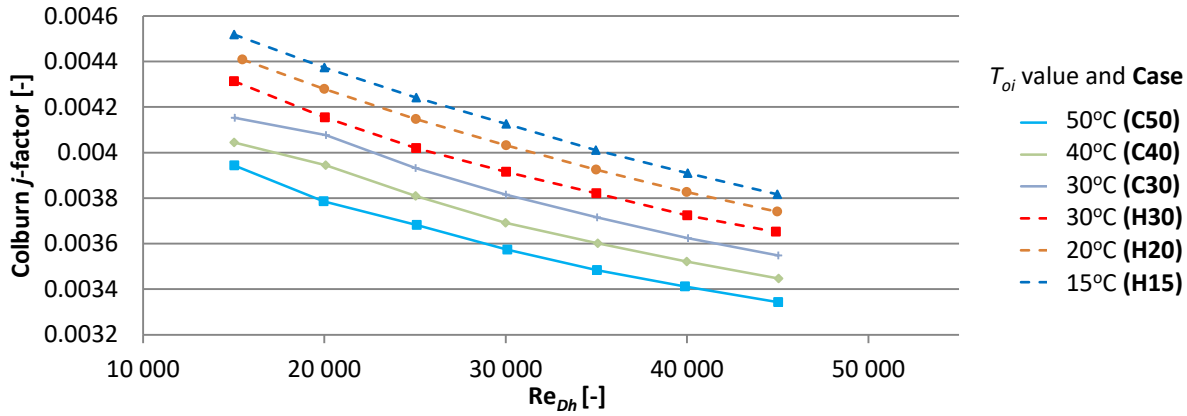
0.409	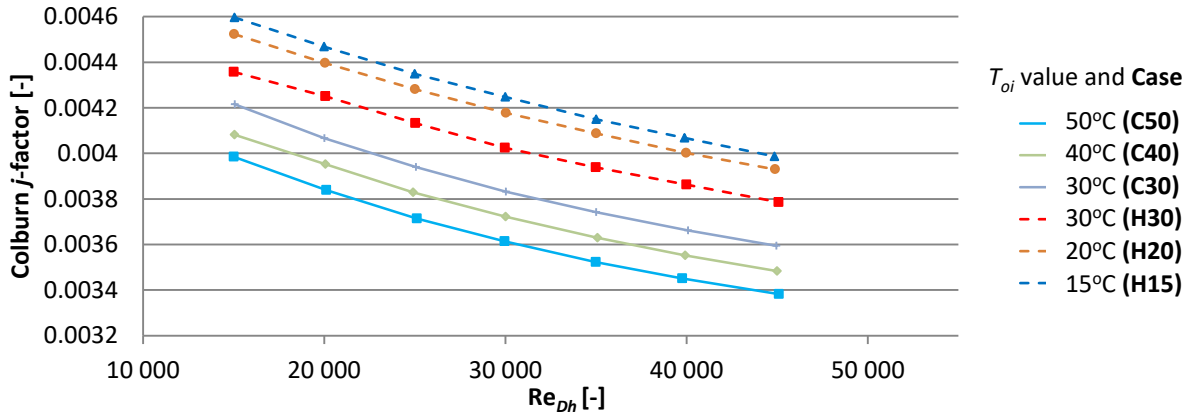
0.483	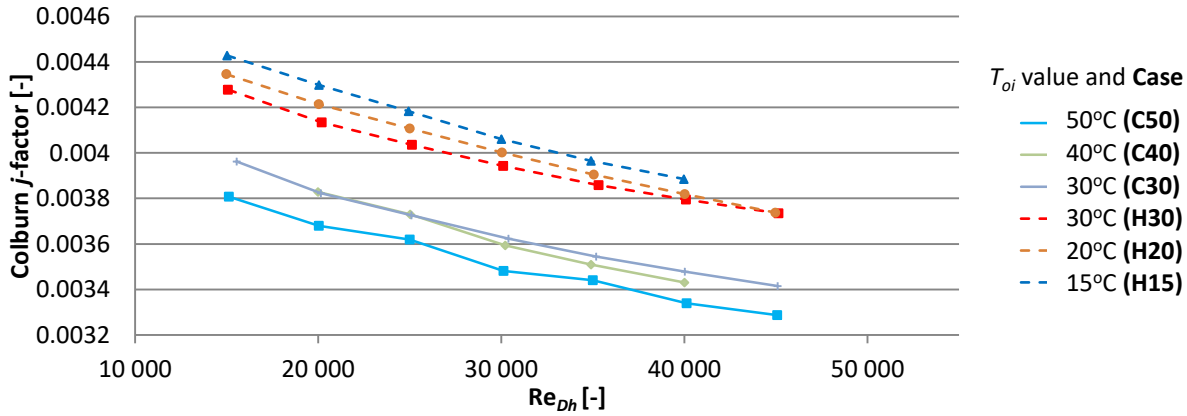

Table B-3: Adjusted Colburn *j*-factor versus Re_{Dh} for the six inlet temperature cases in the 0.327, 0.386, 0.409 and 0.483 test sections with exponent p = 0.542.

a	
0.327	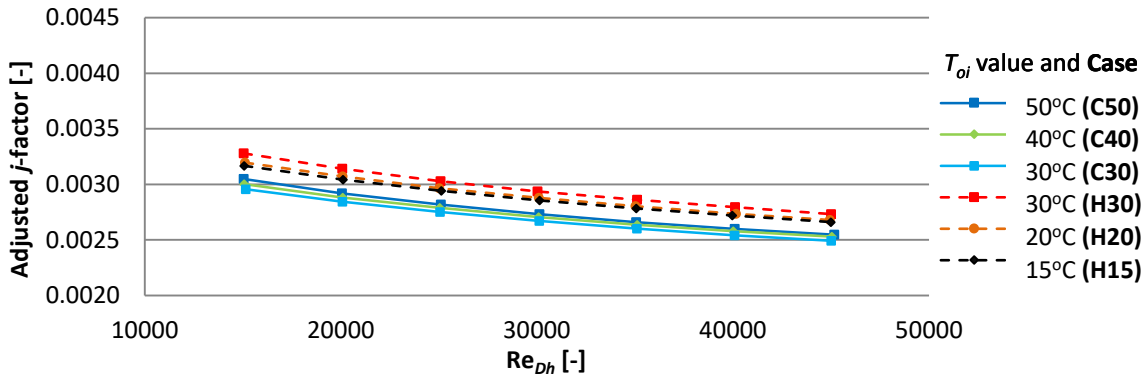
0.386	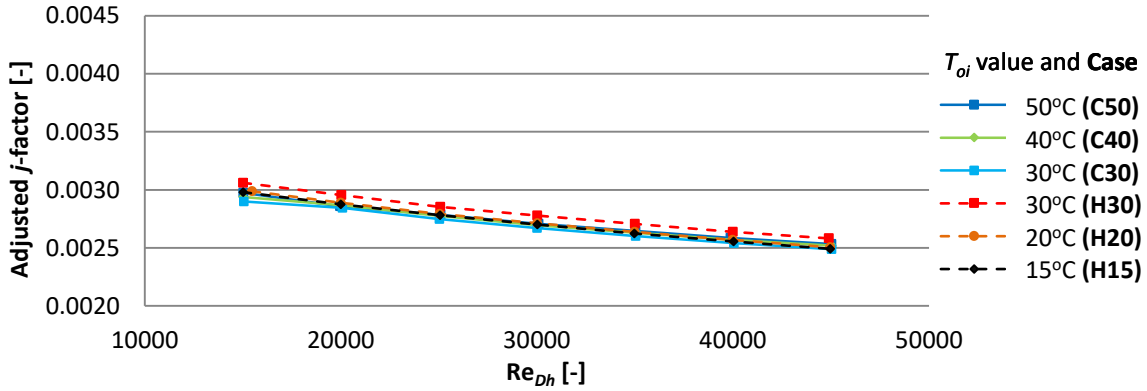
0.409	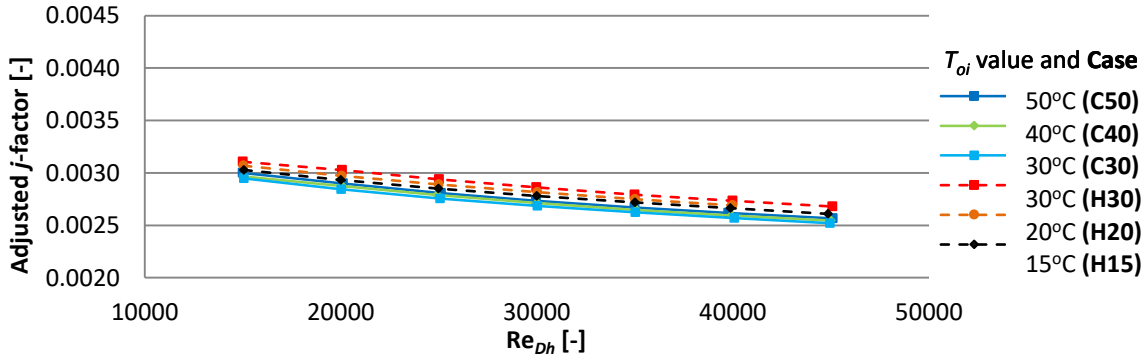
0.483	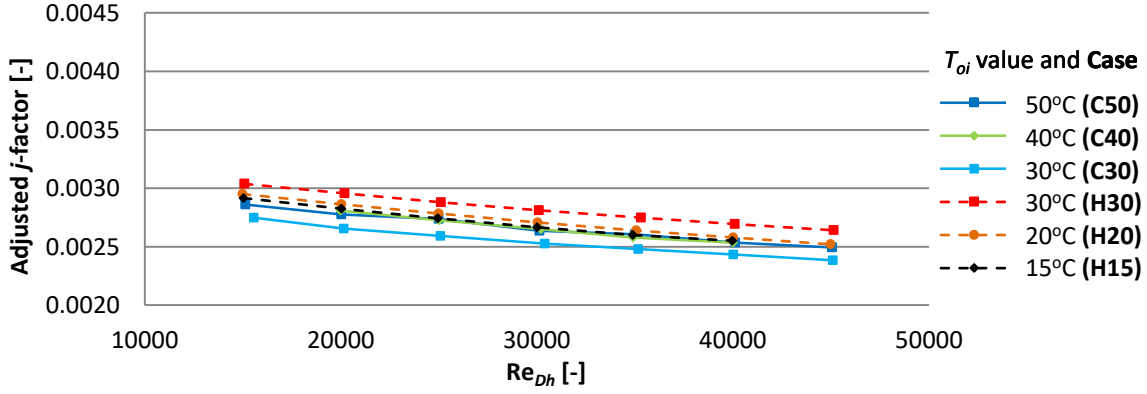

Table B-3: Friction factor versus Re_{Dh} for the six inlet temperature cases in the 0.327, 0.386, 0.409 and 0.483 test sections.

a	
0.327	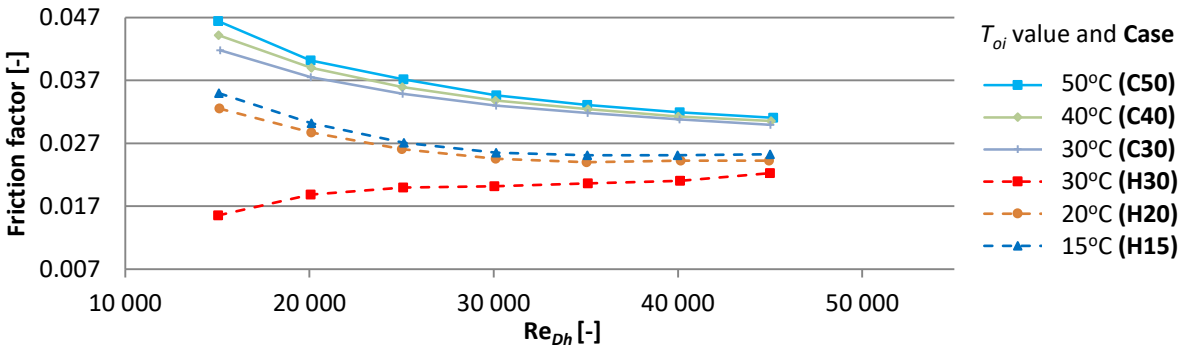
0.386	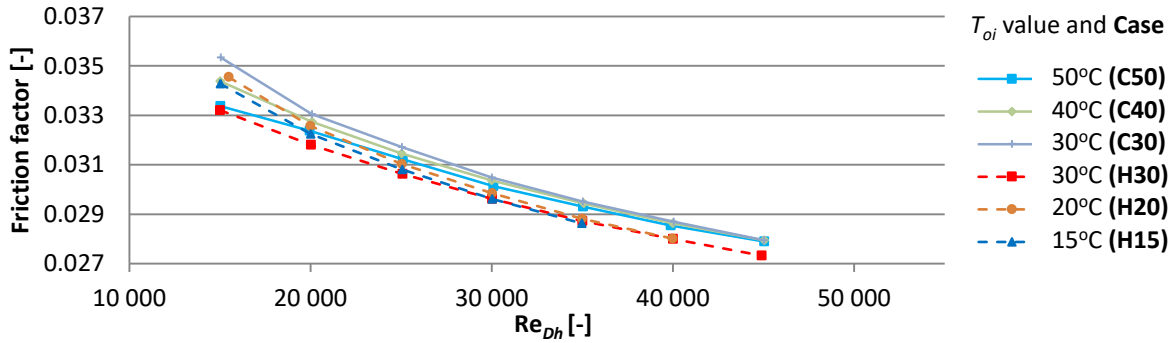
0.409	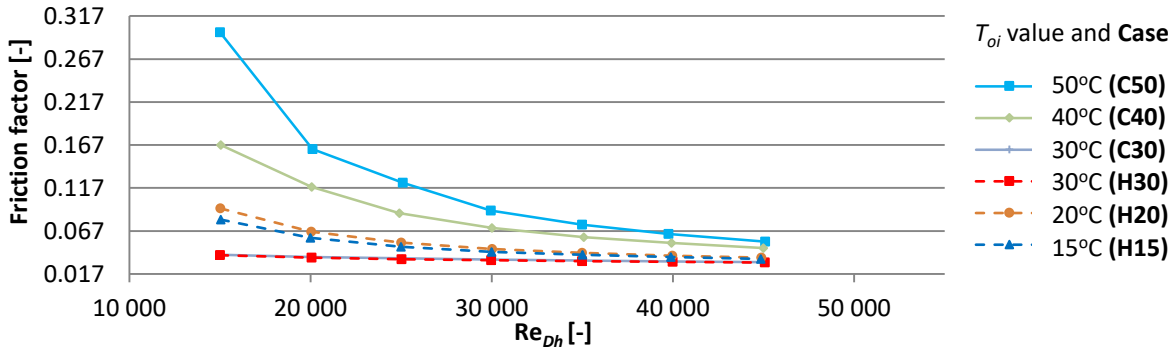
0.483	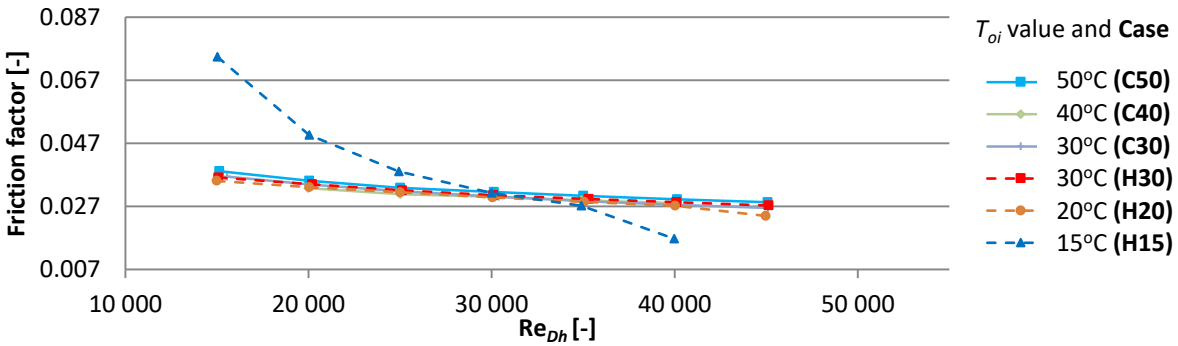

Table B-4: Local Nusselt number along the length of all four test sections for different annular Reynolds numbers at inlet temperatures cases C50 and H15.

a	C50	H15
0.327	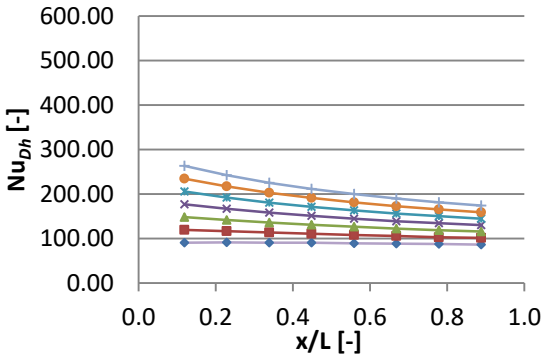	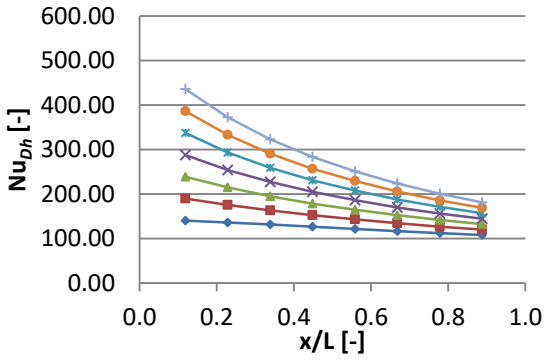
0.386	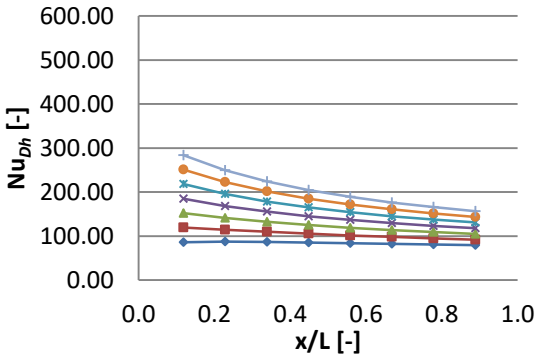	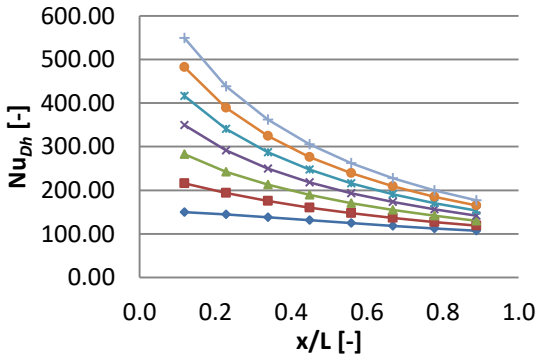
0.409	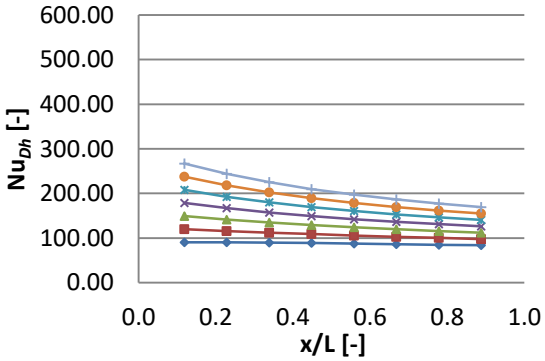	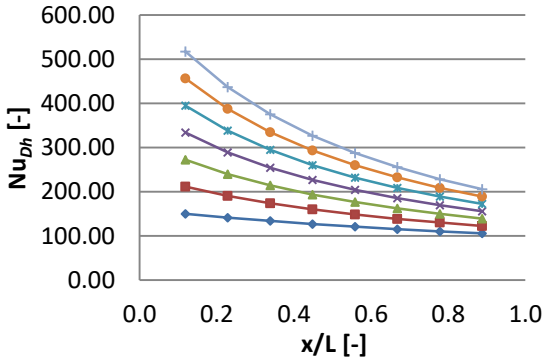
0.483	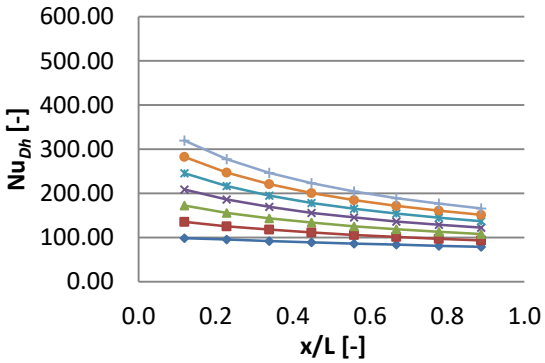	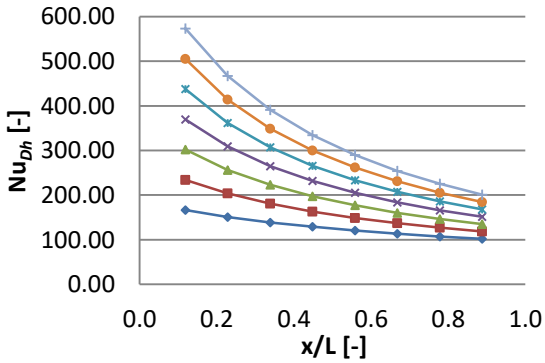

Table B-5: Variation of Nu_{Dh} with T_b for all four test sections at different Re_{Dh}.

a	
0.327	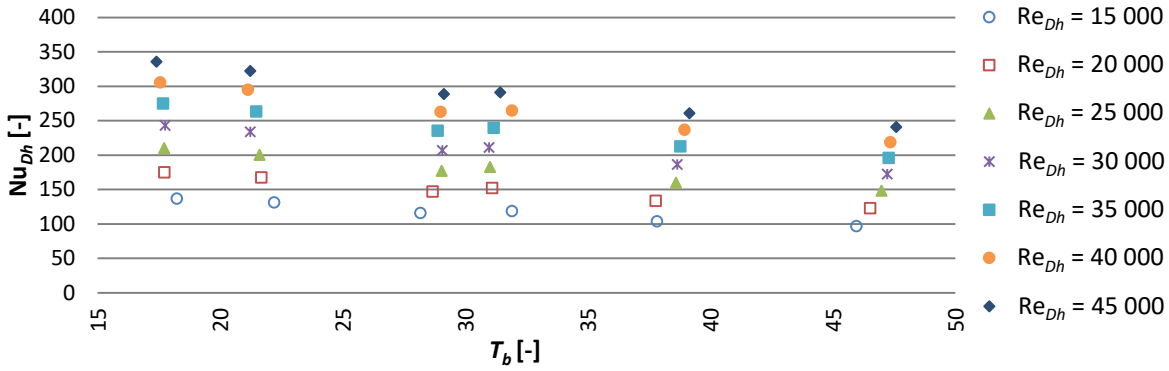
0.386	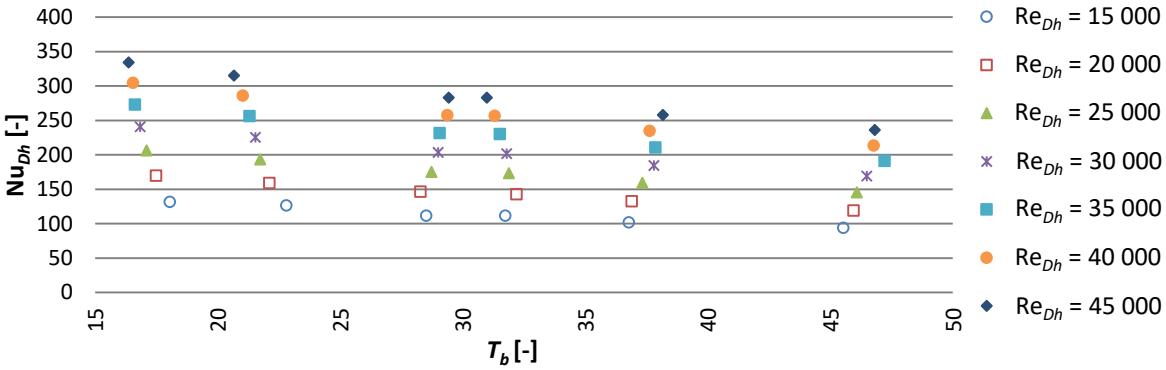
0.409	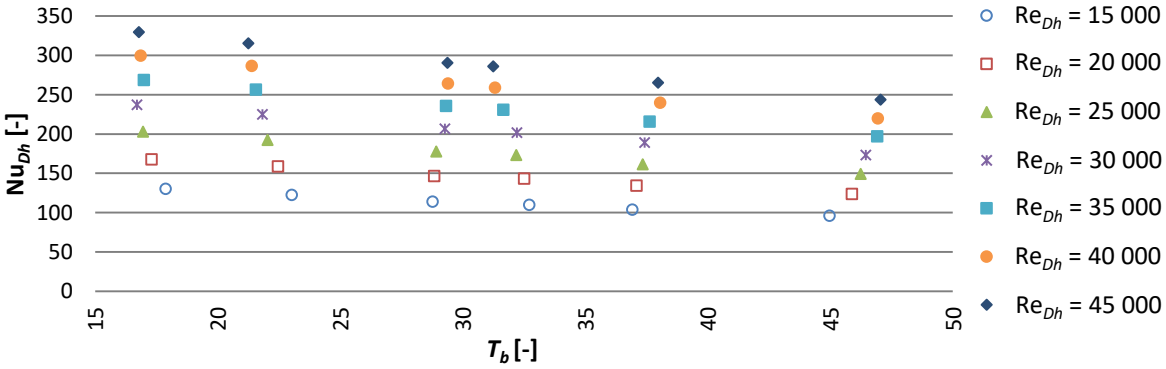
0.483	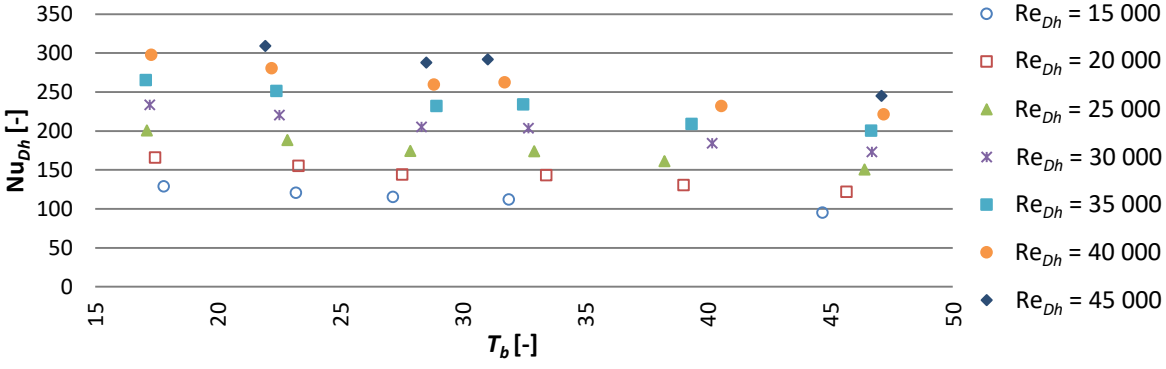

APPENDIX C – NTU AND EFFECTIVENESS ANALYSIS

For this study, the NTU and effectiveness analysis was done to validate the length of the test sections. The NTU-effectiveness method was developed by Kays and London in 1955 to analyse the effectiveness of an existing heat exchanger. In a counter flow tube-in-tube heat exchanger, maximum heat transfer would occur when the temperature of the inner tube outlet reached the temperature of the annulus inlet, or when the annular outlet temperature reached the inner tube inlet temperature. Thus, if $T_{io} = T_{oi}$ or $T_{oo} = T_{ii}$. The maximum heat transfer rate is calculated with

$$\dot{Q}_{max} = C_{min}(T_{h,i} - T_{c,i})$$

where $T_{h,i}$ and $T_{c,i}$ are the hot and cold inlet temperatures into the heat exchanger. The capacity of the inner tube and annulus are compared by taking

$$C_c = \dot{m}_c c_{p,c}$$
$$C_h = \dot{m}_h c_{p,h}$$
$$C_{min} = \text{Minimum of } C_c \text{ or } C_h$$

where subscripts *c* and *h* denote the hot and cold inlets. The capacity ratio is described by

$$c = \frac{C_{min}}{C_{max}}$$

The effectiveness of the heat exchanger is calculated by

$$\varepsilon = \frac{\dot{Q}_{actual}}{\dot{Q}_{max}}$$

where $\dot{Q}_{actual}$ is the actual heat transfer calculated from the inlet and outlet temperatures of either the inner tube or annulus.

The Number of Transfer Units (NTU) signifies the amount of heat transferred in a heat exchanger and is expressed as

$$\text{NTU} = \frac{UA_s}{(\dot{m}c_p)_{min}} = \frac{UA_s}{C_{min}}$$

where A_s is the heat transfer area and U is the overall heat transfer coefficient. The NTU is thus a function of the heat transfer surface and maximum heat will be transferred if the surface area is large enough. A relation exists between the effectiveness of a heat exchanger and the NTU, described by

$$\text{NTU} = \frac{1}{c-1} ln\left(\frac{\varepsilon - 1}{\varepsilon c - 1}\right)$$

where ε is the effectiveness and c signifies the capacity ratio.

Although one might think it is better to transfer the maximum amount of heat possible in the heat exchanger, the required length of such unit makes it uneconomical. Figure C-1 shows that the ratio between the effectiveness of the heat exchanger and the number of transfer units (NTU) increases rapidly while NTU is less than 1.5, but rather slowly for larger a NTU. It is therefore desirable to have heat exchangers with NTU close to 1.5.

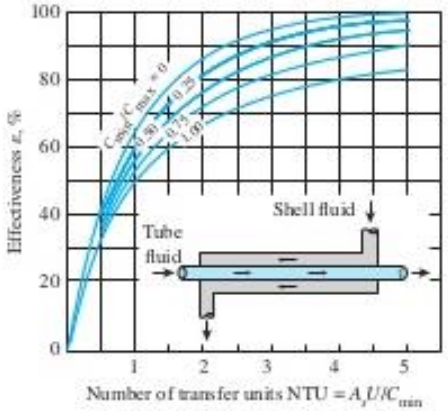

Figure C-1: NTU-effectiveness relation for a counter flow tube-in-tube heat exchanger [2].

Table C-1 gives a summary of the NTU-effectiveness analysis done for the 0.386 test section over the range of inlet temperature cases and at the maximum annular flow rate condition for each inlet temperature case. Overall, the heated annulus conditions had higher NTU values with a maximum of 1.631 for the case H30 at a maximum effectiveness of 0.791.

Table C-1: NTU and effectiveness values of the 0.386 annular ratio test section at different inlet temperature cases for maximum annular flow rate cases.

Case	Re_i	Re_{DH}	Capacity ratio, c	Effectiveness, ε	NTU
H15	20 154	45 057	0.062	0.776	1.543
H20	19 925	44 880	0.068	0.781	1.569
H30	20 065	44 712	0.080	0.791	1.631
C30	20 116	45 115	0.159	0.602	0.977
C40	20 116	45 140	0.174	0.613	1.013
C50	20 079	44 994	0.179	0.640	1.096

For all three heated cases, at the maximum annular flow rates, the NTU was greater than 1.5 with effectiveness values higher than 0.77. This indicates that the heat exchanger length was close to its maximum economical length for these conditions. On the other hand, the cooling cases had NTUs smaller than 1.1 with effectiveness values of less than 0.64. This signifies that the heat exchanger length could still be longer than 5.03 m. The effectiveness could have been improved

by increasing the length of the heat exchanger even more or, alternatively, by increasing the annular Reynolds number.